Master Thesis, Department of Geosciences

Structural analysis of the Leirdjupet Fault Complex in the southwestern Barents Sea

Andreas Bjørnestad

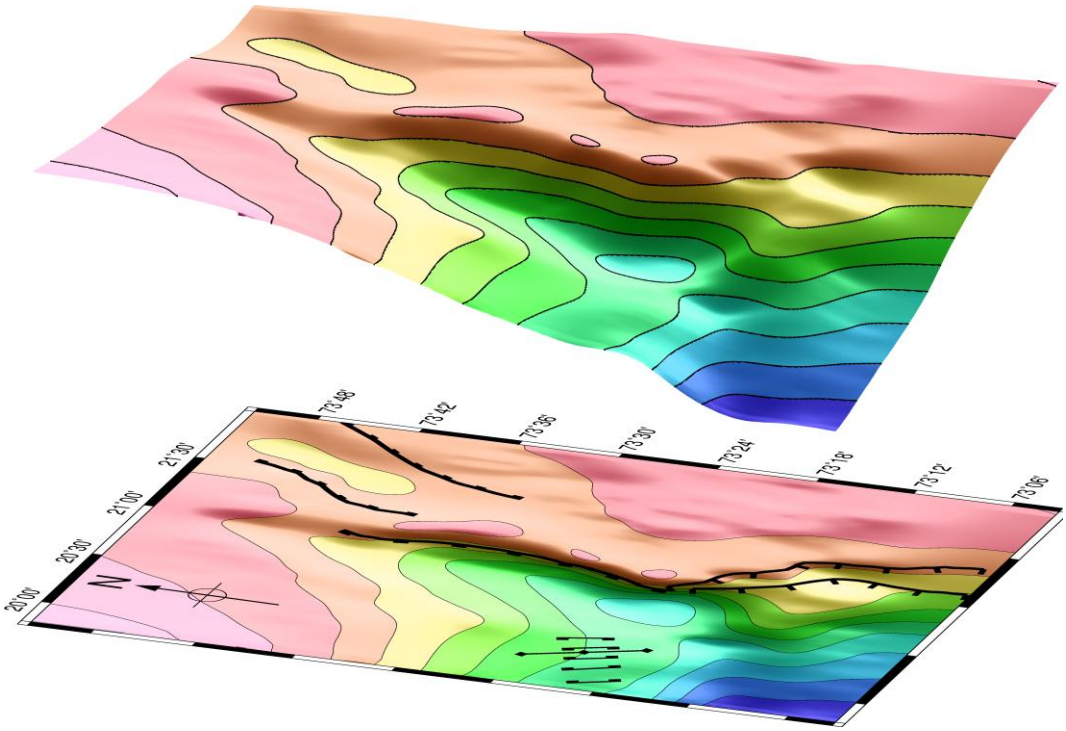

UNIVERSITY OF OSLO

FACULTY OF MATHEMATICS AND NATURAL SCIENCES

Structural analysis of the Leirdjupet Fault Complex in the southwestern Barents Sea

Andreas Bjørnestad

Master Thesis in Geosciences

Discipline: Petroleum Geology and Petroleum Geophysics

Department of Geosciences

Faculty of Mathematics and Natural Sciences

University of Oslo

June 1st, 2012

Tutor(s): **Roy H. Gabrielsen & Jan Inge Faleide**

This work is published digitally through DUO – Digitale Utgivelser ved UiO

http://www.duo.uio.no

It is also catalogued in BIBSYS (http://www.bibsys.no/english)

Abstract

The Leirdjupet Fault Complex is located in the southwestern Barents Sea and trends N - S from the Loppa High towards the Stappen High between 73° - 73°55'N at 21°E. The fault complex divides the Bjørnøya Basin into a deep western part and a shallow eastern part, the latter formally known as the Fingerdjupet Subbasin. A set of 2D seismic lines have been interpreted in order to constrain timing of faulting and study the subsequent structuring the area has been subjected to. The fault complex has been divided up into three segments, each representing different structural settings. The study addresses the possibility of fault segmentation and linkage by examining variations in the fault throw along the Leirdjupet Fault Complex. The Leirdjupet Fault Complex has been affected by at least three tectonic extensional events and subordinate phases of contraction. The extension which occurred during Late Paleozoic may have comprised two discrete phases of tectonic movement, implying that the initial phase of fault movement rapidly was succeeded by renewed activity. The Leirdjupet Fault Complex is a deep seated structure and is assumed to represent a class 1 fault, separating areas of different tectonic outline. The fault complexes, including the Leirdjupet Fault Complex, present in the southwestern Barents Sea are likely to have developed due to deep-seated zones of weakness inherited from earlier periods of tectonic activity. Observations relating the study area to the regional development of the southwestern Barents Sea indicate that the Leirdjupet Fault Complex might bound a northern continuation of the relict structural high, the Selis Ridge, situated below the present day Loppa High.

Preface

This master thesis completes the two year master program in Petroleum Geology and Petroleum Geophysics at the Department of Geosciences, University of Oslo. The master thesis has been supervised by Professor Roy H. Gabrielsen and Professor Jan Inge Faleide.

Acknowledgements

I would like to thank my supervisors, Professor Roy H. Gabrielsen and Professor Jan Inge Faleide, for giving me the opportunity to write this thesis. Their valuable input, constructive comments, encouraging words and suggestions have enabled me to improve the manuscript and has been highly appreciated.

The author would also like to thank Dr. Michel Heeremans for preparing data and Associate Professor Asbjørn Johan Breivik for providing map data of the southwestern Barents Sea.

A big thank you to all the people of 217 (Geir, Håkon, Julie, Katrine, Nicolai and Ronny) for coffee breaks, discussions - both scientific and non-scientific - and many good times.

Fugro and TGS-NOPEC are acknowledged for making seismic data available.

Contents

1 Introduction

The Barents Sea is located at the northwestern corner (Fig. 1.1) of the Eurasian continental shelf (Faleide et al., 2010). The Barents shelf covers a total area of approximately 1.2-1.3 million km^2 (Worsley, 2008; Ritzmann and Faleide, 2007) of which 245.000 km^2 constitutes the Norwegian Barents Sea, covering an area roughly twice the size of the Norwegian North Sea (Ohm et al., 2008).

The Barents Sea is a shallow epicontinental sea, not exceeding 500 m. The present day surficial features such as the Bjørnøya Trench, Finnmark Trench and Ingøy Deep are believed to represent Cenozoic drainage systems and/or the result of glacial erosion (Rønnevik, 1981). Studies of the huge fans observed in the western Barents Sea support the notion of glacial moulding, erosion and other related processes (Dimakis et al., 1998; Eidvin et al., 1993). Several mega failures associated with these structures have been documented (Hjelstuen et al., 2007).

The Leirdjupet Fault Complex is located in the southwestern Barents Sea and trends N - S from the Loppa High towards the Stappen High between 73° - 73°55'N at 21°E (Fig. 2.3). The fault complex divides the Bjørnøya Basin into a deep western part and a shallow eastern part, the latter formally known as the Fingerdjupet Subbasin (Gabrielsen et al., 1990b). The purpose of this study is to perform a structural analysis on the Leirdjupet Fault Complex, with an emphasis on timing of tectonic movement, fault segmentation and geometry. The main focus is given to what in this study is defined as the central segment of the Leirdjupet Fault Complex.

1.1 Historical review

The Barents Sea has been subject to scientific studies for more than 120 years. 2011 was a special year related to the Norwegian history of polar exploration. 150 years have passed since Fridtjof Nansen was born and 100 years since Roald Amundsen reached the South Pole as the first in history. It is truly amazing to see what they accomplished with, what today, would be regarded as primitive and outdated scientific equipment. The Norwegian explorer and scientist Fridtjof Nansen was a pioneer in this respect, commencing his

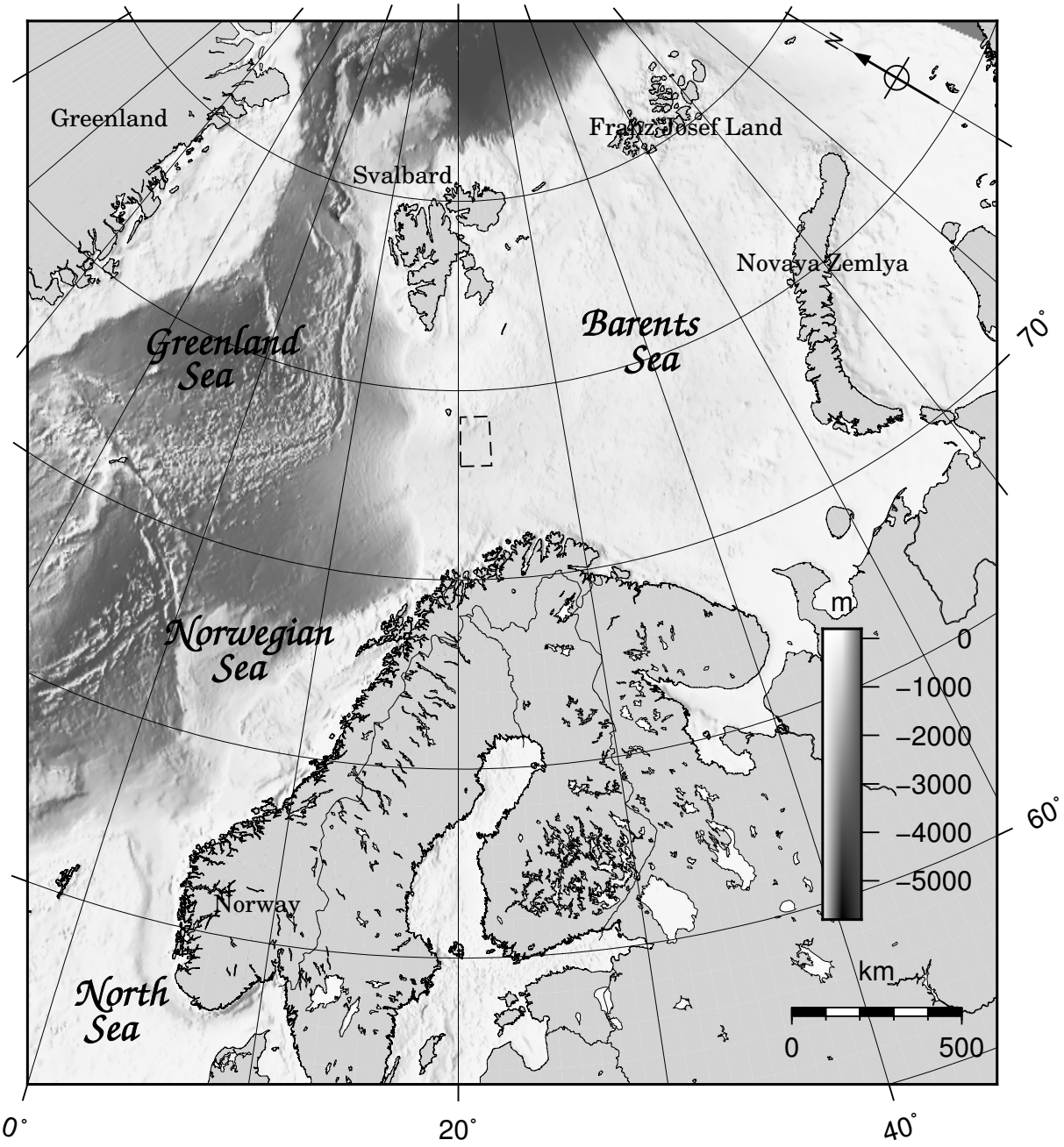

Fig. 1.1 Regional map of the area. Dashed square outlines the location of the study area. See Fig. 2.3 for detailed map of the southwestern Barents Sea. Bathymetry based on the General Bathymetric Chart of the Oceans (*GEBCO*).

research in the 1890s. In July 1893 Nansen and Otto Sverdrup embarked the "Fram" intending to do a series of scientific measurements in the high polar areas. This resulted in one of the first bathymetric maps of the Barents Sea which ultimately would change our view and understanding of the polar areas (Gjelsvik, 1976). The striking similarities with bathymetric maps created today with the help of top modern techniques, truly gives awe for the work they did. Nansen was the first to recognize and model the apparent uplift the area has undergone and his hypothesis was based on the bathymetric data that were collected and geological information from surrounding areas. Today there is a broad consensus of uplift being an important factor in this area (Dimakis et al., 1998; Ohm et al., 2008). Roald Amundsen is best known for his expedition to the South Pole. He was, however, also heavily involved in expeditions in the northern areas, e.g. his attempt to measure the magnetic field (Egeland and Deehr, 2011).

From the 1920s to 1960s Soviet scientists dominated in the field of scientific studies and research in the Barents Sea. Since the 1970s the area has been of interest to several institutions from many nations. The Svalbard archipelago has played an important role throughout these years - and still does - serving as a launch pad for expeditions due to its proximity to the northern areas (Arlov, 2003).

In 1972 the Norwegian government decided to establish the Norwegian Petroleum Directorate (NPD), an institution being the authorities extended arm to administer and manage petroleum resources present on the Norwegian continental shelf. NPD started to systematically map the Barents Sea in 1973 (Rønnevik, 1981), and today the database includes large amounts of data; gravimetric, magnetometric, reflection- and refraction seismic measurements and well data (Smelror et al., 2009).

1.2 Petroleum exploration in the Barents Sea

Exploration for hydrocarbons has been carried out in the North Sea since the 1960s. The first commercial discovery, Ekofisk, was made in 1969 and since then numerous large fields (e.g. Sleipner, Statfjord and Gullfaks etc.) have been discovered (Faleide et al., 2010).

Ever since the North Sea was recognized as being a prolific petroleum system (Magoon

and Dow, 1994) – often termed the Kimmeridgian "Hot Shale"-Brent petroleum system (Klemme, 1994) – the area has been extensively studied and is today very well understood. Especially the Viking Graben, a major Mesozoic rift basin (Fjeldskaar et al., 2004) in the northern North Sea has been subject for thorough exploration (Christiansson et al., 2000; Gabrielsen et al., 1990a; Nøttvedt et al., 1995; Odinsen et al., 2000; Evans et al., 2002) and models that have been developed are capable of reconstructing the basin history with high degree of accuracy (Rüpke et al., 2008).

Exploration for hydrocarbons in the Barents Sea started in the late 1970s/early 1980s (Stewart et al., 1995; Knutsen et al., 2000) and has lead to several discoveries. The early exploration started in the Hammerfest Basin, focusing on reservoirs of Lower- Middle Jurassic age capped by Upper Jurassic and Cretaceous shale. The Hekkingen Formation deposited in Late Jurassic time (Fig. 2.1) is probably the most important source rock in the region. Cored sections from the Nordkapp Basin show that the total organic carbon (TOC) in this formation varies from of 4-21 weight percent (Bugge et al., 2002), i.e. it has substantial potential for generating hydrocarbons.

Although the principal reservoir rock in this area has a large extent, it contained mainly gas and the reservoir quality was poorer than expected, i.e. severe diagenesis (Bjørlykke and Egeberg, 1993; Bjørlykke and Jahren, 2010; Bjørlykke, 2006). Initially this was thought to have been caused by anomalous geothermal gradients in the area. Later studies have shown that these rocks originally were buried to greater depths, but was uplifted to present depth during the Cenozoic (Stewart et al., 1995; Green and Duddy, 2010). The integrated time-temperature is known to be crucial for thermal cracking of kerogen (Tissot et al., 1987; Waples, 1994) and for subsequent expulsion and migration (England, 1994) to take place, and thus would to a high degree have affected the petroleum potential. Gaining more experience and knowledge throughout the years, other plays have become important and interesting (Knutsen et al., 2000; Østvedt et al., 2005).

It is a common misconception that the the success rate regarding petroleum exploration is low in the Barents Sea. Compared to the Norwegian North Sea where 32 dry wells were drilled before the major discovery of Ekofisk, the success rate is high - about one of three wells resulting in a discovery. Despite of this, the commercial implications have

been rather limited, as the findings mainly represent gas (Ohm et al., 2008; Stewart et al., 1995). The most significant discoveries in the area up until recently included the Snøhvit and Goliat fields, representing a gas field and an oil field, respectively. To this date, the Shtokman discovery in the Russian sector represents the largest natural gas field in the world.

The recent giant discoveries of the Skrugard prospect (well 7220/8-1) and the Havis prospect (7220/7-1) indicates that significant volumes are still to be found in less explored areas. These findings and the decreasing production in the North Sea makes the Barents Sea an interesting and important area in the future.

2 Geological framework

The Norwegian continental shelf is divided into three provinces; i)the North Sea, ii)the mid-Norwegian continental shelf and iii)the western Barents Sea. Prior to the break up of the Norwegian-Greenland Sea all these provinces were part of a major epicontinental sea. This is readily recognized by the similar stratigraphy and geological evolution of the different provinces (Gabrielsen et al., 1990b; Faleide et al., 2010).

2.1 The Barents Sea

The Barents Sea is an epicontinental sea overlying an intracratonic basin (Rønnevik and Jacobsen, 1984) located approximately between 70°and 80°N in the northern part of the post-Caledonian North Atlantic rift system (Breivik et al., 1998). It is bordered in the west by the Norwegian-Greenland Sea, the Svalbard archipelago in the northwest and Franz Josef Land and Novaya Zemlya in the northeast and east, respectively (Fig. 1.1).

On basis of sediment thickness, the Barents Sea may be divided into two regions; a western and an eastern. These two regions are separated by a north-south trending monoclinal structure (Worsley, 2008). The eastern region is dominated by very deep sedimentary basins, reaching depths of $>$ 20 km (Smelror et al., 2009) in some places (i.e. South Barents Basin). The western part comprises shallower basins, and the structural trends are more complex, hence the same division can be made on basis of structural evolution. The Norwegian part of the Barents Sea has traditionally been divided into three major provinces; the Barents Sea east of 25°E, the area between 20°E and 25°E and the area west of 20°E (Rønnevik, 1981). The area towards the west displays increasing tectonic complexity. These contrasts have their offspring in the different type and degree of tectonics that have acted in the various regions.

The study area is located in the southwestern Barents Sea, and the main focus will be on this area.

2.2 Structural and stratigraphic evolution

The western Barents Sea area is in general dominated by thick sequences of sediment deposited during the Late Paleozoic through Cenozoic. Structurally the area has been divided into three distinct regions. 1)The Svalbard Platform - an area comprising relatively flat-lying Paleozoic to Mesozoic, predominantly Triassic sediments. 2)A basin province between the Svalbard Platform and the Norwegian coast. This area is characterized by several basins and structural highs. 3)The continental margin, subdivided into i)a southern sheared margin following the Senja Fracture Zone ii)a central rifted complex southwest of Bjørnøya and iii)a northern sheared and later rifted margin following the Hornsund Fault Zone (Faleide et al., 2010). The area shows large variation in terms of potential field and magnetic anomalies. This is in large parts related to the processes and geologic evolution during the orogenies the area has been exposed to (Barrère et al., 2009).

The regional geologic history of the south western Barents Sea, both in terms of structural configuration and stratigraphy, has been subject to many studies (Rønnevik, 1981; Rønnevik and Jacobsen, 1984; Worsley, 2008; Gudlaugsson et al., 1998; Faleide et al., 1984, 1996, 2008, 1993b; Smelror et al., 2009; Glørstad-Clark et al., 2011, 2010) and is generally well understood.

The present day western Barents Sea shelf has been formed through several post-Caledonian tectonic phases. These tectonic events are responsible for the gross structuring observed today. Superimposed on these are subordinate events which caused local depositional variations (Smelror et al., 2009). The major features and structural elements were properly described and formalized by Gabrielsen et al. (1990b). The structural evolution since Late Paleozoic times has been suggested to be closely connected to weaknesses in the basement. These weakened areas have been thought to be caused by three major compressional orogens; Baikalian, Caledonian and Innuitian (Gudlaugsson et al., 1998). It is plausible that the later structuring has been affected and biased by deep seated zones of weakness inherited from these tectonic events, and they have been shown to be traceable and correlate with detachment zones in the south western Barents Sea basins

(Gabrielsen, 1984).

The main post-Caledonian events include three major rift phases; Late Devonian(?)-Carboniferous, Middle Jurassic-Early Cretaceous and early Cenozoic. Each of these events comprised several pulses of movement. The rifting in Late Paleozoic affected the whole Barents Sea, whereas the later rifting tended to migrate westwards. This created rift and pull-apart basins in the southwest, and several strike-slip faults in the north (Faleide et al., 1993b). Hence, the eastern Barents Sea has been relatively stable since Late Paleozoic times which is readily recognized in regional geological profiles (Smelror et al., 2009).

The lithostratigraphy of the western Barents Sea is shown in Fig. 2.1.

The sediments deposited in Paleozoic mainly comprise mixed carbonates, evaporites and clastic material. The Mesozoic and Cenozoic deposits primarily consist of clastic material. A brief review of the regional geological history of the Barents Sea from Upper Paleozoic through Cenozoic based on Gudlaugsson et al. (1998) and Faleide et al. (2010) is given below.

Upper Paleozoic The 300 km wide and at least 600 km long rift zone covering the western Barents Sea was established mainly in mid-Carboniferous time. This zone comprises several rift basins and intrabasinal highs. The extensional basins are characterized by half-graben geometries and several of them are interconnected. Syn-rift deposits are present, separated by the fault bounding highs. Basins formed at this time include the Tromsø, Bjørnøya, Nordkapp, Fingerdjupet, Maud and Ottar Basins. By the end of Carboniferous the faulting ceased.

The structural relief was later infilled and covered by successions of platform forming strata. The lower part of these deposits comprise dolomite and evaporites underlying massive limestone. The evaporites deposited during this period (late Carboniferous - early Permian) have a widespread extent, covering large parts of the southwestern Barents Sea. In the Nordkapp Basin the thickness is inferred to reach up to 4-5 km. This has been interpreted as being related to depressions created by faulting, either in place, or developing by early Late Carboniferous and subsequent (but subordinate) thermal

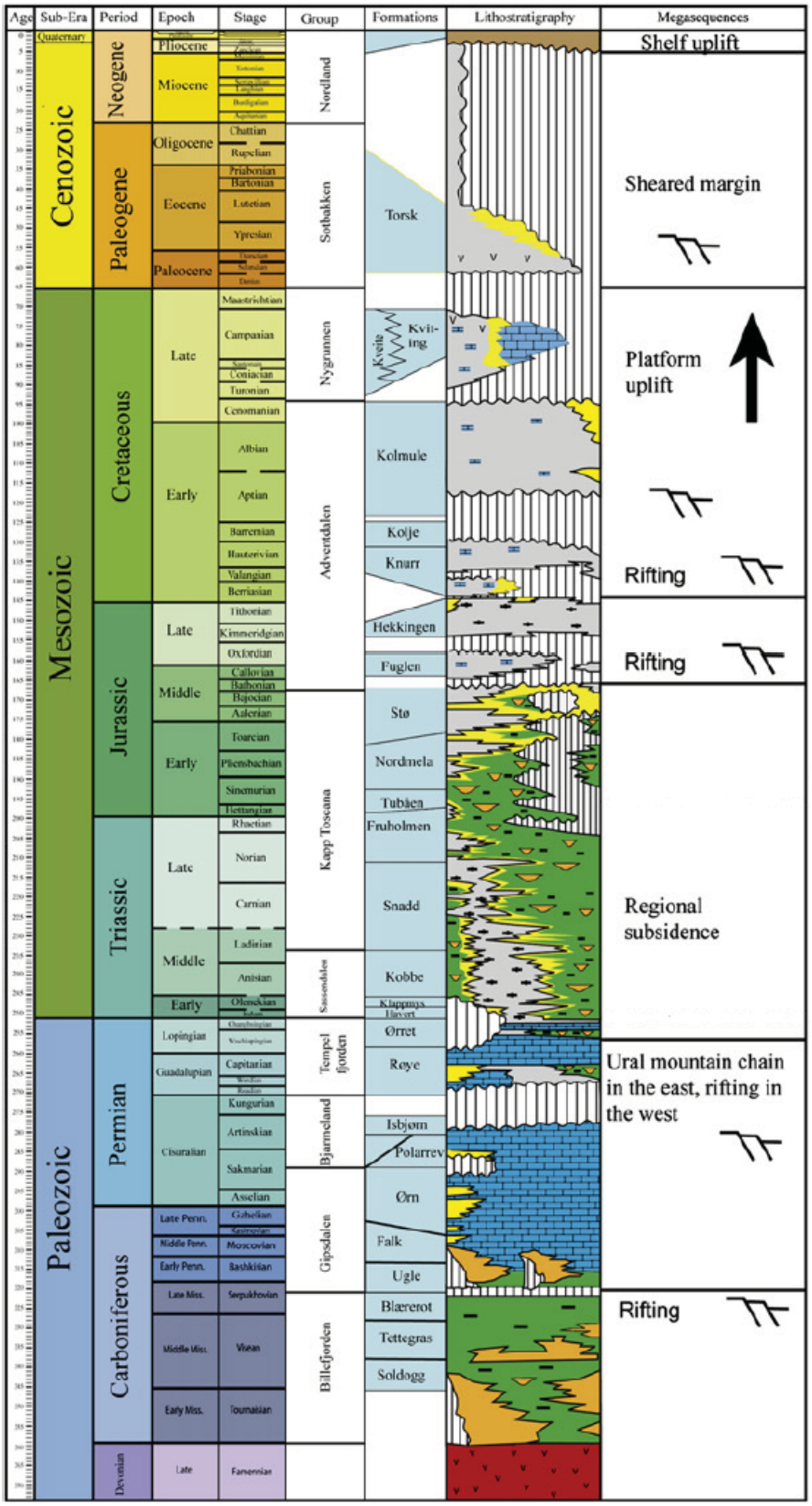

Fig. 2.1 Lithostratigraphy of the western Barents Sea. Modified from Glørstad-Clark et al. (2010).

subsidence.

Carbonate and evaporite deposition is thought to have been dominating the sedimentation from mid-Carboniferous until Early Permian, when input of clastic material increased. In Permian - Early Triassic the western part of the fault system experienced renewed faulting, uplift and erosion. This rift phase is associated with erosional surfaces extending from Loppa High to Stappen High, as well as fault movements as far north as the Fingerdjupet Subbasin. The magnitude of this event must therefore have been significant, affecting a narrow zone along the entire present western margin.

Mesozoic At Early Triassic times a large part of the Barents Sea was covered with a regional deep water basin. During the Triassic, clastic sediment input was high. Sources included the Uralian highlands, the Baltic shield and other local source areas. The strata deposited during this time were dominated by shales and sandstones. Marine conditions prevailed from Late Permian to Early Triassic time. Up until Middle Triassic shallowing and exposure of some areas caused continental conditions. By this time prograding deltaic systems continued to fill in the regional basin.

The northern and central areas still had marine conditions and source rocks from this time are recognized from Svalbard. This source rock is thought to be present in most parts of the western Barents Sea. By the end of Triassic, regression and erosion took place.

In Lower-Middle Jurassic, sandstones were deposited in the whole Barents Sea region. These sandstones act as the main reservoir rock in the southwestern Barents Sea, e.g. Snøhvit field in the Hammerfest Basin (Fig. 2.3). These sandstones are believed to have covered the Loppa High and Finnmark Platform as well, but were later eroded due to tectonic activity. The Middle Jurassic marks the initiation of rifting and Late Jurassic - earliest Cretaceous is characterized by extension along with strike-slip displacement along the old zones of weakness (i.e. old structural elements). The extension caused the Bjørnøya, Tromsø and Harstad basins to develop and become prominent rift basins.

This phase of rifting continued in Early Cretaceous. The period is dominated by deposition of shales and claystones, and some silt limestone and dolomite. These deposits

are typical infill of the deep basins in the southwestern part of the Barents Sea.

During Early Cretaceous the northern Barents Sea was subjected to magmatism, and associated extrusives and intrusives have been identified both on- and offshore. This magmatism caused regional uplift and is thought to be associated with a rift event affecting the Amerasia Basin and the subsequent formation of the Alpha Ridge. During Upper Cretaceous the southwestern part of the region continued to subside due to pull-apart related faulting. This area is the only part subjected to deposition in this time period. The deposits vary in thickness, but in e.g. the Tromsø Basin sequences of shale up to 2-3 km are inferred from seismic data (Faleide et al., 2010).

Cenozoic This period was dominated by the opening of the Norwegian-Greenland Sea which occurred after a period of rapid subsidence taking place in late Paleocene. Fig. 2.2 shows a simplified tectonic map illustrating how the Norwegian-Greenland sea developed during Cenozoic.

The western Barents Sea-Svalbard margin is thought to have originated from a mega shear zone which connected the Norwegian-Greenland Sea and the Eurasia Basin. It is believed that the evolution of this margin has been controlled by three parameters. These include the 1)pre-break up structure, 2)the orientation and geometry and 3)the plate boundaries by the onset of the opening and the relative movement of the plate. The interplay of these various parameters caused several structural styles of the different margin segments. During break-up in Paleocene - Eocene, and later in Oligocene, the central rifted margin near Bjørnøya experienced magmatism (Vestbakken Volcanic Province). East of Svalbard as well as further north, between Svalbard and Greenland, strike-slip movement occurred. This caused compressional deformation that occurred within the Spitsbergen Fold and Thrust Belt. This is thought to have created the domal structures in the eastern part of the Barents Sea.

The late Cenozoic development is characterized by further subsidence with increasing input of sediments causing burial of the margins by a thick clastic wedge. The sediment input originated from the uplifted Barents Sea area. Due to the uplifting, large amounts of the Cenozoic and older deposits have been eroded away. As much as 3000 m of

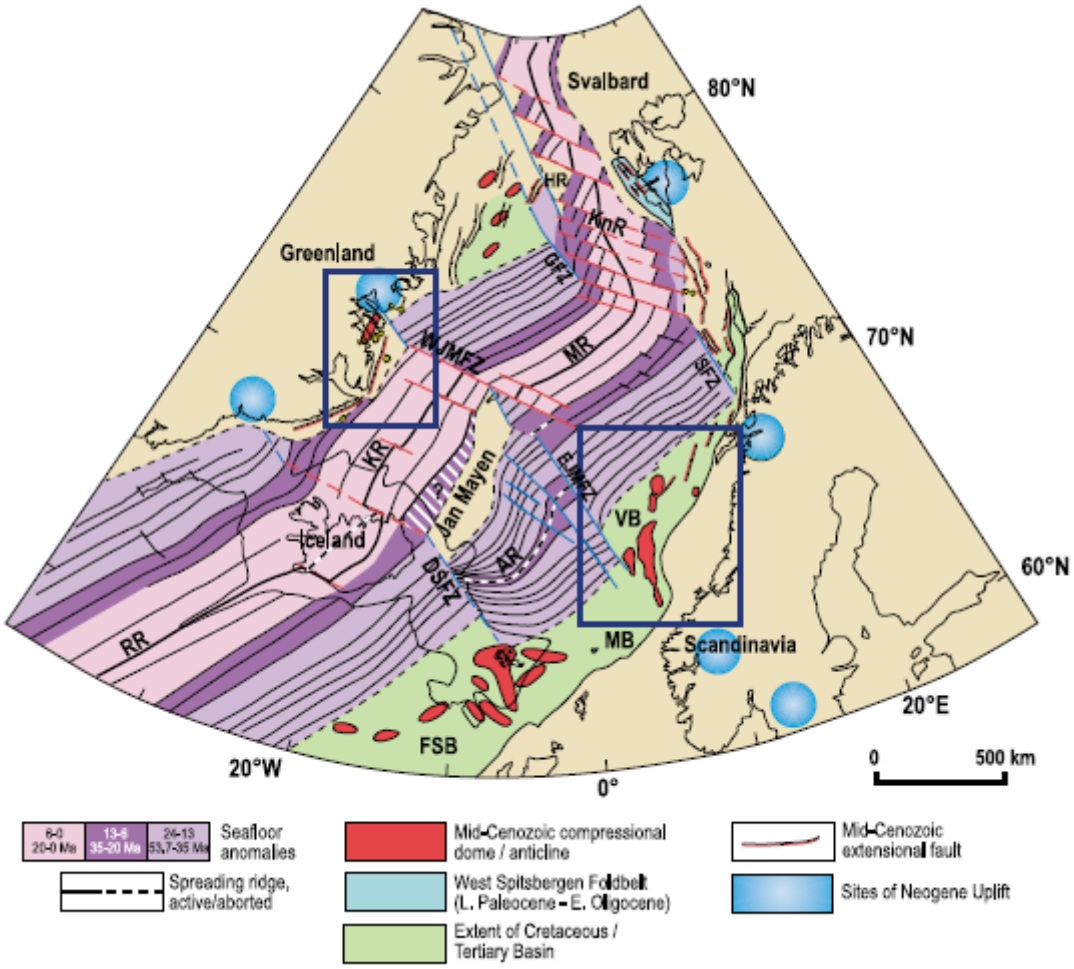

Fig. 2.2 A simplified tectonic map illustrating the evolution of the Norwegian-Greenland Sea during Cenozoic. From Lundin and Doré (2002).

strata has been eroded in the western Barents Sea, most notable in the northwestern part including Svalbard, whereas the southwestern part only experienced 1000-1500 m of erosion (Faleide et al., 2010).

2.3 The Bjørnøya Basin

The Bjørnøya Basin is a complex basin located between 32°30'N - 74°N in N-S direction and 18°E - 22°E in W-E direction. It trends north-northeast and increases both in depth and width westwards (Faleide et al., 1984). The basin is divided into a deep western part and a shallow eastern part by the Leirdjupet Fault Complex (see section 2.4) (Gabrielsen et al., 1990b). The Bjørnøya Basin together with the Hammerfest, Sørvestsnaget Basins and the Samson Dome are all associated with negative gravimetric anomalies, around -10 mGal (Gabrielsen et al., 1990b; Barrère et al., 2009). It borders against the Stappen High to the north, Sørvestsnaget Basin to the west and Loppa High and Vesleøy High to the southwest and south, respectively (Fig. 2.3). The basin is characterized by particularly deep Cretaceous and Cenozoic sediment infill (Faleide et al., 1993b; Ryseth et al., 2003), as the other basins in the province (i.e. Harstad, Tromsøand Sørvestsnaget Basins). However, the basins and highs between 20 - 25 °E do not exhibit the same subsidence pattern. This is clearly seen in the case of Fingerdjupet Subbasin (Fig. 2.5). The genesis of the Bjørnøya Basin is believed to have started during Late Jurassic-Early Cretaceous. This was a period of rifting which is assumed to have caused the NE-SW trending structures, such as the Bjørnøya Basin. The subsequent subsidence included a large area, which was covered with thick Cretaceous strata.

In the adjacent Tromsø Basin the top of the crystalline basement has been suggested to be located at a depth of 18 - 20 km. A similar depth has been inferred for the Bjørnøya Basin as well (Gabrielsen et al., 1997).

Other Late Paleozoic rift basins such as the Ottar (Breivik et al., 1995) and Nordkapp basins (Bugge et al., 2002) both comprise accumulations of Paleozoic deposits. These basins include large amounts of salt deposited during Carboniferous-Permian (see section 2.2), reaching thicknesses of several km in the Nordkapp Basin. This has been shown

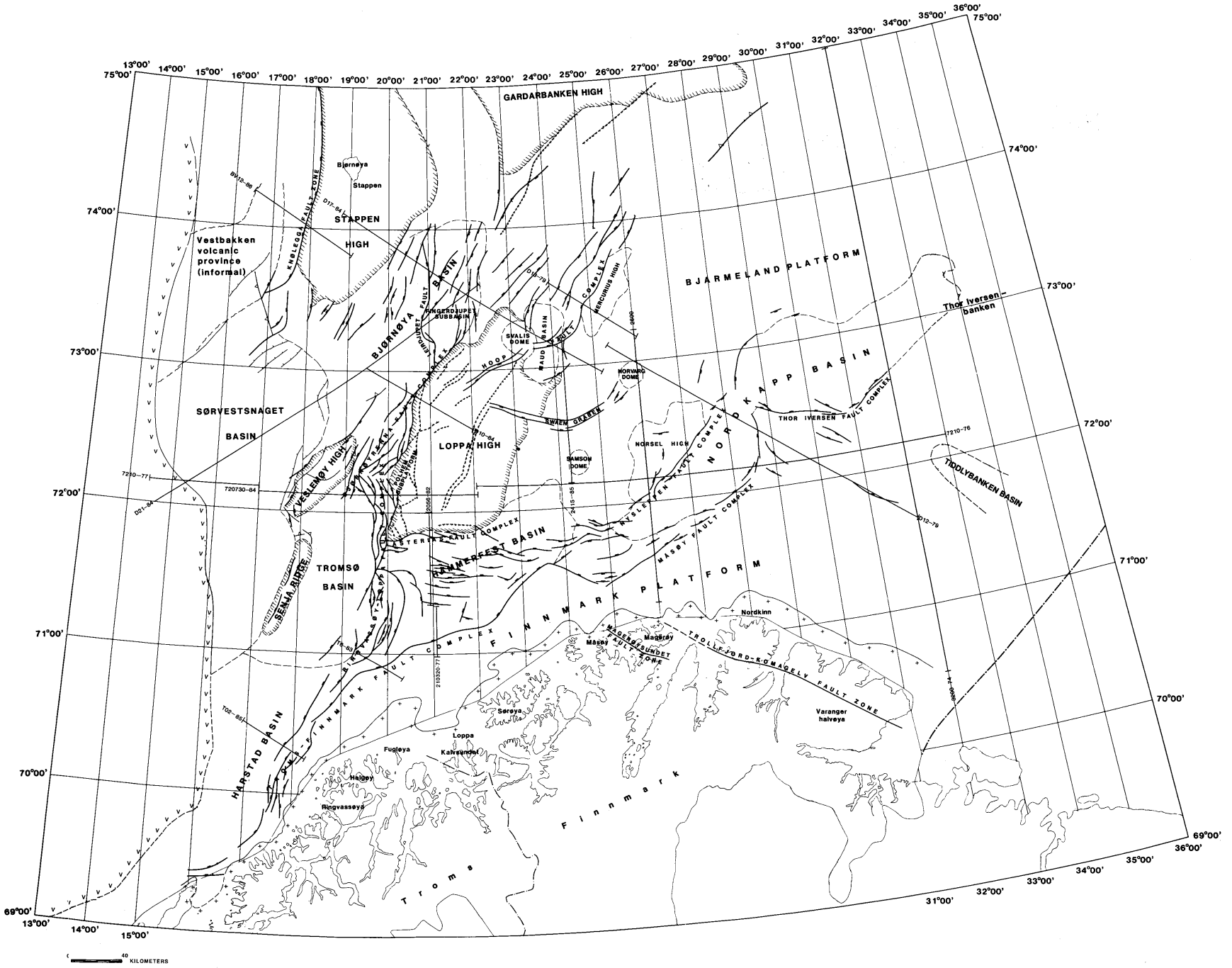

Fig. 2.3 Map of southwestern Barents Sea and its structural elements. From Gabrielsen et al. (1990b)

to to be very important in the later structural development. The Nordkapp Basin experienced uplift due to salt diapirism in the Early/Middle Triassic, Late Jurassic, Late Cretaceous and Cenozoic. This halokinesis combined with Late Pliocene/Pleistocene glaciation caused some 1200 m of Mesozoic and Cenozoic strata to be eroded, tilted and truncated.

2.4 The Leirdjupet Fault Complex

The Leirdjupet Fault Complex (also called Leirdjupet Fault Zone or simply Leirdjupet Fault) was first referred to by Rønnevik and Jacobsen (1984). They recognized that the area marks a transition zone that divides the Bjørnøya Basin into a deep western part and a shallow eastern part, the latter formally known as the Fingerdjupet Subbasin (Gabrielsen et al., 1990b). The fault complex trends N-S from the Loppa High towards the Stappen High between 73° - 73°55'N at 21°E. The name originates from the bathymetrical trough at the northern end of the complex. The individual faults constituting the fault complex have been active through several time periods, the main movement taking place in the Carboniferous, Mid Jurassic and Early Cretaceous (Gabrielsen et al., 1990b). The Leirdjupet Fault Complex, together with the adjacent Ringvassøy - Loppa Fault Complex and the Bjørnøyrenna Fault complex are thought to be closely linked to the mega shear zone that developed during Late Mesozoic and Cenozoic. Though many different names exist for this zone, the term *de Geer Zone* is widely recognized. This zone created a link between the North Atlantic and Arctic before continental breakup (Breivik et al., 1998). In pre-drift reconstructions these fault complexes bounded the de Geer Zone (Faleide et al., 1993b). The fault complexes represent the first order boundary between the eastern province, dominated by platforms and terraces, and the basin province in the west (Ritzmann and Faleide, 2007). Although the Leirdjupet Fault Complex *sensu stricto* is an extensional fault dividing the Bjørnøya Basin, the zone displays several characteristics of a linked fault system.

Three of the seismic lines used in this thesis were interpreted by Gabrielsen et al. (1990b) and Faleide et al. (1993b), in a regional study of the area, as shown in Figs.

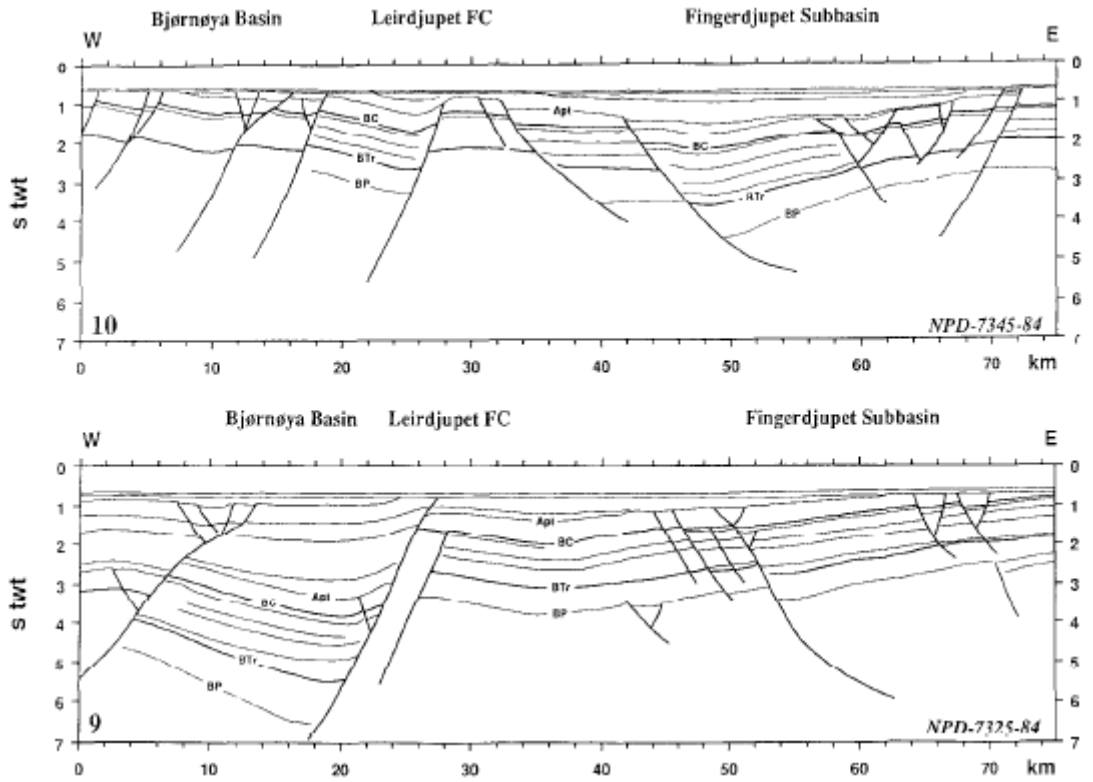

Fig. 2.4 Interpreted seismic lines going through Bjørnøya Basin, Leirdjupet Fault Complex and Fingerdjupet Subbasin. Upper image shows NPD-7345-84 and lower image shows NPD-7325-84. From Faleide et al. (1993b). Apt. - Aptian (mid-Cretaceous), BC - Base Cretaceous, BTr - Base Triassic and BP - Base Permian.

2.5 and 2.4, respectively. Identification of reflections, especially in the hanging wall (i.e. Bjørnøya Basin), that are deeper than well penetration is primarily based on these studies.

A composite seismic profile going through the Sørvestsnaget Basin, Bjørnøya Basin and Fingerdjupet Subbasin is shown in Fig. 2.5.

2.5 Loppa High

The Loppa High and the Polheim Platform, which it incorporates, is a large diamond shaped structural feature located southeast of the Bjørnøya Basin (Fig. 2.3) between 71°50'N, 20°E and 71°55'N, 22°40'E, and 72°55'N, 24°10'E and 73°20'N, 23°E (Gabrielsen et al., 1990b). The western crest of the Loppa High represents an area which has acted as a high at least four times since Devonian times (Gabrielsen et al., 1990b), illustrating

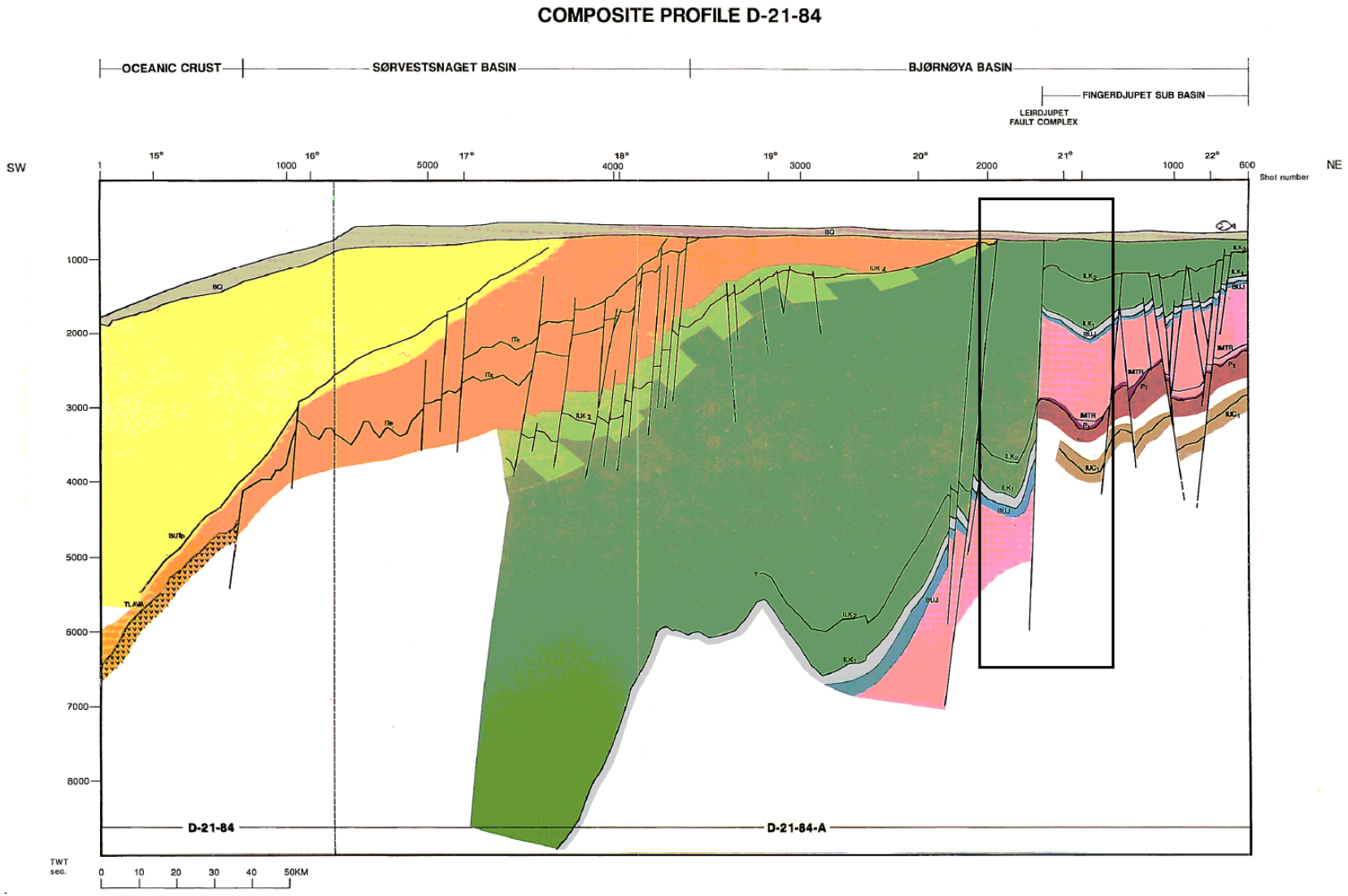

Fig. 2.5 Composite profile of line D-21-84. See Fig. 2.3 for location. Quaternary (gray), Pliocene & Oligocene (yellow), Eocene & Paleocene (orange), Cretaceous (green), Jurassic (light and dark blue), Triassic (pink), Permian (violet & brown). Note vertical exaggeration. The black rectangle indicate the area discussed in this study. Modified from Gabrielsen et al. (1990b).

the dynamic and complex geological history of the area which have involved alternating phases of uplift and subsidence (Glørstad-Clark, 2011). It is bounded by the Asterias Fault complex in the south and the Ringvassøy-Loppa and Bjørnøyrenna Fault complexes to the west (Gabrielsen et al., 1990b).

The current day Loppa High overlies an older relict structural high which was initiated during Late Carboniferous, but major uplift of the ridge did not occur until Late Permian. This Late Paleozoic high, often referred to as the paleo-Loppa High, but defined as the *Selis Ridge* by Glørstad-Clark (2011), is characterized by a distinct, narrow ridge trending north-south beneath the western part of the area. It is bounded to the west by the Jason Fault Complex (Fig. 4.23).

3 Seismic interpretation

3.1 Data and methods

This study is based on a set of regional 2D reflection seismic lines (Fig. 3.1).

Wells and associated well tops have been used to identify and constrain selected seismic horizons (Table 3.1). All wells are located in the Fingerdjupet Subbasin (see Fig. 2.3 for map and Fig. 3.1 for seismic lines and wells). 7321/7-1 and 7321/9-1 were drilled in 1988 and 7321/8-1 was drilled in 1987. The wells are exploration wells and wellbore contents contained shows. They were all plugged and abandoned.

Well 7321/8-1 is the deepest well and is the only one encountering Paleozoic rocks of Upper Permian age. This well does not line up with any of the seismic lines, though it is reasonably close and has been used as a control well only. No wells used in the study are located on the western side of the fault complex, i.e. the hangingwall (Bjørnøya Basin), making horizon interpretation to a large degree tentative. A map of the seismic lines and wells used in the study is shown in Fig. 3.1. Note that the regional 2D lines have a large extent, and thus covering regions outside of the main core area of this study. The interpretation will focus on the area proximal to the Leirdjupet master fault. This includes the eastern margin of Bjørnøya Basin and the western margin of the Fingerdjupet Subbasin along the master fault segment.

The 2D seismic lines used in this study come from multiple surveys, and display considerable variation in quality, both in terms of lateral and vertical resolution, phase and polarity. Fig. 3.2 demonstrates these differences.

Two things are important to keep in mind while interpreting seismic reflection data; seismic phase and polarity. The seismic phase defines the shape of the wave, which usually is minimum phase or zero phase. The polarity describes the nature of the positive and negative portions of the seismic wavelet. Fig. 3.3 shows the typical seismic phases and polarities encountered in seismic reflection surveys. By looking at the seismic response at the seafloor one can usually determine these seismic properties. Given the increase in acoustic impedance going from water to (unconsolidated) sediments, the seismic phase and polarity for line IV is interpreted as being zero-phase and normal, respectively. Line

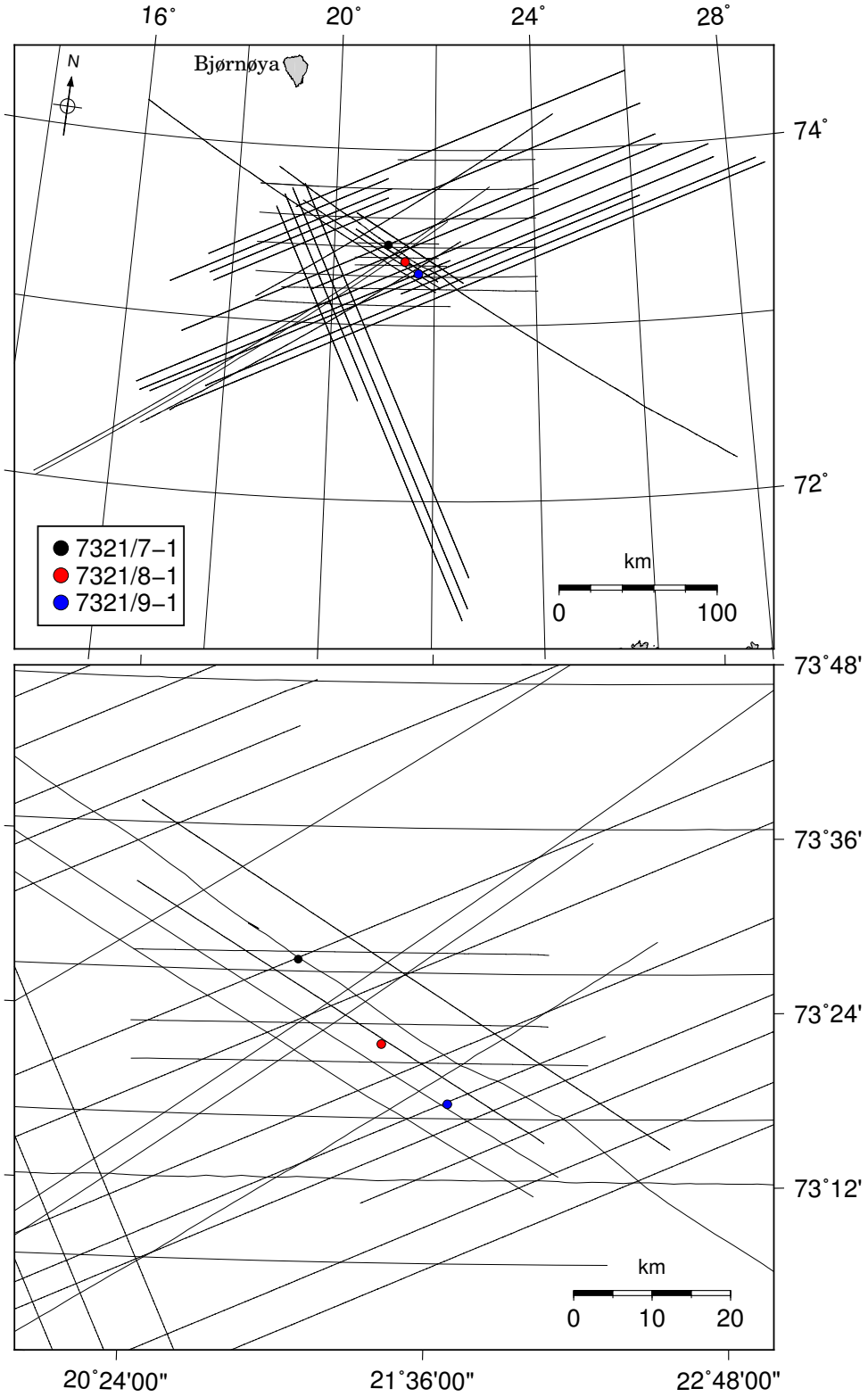

Fig. 3.1 Map of the seismic 2D lines and the location of wells (Table 3.1) used in the study.

Table 3.1 Wells used in the study. Lithostratigraphy and associated time periods based on Glørstad-Clark et al. (2010) as shown in Fig. 2.1 (source: NPD).

Age		Lithostratigraphic unit		Well		
Epoch	Period	Gr.	Fm.	7321/7-1	7321/8-1	7321/9-1
Cenozoic	Neogene	Nordland		499	491	483
Mesozoic	Cretaceous	Adventdalen	Kolmule	526	546	558
			Kolje	1145	852	892
			Knurr	1892	1352	986
	Jurassic		Hekkingen	1918	1383	1317
			Fuglen	1965	1427	1367
		Kapp Toscana	Stø	1999	1437	1379
			Nordmela	2022	1455	1417
	Triassic		Fruholmen	2039	1467	1424
			Snadd	2207	1626	1572
		Sassendalen	Undifferentiated	-	3362	-
Paleozoic	Permian	Tempelfjorden	Røye	-	3398	-

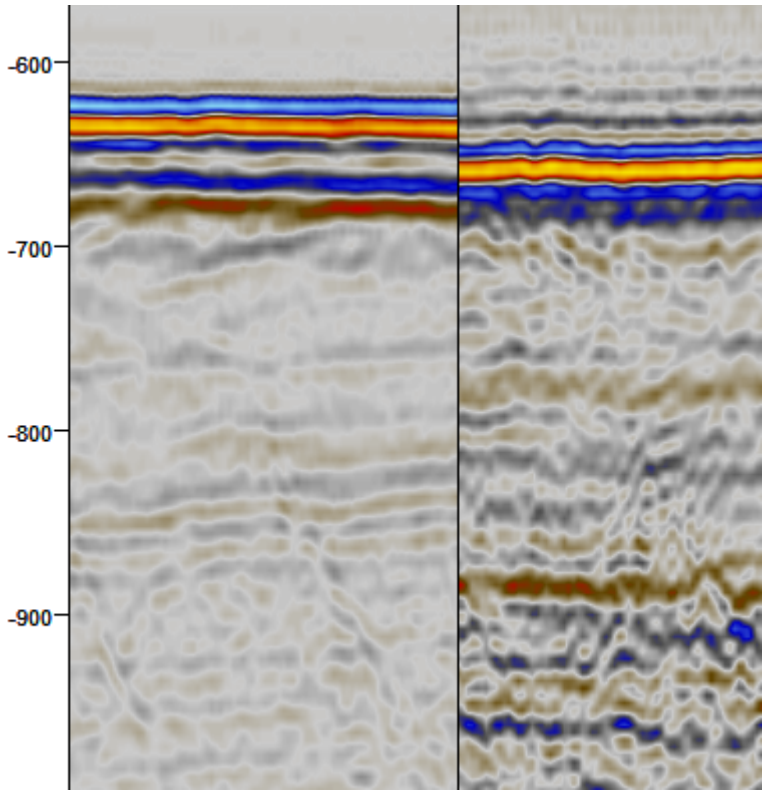

Fig. 3.2 Composite display of line II (left) and line IV (right) demonstrating varying quality between the different surveys.

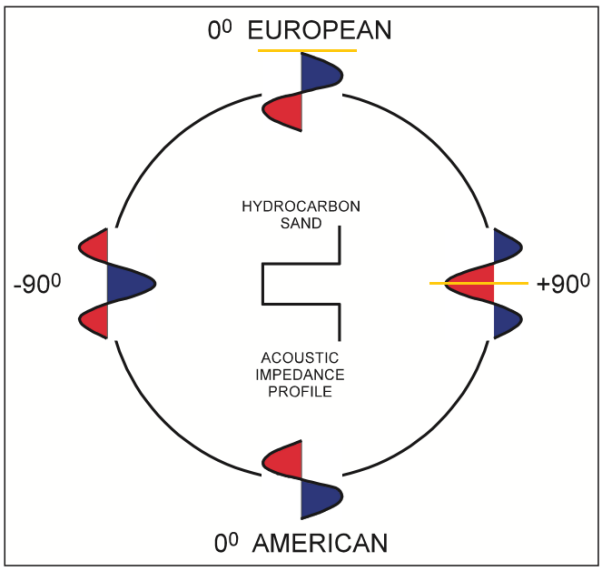

Fig. 3.3 The principal phases and polarities encountered in reflection seismic data. Compare with Fig. 3.2 and the differences between the two surveys. Line II is interpreted as being minimum-phase, while line IV is interpreted as being zero-phase. The added orange lines mark where the interface is situated for a minimum-phase and zero-phase wavelet, respectively. Modified from Brown (2004).

II line is interpreted as being minimum-phase and normal polarity.

The differences between the two surveys displayed in Fig. 3.2 will be briefly pointed out and discussed in the paragraph below.

Between ca. -600 og -700 TWT the seismic response of the seabed is seen. In the left image (Line II) there is a distinct bright blue, i.e. negative reflection above an equally bright red (positive) reflection. The corresponding seismic response to the seabed in the right part (line IV) shows a bright red reflection situated between two less bright blue reflections. While the seabed reflection for line II is received at about -620 ms, it is delayed by ca. 30 ms. in the IV line (i.e. the point of symmetry of the seismic wavelet, see Fig. 3.3), and received at ca. -650 ms. This may be due to different datums used in the two seismic surveys. It is also important to keep in mind the variations in the response of different seismic phase related to the interface between two layers of contrasting acoustic properties. In the case of minimum-phase, the seismic response to the interface between two layers of different acoustic impedance will be placed *above* the initial downkick (in

a normal polarity case). In the case of a zero-phase seismic response, the interface is represented by the reflection which is placed at the central point of symmetry (Fig. 3.3). At ca. -790 ms in line II a negative reflection is seen, with a duration of about 20 ms. The corresponding response for line IV is a positive reflection with a duration of about 30 ms. Hence, the vertical resolution in the latter is generally lower compared to the other survey. The seismic reflection patterns in deeper parts of the image show that line IV in general shows higher amplitude values compared to the other survey. These differences may be related to the signal processing, i.e. use of different filters, deconvolution etc., and the parameters used in the processing stage.

The seismic lines can roughly be divided into three groups based on orientation; i)SW-NE, ii)NNW-SSE and iii)E-W.

The E-W lines represent lines that are (sub) perpendicular to the master fault segment (F1), and thus gives the best geometrical representation of the fault zone.

Key horizons have been identified across the study area in order to constrain timing of structural deformation and tectonic movement. These include the intra Cretaceous (Aptian), Early Cretaceous and Jurassic. Its respective formations include the Kolje Formation, Knurr Formation and Fuglen Formation (Fig. 2.1). Deeper horizons are based on Faleide et al. (1993b) and Gabrielsen et al. (1990b), shown in Fig. 2.4 and Fig. 2.5.

It should be noted that the Base Permian reflections are difficult to track in many of the seismic sections. To further complicate interpretation, the Base Permian reflections in some of the seismic lines are deeper than seismic recording length.

3.1.1 General outline of the stratigraphy

A brief description of the formations encountered in the three different wells (Table 3.1) is given below and based on Dalland et al. (1988).

Kolmule Formation. Part of the Adventdalen Group. Consists of claystone and shale, with some siltstone interbeds, limestone and dolomite stringers. Age is suggested to be mid Cretaceous (Aptian to mid-Cenomanian). Depositional environment is thought to be open marine.

Kolje Formation Part of the Adventdalen Group. and consists mainly of shale and claystone with minor interbeds of limestone and evaporites. Depositional environment was distal open marine, with good water circulation An age of Lower Cretaceous (Barremian to late Barremian/early Aptian) is suggested.

Knurr Formation Part of the Adventdalen Group. Claystones with thin limestone and dolomite interbeds. Age is suggested to be Ryazanian/Valanginian to early Barremian.

Hekkingen Formation Part of the Adventdalen Group. Mainly consists of shale and claystone with occasional limestone, dolomite, siltstone and sandstone interbeds. Age is suggested to be late Oxfordian/early Kimmeridgian to Ryazanian.

Fuglen Formation Part of the Adventdalen Group. Mudstones with interbedded thin limestones. Age is suggested to be late Callovian to Oxfordian.

Stø Formation Part of the Kapp Toscana Group. Sandstones dominate. In some wells phosphatic conglomerate occur. Age is suggested to be late Pliensbachian to Bajocian.

Nordmela Formation Part of the Kapp Toscana Group. Interbedded siltstones, sandstones, shales and claystones. Sandstones tend to dominate towards the top of the formation. Age is suggested to be Sinemurian to the late Pliensbachian.

Fruholmen Formation Part of the Kapp Toscana Group. Shales which gradually pass upwards into interbedded sandstones, shales and coals. Age of the base of the formation is suggested to be early Norian. The upper parts of the formation is thought to correspond to the Triassic/Jurassic transition.

Snadd Formation Part of the Kapp Toscana Group. Mainly shale which coarsens upwards with interbeds of siltstones and sandstones. In the the lower and middle parts of the formation, limestones and calcareous interbeds are common. The formation varies both laterally and vertically. Age is suggested to be Ladinian to early Norian

Sassendalen Group. Shale and siltstone dominate with subordinate sandstones and minor amounts of carbonate rocks. Age is suggested to be Early and Middle Triassic.

Røye Formation Part of the Tempelfjorden Group. The lower parts of the formation (towards the Loppa High) are characterised by marls, silty carbonate mudstones and claystone with some thin beds of chert. The upper part contains interbedded chert, limestone, carbonate mudstone, marl and calcareous claystone. Age is suggested to be Kungurian to Kazanian - (Tatarian) age.

The whole study area shows a similar preservation of the lithostratigraphy and no significant or major changes occour along the transect of the master fault. A brief description of the lithostratigraphy of the two subareas is given below.

The deepest reflector in the study area is interpreted to be of Permian age and is denoted base Permian. This reflector is very difficult to interpret on several of the seismic lines, as the data becomes progressively noisier with increasing depth. Triassic sediments underlie a thin package of Jurassic deposits. The very thick succession of Cretaceous sediments is by far the dominating stratigraphic feature and constitutes the gross basin fill all up to base Quaternary (see Fig. 2.5) which defines the regional unconformity (Gabrielsen et al., 1990b).

Subarea 1 contains the same sequences as subarea 2, but are in general not as thick. This is especially the case for the Jurassic strata. This is probably related to the erosion or hiatus that is recognized in the area during Late Jurassic (Fig. 2.1). As subarea 1 has not undergone the same amount of subsidence as subarea 2, the Cretaceous infill is naturally much thinner. However, similar to subarea 2 the dominating infill is of Cretaceous age. The Jurassic succession is very thin and is difficult to map where well tie is available due to the interference between the reflectors (Fig. 3.4). An interval of Triassic sediments rests below.

Fig. 3.7 shows an uninterpreted version of line II. Note the location of well 7321/7-1 which is closest to the master fault (ca. 5 km). The other two wells, 7321/8-1 and 7321/9-1, are located ca. 10 km and 15 km from the master fault, respectively.

Checkshots and survey data for all wells have been retrieved and formed the basis for

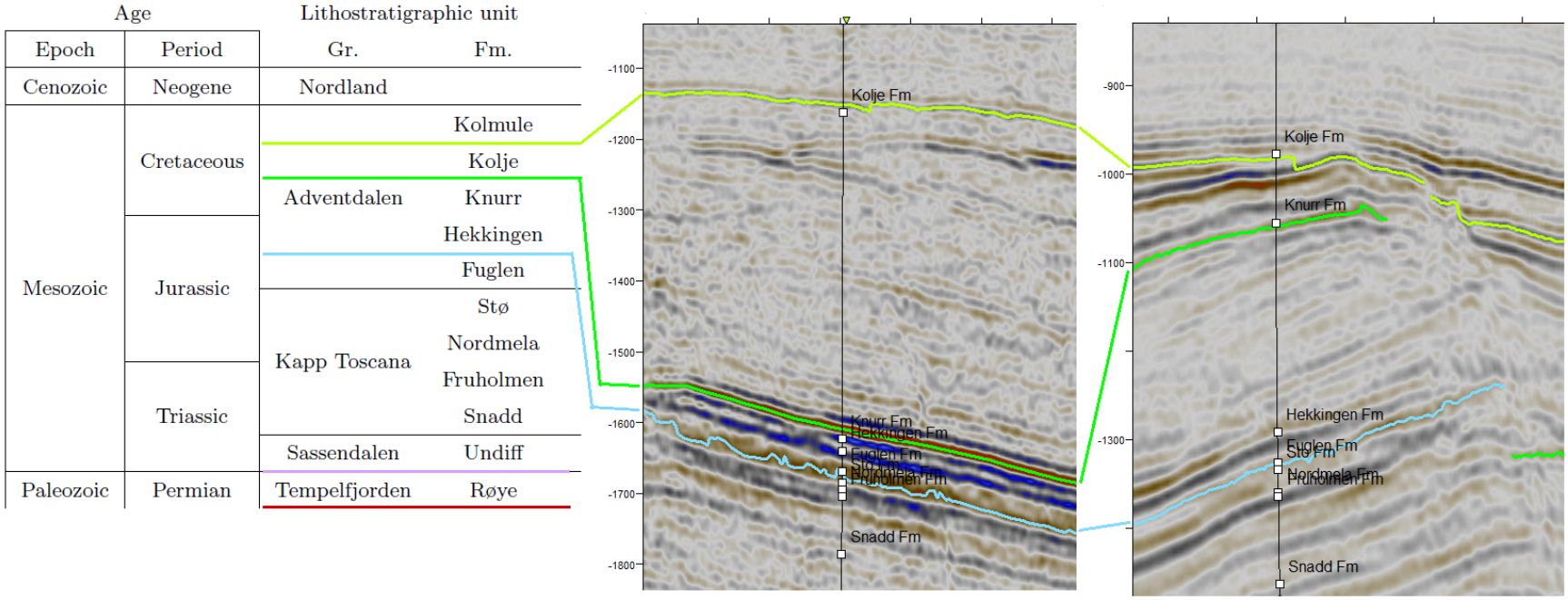

Fig. 3.4 Well 7321/7-1 and well 7321/9-1 with its associated well tops and seismic tie. Notice how vertically close the Knurr Formation through Fruholmen Formation are situated in 7321/7-1, possibly causing interference (Fig. 3.8). See Fig. 3.5 and Fig. 3.6 for uninterpreted versions of well 7321/7-1 and 7321/9-1, respectively. Table 3.1 shows the depth down to each formation. Note the color codes used for the different reflections mapped.

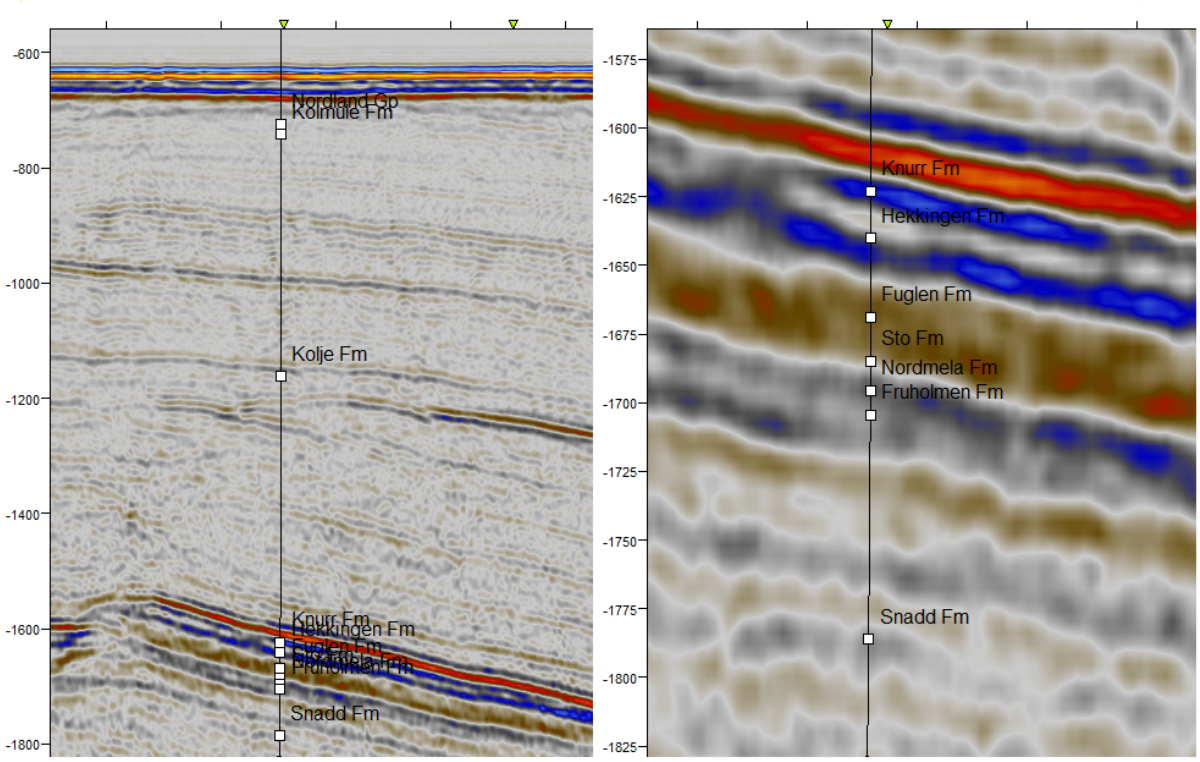

Fig. 3.5 Seismic line II with well 7321/7-1 uninterpreted

the well ties and depth conversion. Fig. 3.4 shows well 7321/7-1 and well 7321/9-1 with their associated well tops. Note the color codes used for the different reflections mapped, which are used throughout this study and in the seismic sections presented. Fig. 3.5 and Fig. 3.6 show the same wells uninterpreted. Note that the two uppermost well tops (Nordland Group and Kolmule Formation) in 7321/7-1 are erroneous. This is due to lacking checkshot data in this shallow interval.

Note that the Knurr Formation through Fruholmen Formation are vertically very close to each other in well 7321/7-1. This may have caused misinterpretation. It is highly plausible that the thickness of one or more of these intervals are below the limit of separability or even visibility (Brown, 2004). This is a function of wavelength where the limit of separability is given as $\frac{\lambda}{4}$, also called the *tuning thickness* (Fig. 3.8). This is important to take into consideration while interpreting, especially when dealing with 2D seismic reflection data, as this is likely to have lower resolution compared to 3D seismic reflection data.

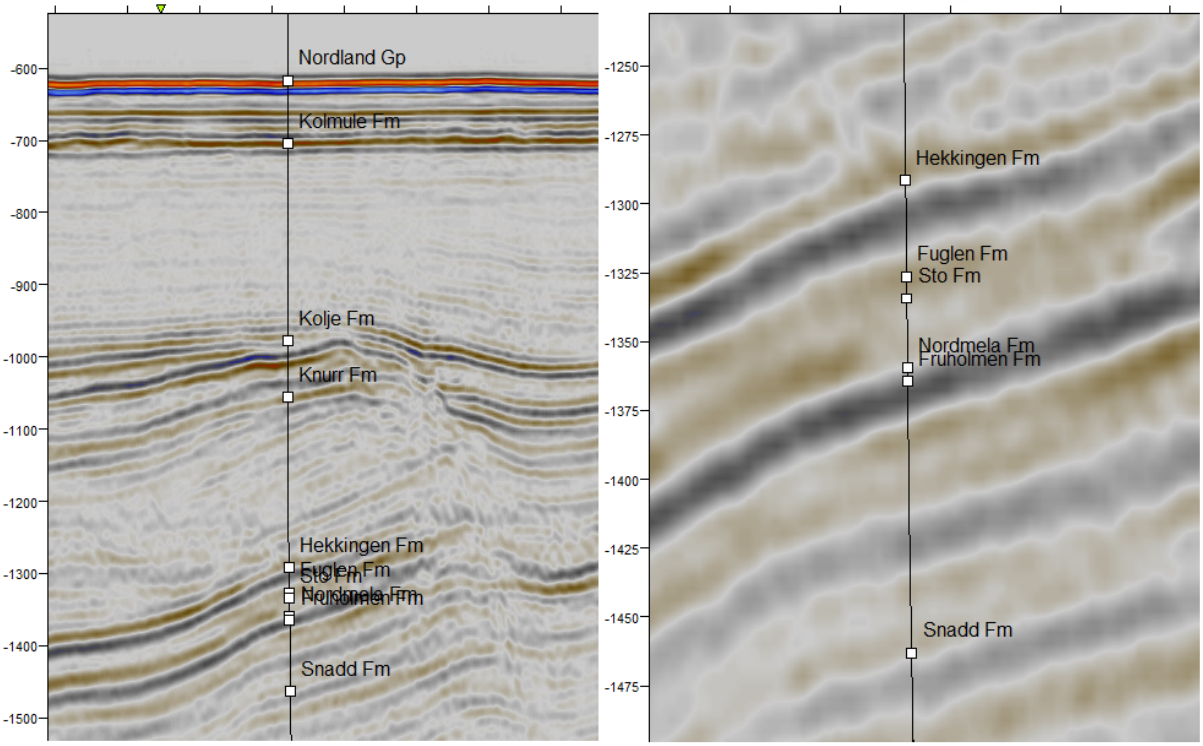

Fig. 3.6 Seismic line with well 7321/9-1 uninterpreted

Even though only 2D seismic reflection data is used, it allows generation of valuable types of maps, e.g. time-structure maps and time-thickness maps. Time-structure maps give information related to the structure of the subsurface. Time-thickness are in general contour maps that displays the difference in time between two seismic events, e.g. between two seismic horizons. This may yield valuable information regarding basin infill, depositional patterns etc. It should be noted that the fault maps have been created on basis of hard data (i.e. the seismic lines), rather than the generated time-structure maps. The relatively wide spacing between the seismic lines does not allow for confident mapping of faults due to the contour algorithm which tends to smooth out abrupt changes - which typically indicate faulting or other important structures; thus the faults in the fault maps have been manually made.

Both these types of maps, including fault maps have been made in order to obtain a better understanding of the Leirdjupet Fault Complex.

It is important to keep in mind that the data are shown in TWT (two way time). This

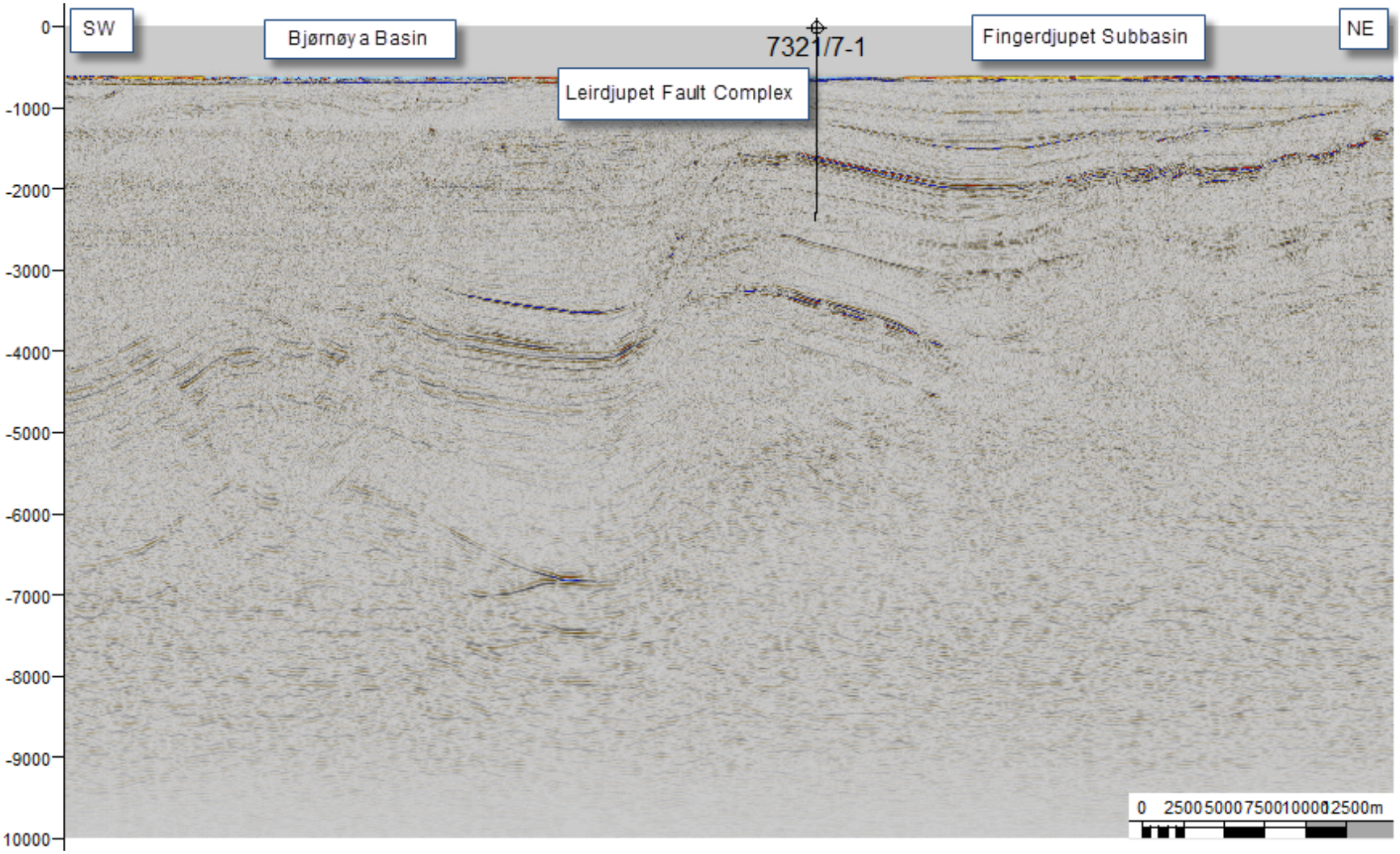

Fig. 3.7 An uninterpreted section of seismic line II which gives an impression of the major structural elements and configuration; The Bjørnøya basin, Fingerdjupet Subbasin and Leirdjupet master fault. See Fig. 3.11 for location of the seismic line and Fig. 3.1 for location of the different wells. An interpreted version of this line is shown in Fig. 3.15.

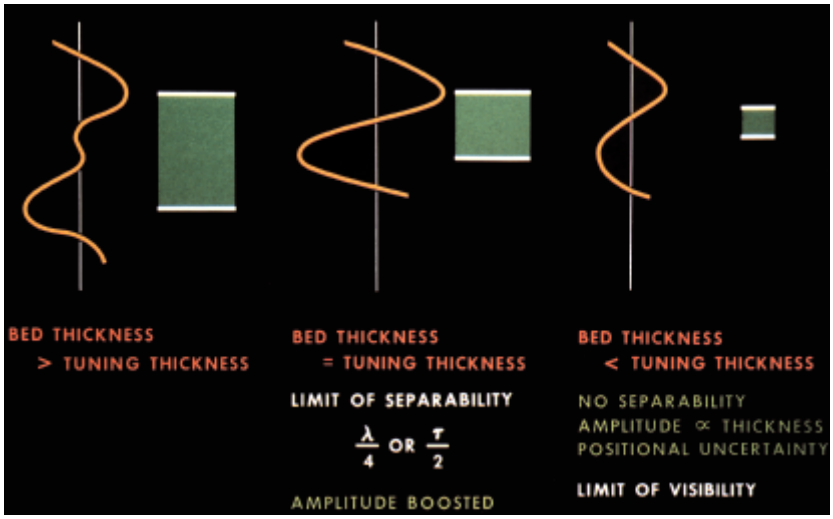

Fig. 3.8 The vertical resolution of seismic data is highly dependent on the wavelength of the seismic wavelet. Beds thinner than the tuning thickness will cause uncertainty with respect to position and interference. The frequency typically decreases with depth, hence increasing the wavelength. These two wave properties are related and given by the formula $\lambda = \frac{v}{f}$. From Brown (2004).

does not reveal the true geometry of structures, e.g. faults and fault planes. Faults which appear to be of listric nature may indeed be more or less planar when depth converted. This is related to the general velocity increase, which typically is a function of depth due to higher degree of sediment compaction and consolidation. The velocity changes are however related and dependant on several other rock properties such as grain size, sorting, shape and mineralogy (e.g. smectite vs. kaolinite content) (Mondol et al., 2007; Fawad et al., 2011).

In many of the seismic 2D lines it is difficult to properly map the fault plane to the point where it dies out. This may be related to several factors; i)With increasing depth the resolution drastically decreases (Fig. 3.8), and the fault plane may not manifest itself in a consistant way. ii) The fault may have a listric nature and may not necessarily juxtapose lithologies of very different acoustic impedance. As a consequence, the fault trace may be obscured and not readily visible.

All interpretation was done in Schlumbergers's Petrel, post-processed and plotted with GMT (Wessel and Smith, 1998).

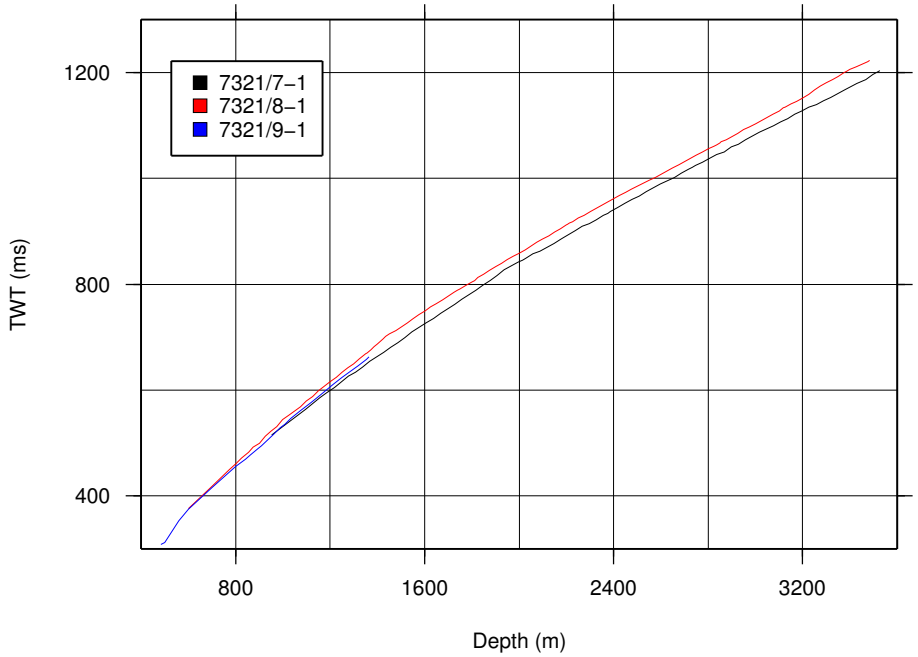

Fig. 3.9 Depth (m) versus TWT (ms) curve for all three wells based on checkshot data for the respective wells. They all show a similar velocity trend with increasing depth.

The seismic data are, naturally, placed along track lines, i.e. along the 2D seismic lines. Given the differences in seismic resolution and seismic phase mentioned above, when gridded - though subtle - these differences may cause short-scale features or *artifacts*. The scale of the artifacts are very short compared to the typical distance between survey track lines. In order to remove these artifacts a filter in space-domain was applied on the 2D grids, involving convolution of a boxcar function.

3.1.2 Depth conversion

In order to obtain a more realistic presentation of the geometry of the structural elements, depth conversion was done on two of the key seismic lines. The velocity model is based on well 7321/7-1 (Fig. 3.1) and its respective checkshot data. All three wells display a very similar velocity trend (Fig. 3.9), but due to the location of 7321/7-1 - being closest to the depth converted lines - only this well was used. An obvious shortcoming of this conversion scheme is the lack of data in the Bjørnøya Basin and in the deeper parts of the seismic lines (i.e. > -2500 ms TWT).

In order to go from time domain to depth domain a velocity model was created. This typically involves making a velocity - time relation which is used to yield a a correct velocity for a given TWT. The velocity model which was used is given by the linear equation

$$v = v_0 + kz$$

where v_0 is the initial velocity, k is a factor (coefficient) which gives the velocity increase with increasing TWT depth and z is the time. This calculates the velocity which is used for the depth conversion.

The P-velocity in water typically ranges between 1.4-1.5 km/s (Mussett and Khan, 2000). Well 7321/7-1 falls on one of the lines which has been depth converted (Line II, Fig. 3.15) and the P-wave velocity in the water column has been derived by solving the equation $x = v \times t$, where x, v and t denote distance, velocity and time, respectively. The water depth at the well location is 475 m (source: NPD) and the reflection from the seabed is received at ca. -630 ms TWT. Inserting these values into the equation and solving for v yields

$$v = \frac{475}{0.630/2} \approx 1508 \text{ m/s}$$

Checkshot data from well 7321/7-1 has formed the basis for determining the parameters (v_0 and k) in the intervals below the seabed. Due to the limited well data at depth, the velocity model was divided into three effective intervals; I)water column, II) seabed - Aptian, III)Aptian - base Perm. See Table 3.2 for the v_0 and k values employed in the three different interals.

Table 3.2 The values of v_0 and k for the intervals used in the velocity model.

Interval	v_0	k
I	≈ 1508	$= 0$
II	≈ 2169	≈ -0.0088
III	≈ 3097	≈ -0.3349

A quick way of assessing the validity of the velocity model employed is to see if the

well tops falls on the same reflection patterns in depth domain as they do in time domain (Fig. 3.10).

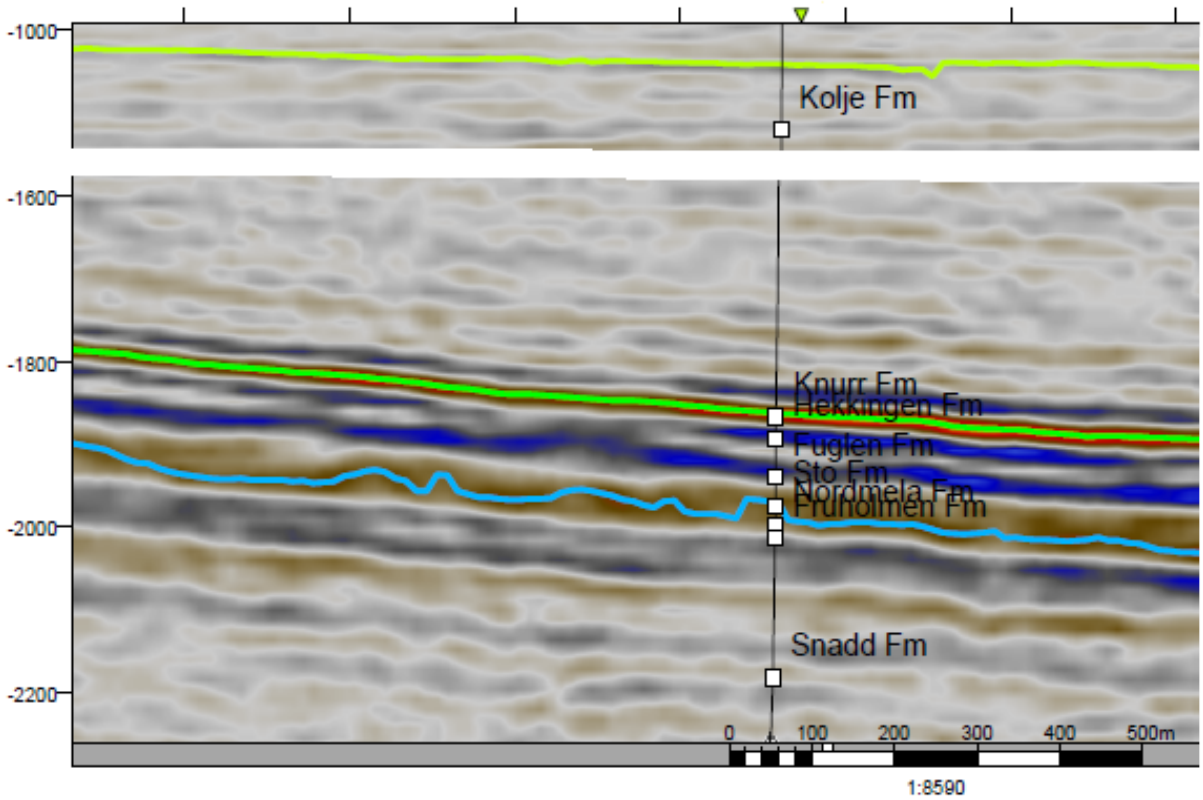

Fig. 3.10 Line II in depth domain. The well tops fall close to the same reflection patterns as they do in time domain (Fig. 3.5) - indicating that the velocity model is a good approximation.

3.2 Geometry and structuring of the Leirdjupet Fault Complex

In the following sections key seismic lines, time-structure maps and time-thickness maps which represents the geometry of the individual segments of the area will be presented. Each seismic line is presented individually and annotations related to structural features are valid only for its respective line.

3.2.1 Segmentation of the fault complex

The study area has been divided into segments based on geometry and structuring (Fig. 3.11).

The Leirdjupet Fault Complex was early recognized as a major feature dividing the Bjørnøya Basin from the shallow Fingerdjupet Subbasin by Rønnevik and Jacobsen (1984). This divides the study area into two naturally separated areas; the Fingerdjupet Subbasin and the downthrown Bjørnøya Basin, which during the rest of this chapter will be referred to as subarea A and subarea B, respectively (Fig. 3.11). Gabrielsen et al. (1990b) recognized that the fault complex changes structural style along the strike. The central area (segment 2) is characterized by a single fault with a large throw towards the Bjørnøya Basin. The northern area (segment 1) is dominated by a horst and graben topography. The southern area (segment 3) splits up into several smaller normal faults which have been rotated. Based on this and the interpretation presented in this study, the area has been further divided up into a total of three segments, as shown in Fig. 3.11. Based on seismic coverage, the main emphasis is given on the northern and central segment.

3.2.2 2D seismic interpretation

Line I Line I (Fig. 3.12) displays a northeast-southwest-oriented section through the northern segment, i.e. segment 1 (Fig. 3.11), of the Leirdjupet Fault Complex. The line is parallel to line II and line III. The line comprises several characteristic geometries found in extensional regimes; the downfaulted subarea B to the southwest defining a half-graben, a central feature defining a horst and a half-graben to the northeast representing subarea A, i.e. the master fault splits up and makes a horst- and graben topography as pointed out by Grunnaleite (2002).

The seismic reflections in the horst structure are very disturbed and noisy. Except for the shallow part (down to ca. 1500 ms TWT) no continous reflections are observed.

The most evident structural features of this line are the well developed half-graben patterns present in both subarea A and subarea B.

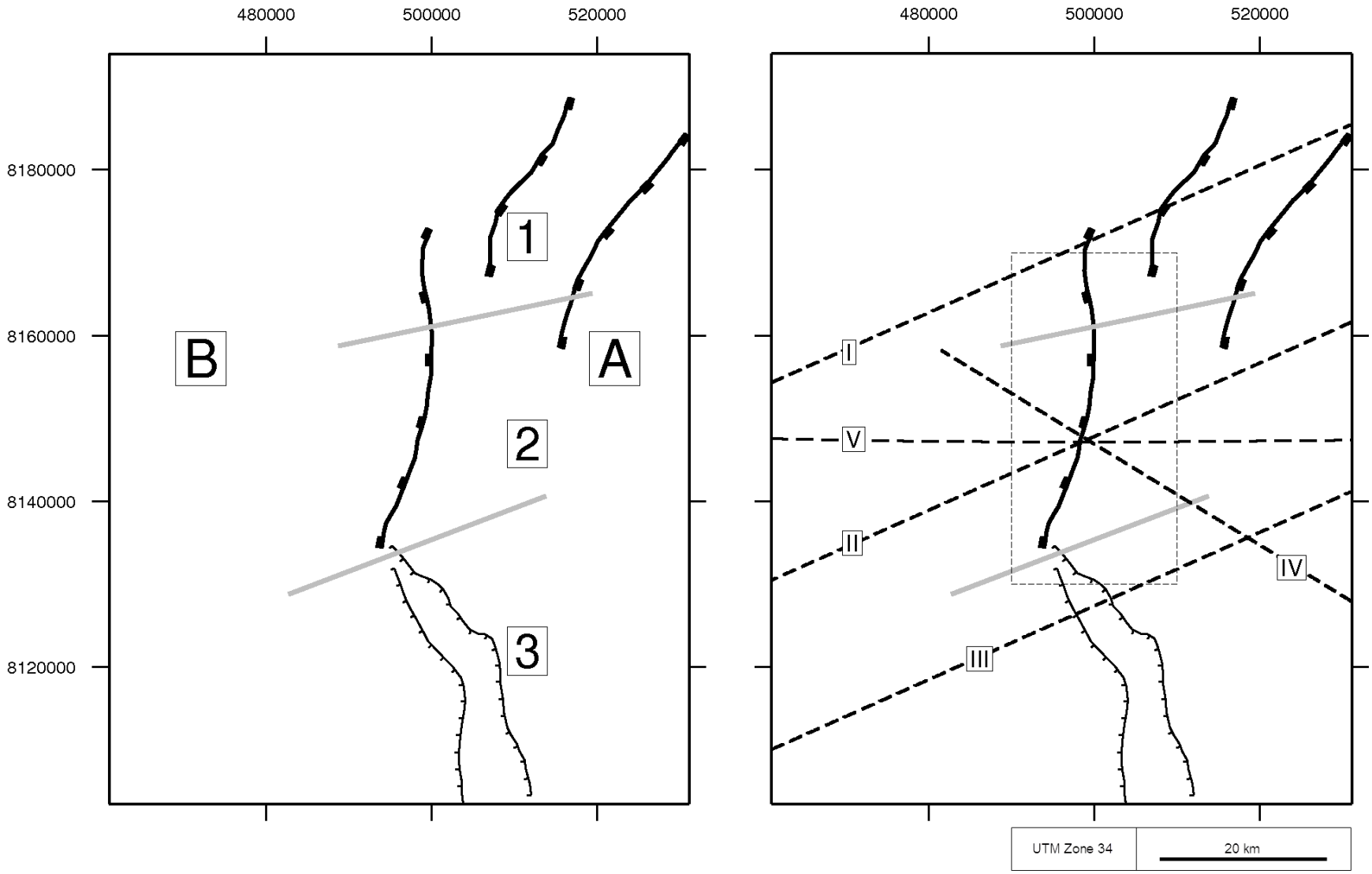

Fig. 3.11 Left: Principal fault map showing the two subareas and the three segments that the study area has been divided into. The different segments are separated by the solid gray lines. Right: Dashed lines represent key seismic sections which are structurally described and presented; Line I (Fig. 3.12), Line II (Fig. 3.15), Line III (Fig. 3.20), Line IV (Fig. 3.21) and Line V (Fig. 3.23). The dashed square outlines the location where detailed mapping of the fault throw has been done (Fig. 4.6).

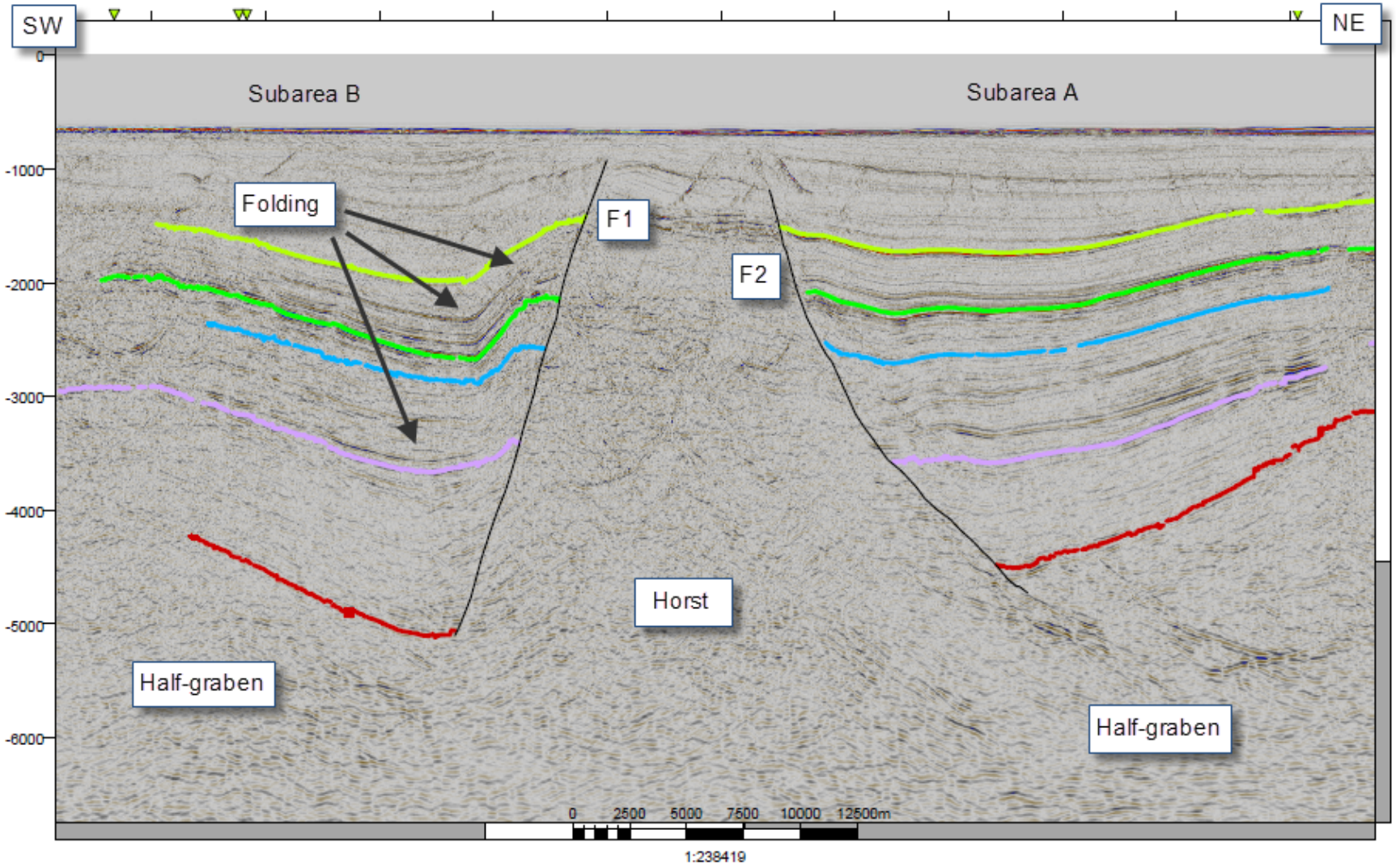

Fig. 3.12 Interpretation of line I. See Fig. 3.11 for location of line and Fig. 3.4 for color codes. See Fig. 3.13 and Fig. 3.14 for detailed images of F1 and F2, respectively.

Subarea B is in general affected by very few small scale features (e.g. faults), and the master fault (F1) is the structural element which is dictating the overall geometry. The strata is seen to thicken towards the fault between some of the seismic reflections mapped.

As opposed to line II, the master fault (F1) displays a simpler geometry; the fault only consist of one major fault branch. The fault appears to be fairly planar, though it is difficult to accurately position the fault plane due to incoherent seismic data. The reflections in subarea B close to the fault from ca. -1000 ms TWT down to -3500 ms TWT are seen to be affected to folding (see fault map, Fig. 3.31). The folding with its sub-horizontal limb which is extending westwards, show some characteristics of a monocline. Analogous to line II (Fig. 3.15 and Fig. 3.19) the lower part of the section shows a considerable thickening of the strata towards the fault (Fig. 3.13).

The eastern major fault (F2) defining subarea A has a listric nature, causing a very pronounced half-graben geometry. Similar to subarea B, several intervals of sediment thickening towards the fault plane are observed (Fig. 3.14).

Line II This line (Fig. 3.15) displays a northeast-southwest-oriented section through the central segment, i.e. segment 2 (Fig. 3.11), of the Leirdjupet Fault Complex. The line is paralell to line I and line III. The major structural features comprise a folded and slightly faulted footwall (subarea A) to the northeast and a folded hanging wall (i.e. subarea B) to the southwest. These are separated by a normal fault (F1) consisting of two fault branches (F1a and F1b) which are the main controlling structural features.

In subarea A, a set of normal faults (Fa1-Fa10, see Fig. 3.16) are seen to define several minor rotated fault blocks and small scale horst-and-graben and half-graben structures, i.e. synthetic and antithetic faults, which involve the base Cretaceous and Jurassic reflections. They all have planar geometry. A set of faults affecting the Aptian reflections are seen above (Fa15-Fa17). In the far northeast part of the section, another set of normal faults (Fa11-Fa13) are seen to affect the Jurassic and base Cretaceous reflections. To the far northeast a normal fault (F14) affecting the base Cretaceous and Jurassic is seen (Fig. 3.15).

Folds affecting the Aptian, base Cretaceous, Jurassic and Triassic reflections are clearly

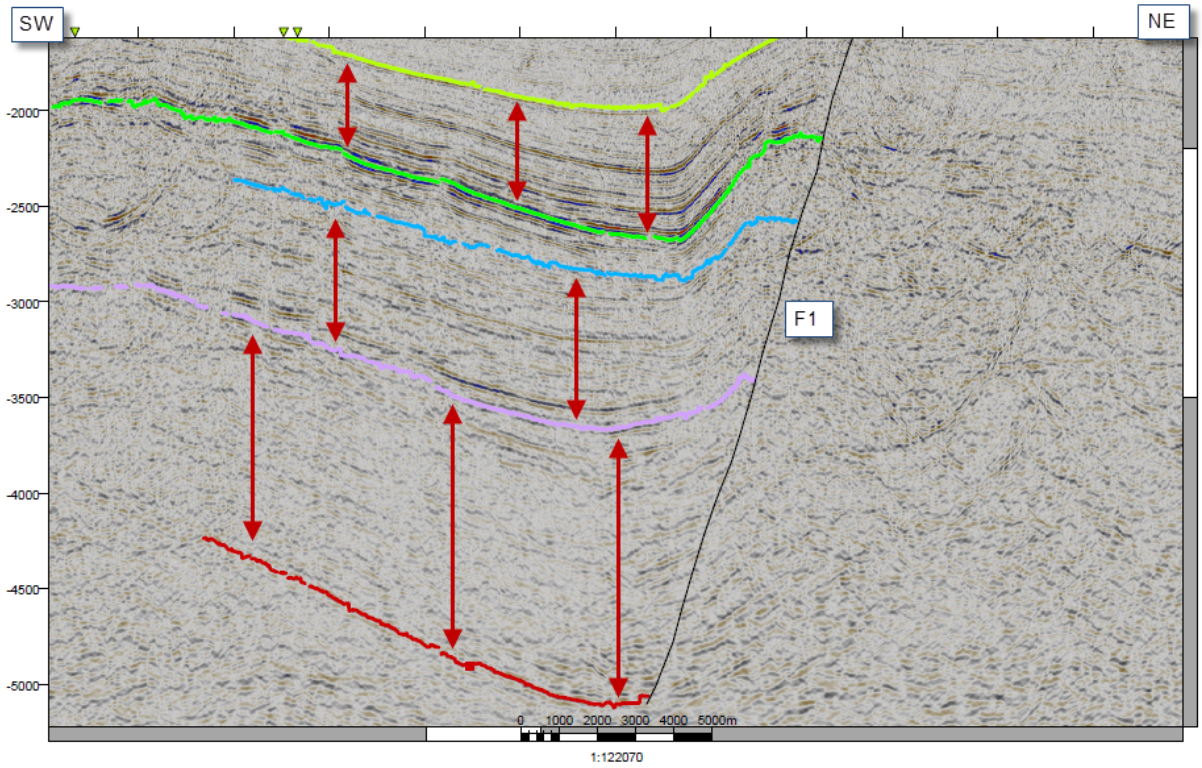

Fig. 3.13 Close-up of the area southwest of F1 in line I. Note sediment thickening towards the fault.

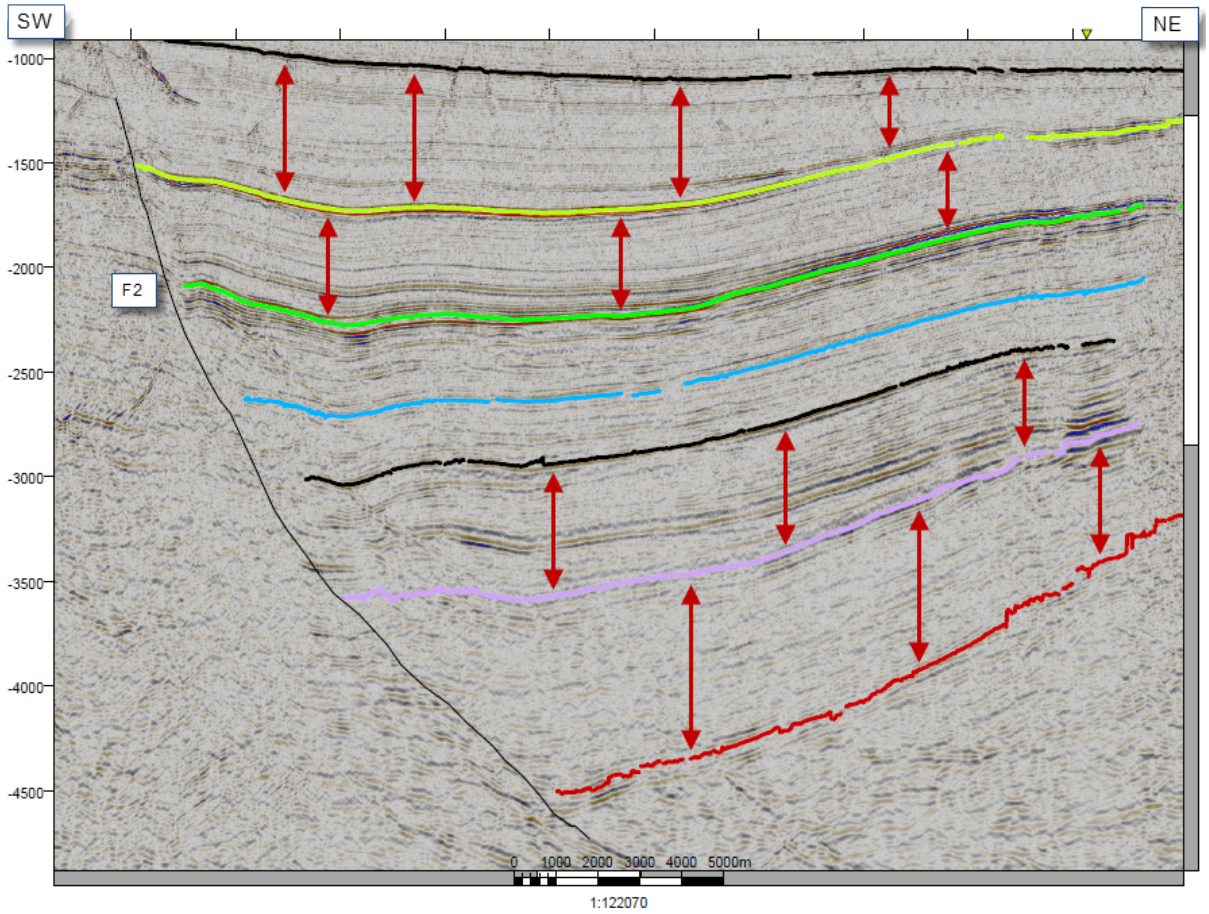

Fig. 3.14 Close-up of the area northeast of $F2$ in line I. Note half-graben geometry and sediment thickening towards the fault.

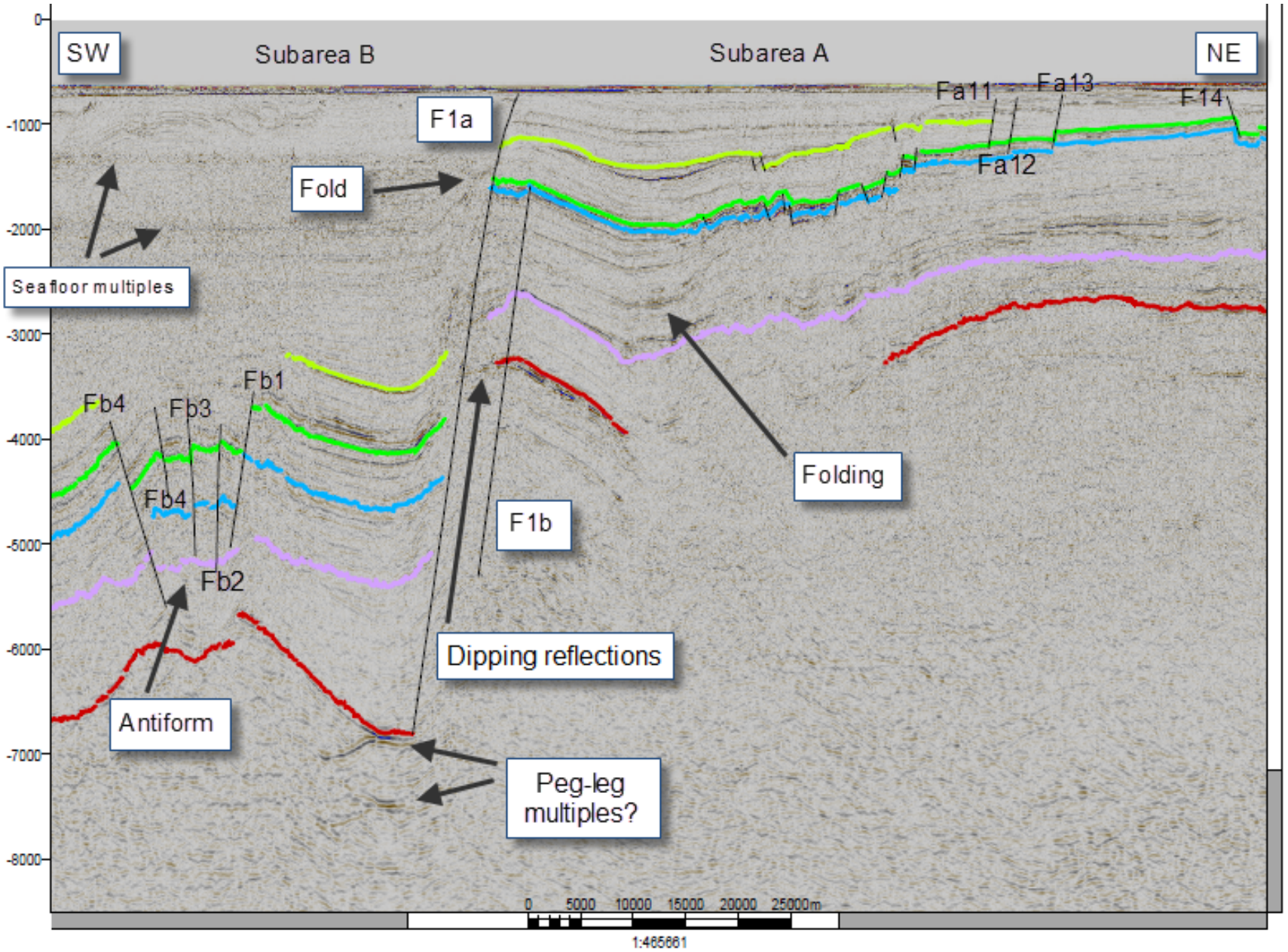

Fig. 3.15 Interpretation of line II. See Fig. 3.11 for location. Fig. 3.16 shows a close-up of the faults in subarea A. See Fig. 3.4 for color codes.

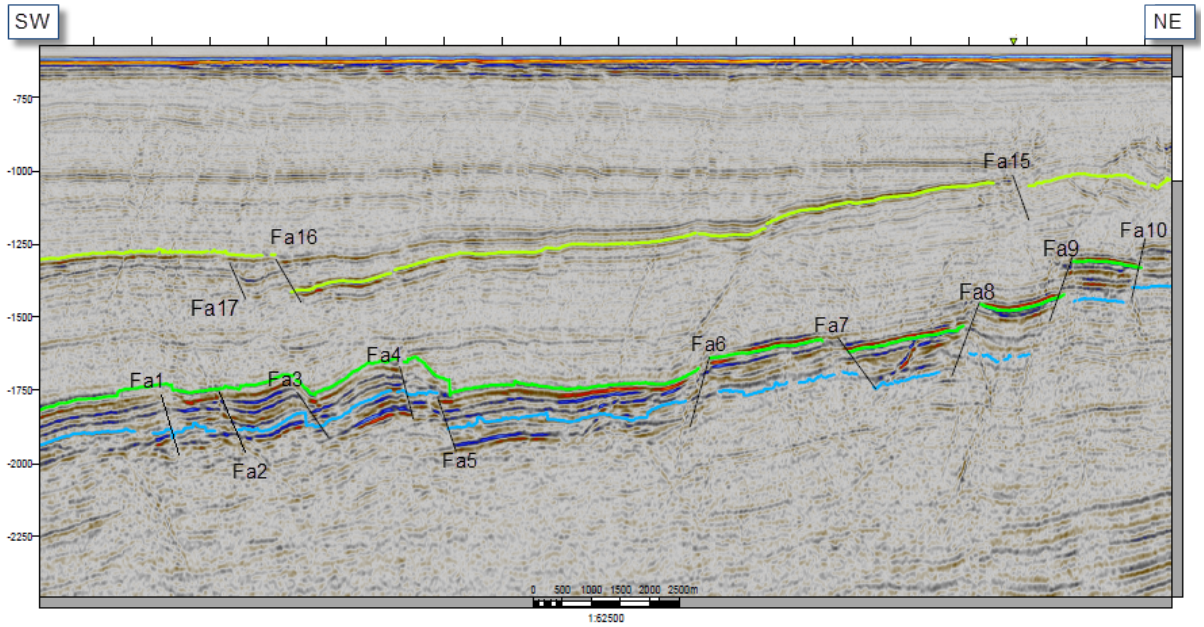

Fig. 3.16 Close-up of faults in subarea A.

defined in subarea A; immediately east of the master fault the reflections dip to the east, and in the central part then change polarity and gradually begin to dip towards west. This may also be the case for the Permian reflection, but this is hard to determine due to very noisy seismic data. The base Permian reflection does none the less display steeply dipping reflections towards the east and the apparent apex of the fold.

A clinoform can be seen in the lower parts of subarea A within the Triassic interval (Fig. 3.17).

Subarea B is dominated by an antiform with an apparent apex in the central part of the basin. The Aptian reflection is very difficult to interpret in this area, and the seismic reflections from the top of the antiform (ca. -3500 ms TWT) up to ca. -1000 ms TWT are very noisy and obscured. The shallow reflections at ca. -1000 ms TWT, display open folds. Whether this is associated with the deeper antiform is difficult to determine. The base Cretaceous through Permian reflections are all affected by the antiform. The base Cretaceous is offset by ca. 400 ms TWT, though the offset varies along the structure. A set of normal faults are seen in the central part of the antiform (Fb1-Fb4). The faulting changes polarity approximately at the apex of the structure; on the western side the

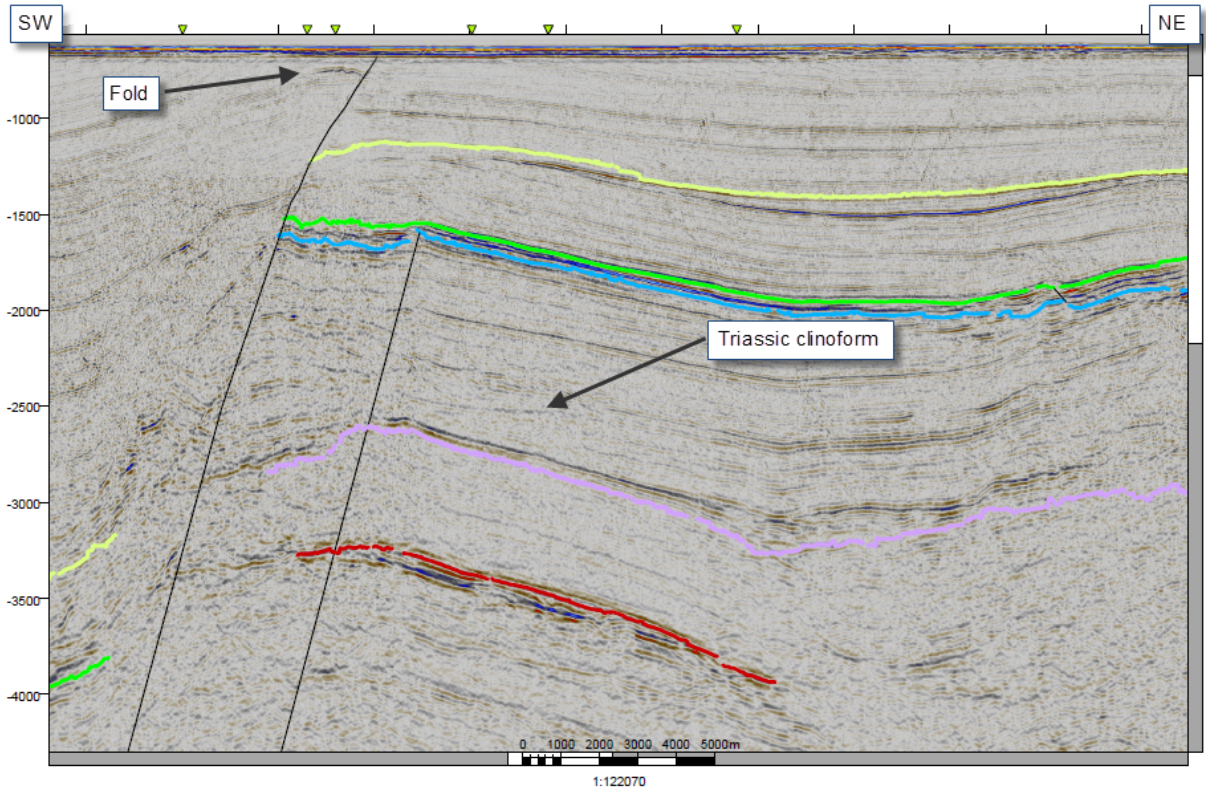

Fig. 3.17 Subarea A and mapped reflections. Note the clinoform indicating Triassic sediment infilling and progradation.

faults dip toward the northeast, whereas the faults on the eastern side dip towards the southwest (see fault map in Fig. 3.29). No drag is apparent along the faults and the internal structure in the downfaulted segments appears to be little affected.

Fig. 3.18 shows a close-up of the sedimentary infill in subarea B. The Aptian reflection is seen to form the base of a wedge which increases in thickness towards F1a.

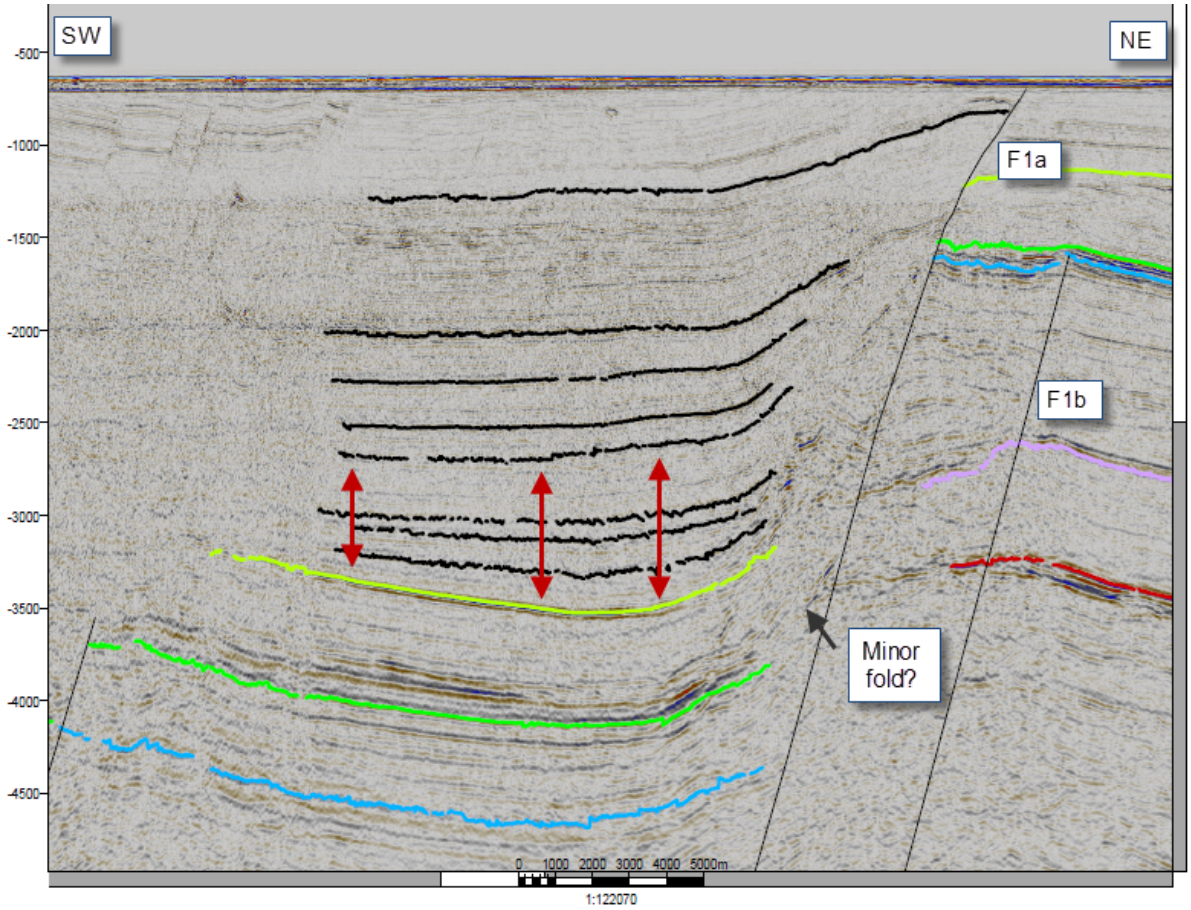

Fig. 3.18 Interval in Subarea B with wedge geometry. Sediment thickening is indicated by the red arrows. The height of the arrow to the left is 557 ms TWT, the arrow in the middle is 696 ms TWT and the arrow to the right is 822 ms TWT, i.e. a substantial thickening.

A more complex pattern of seismic facies and boundaries is observed between the Permian through Jurassic reflections. The seismic data are clearly affected by the great depth, but the gross internal structure within this interval is recognizable (Fig. 3.19). The concept of onlap and downlap has been used to define sequences within this interval.

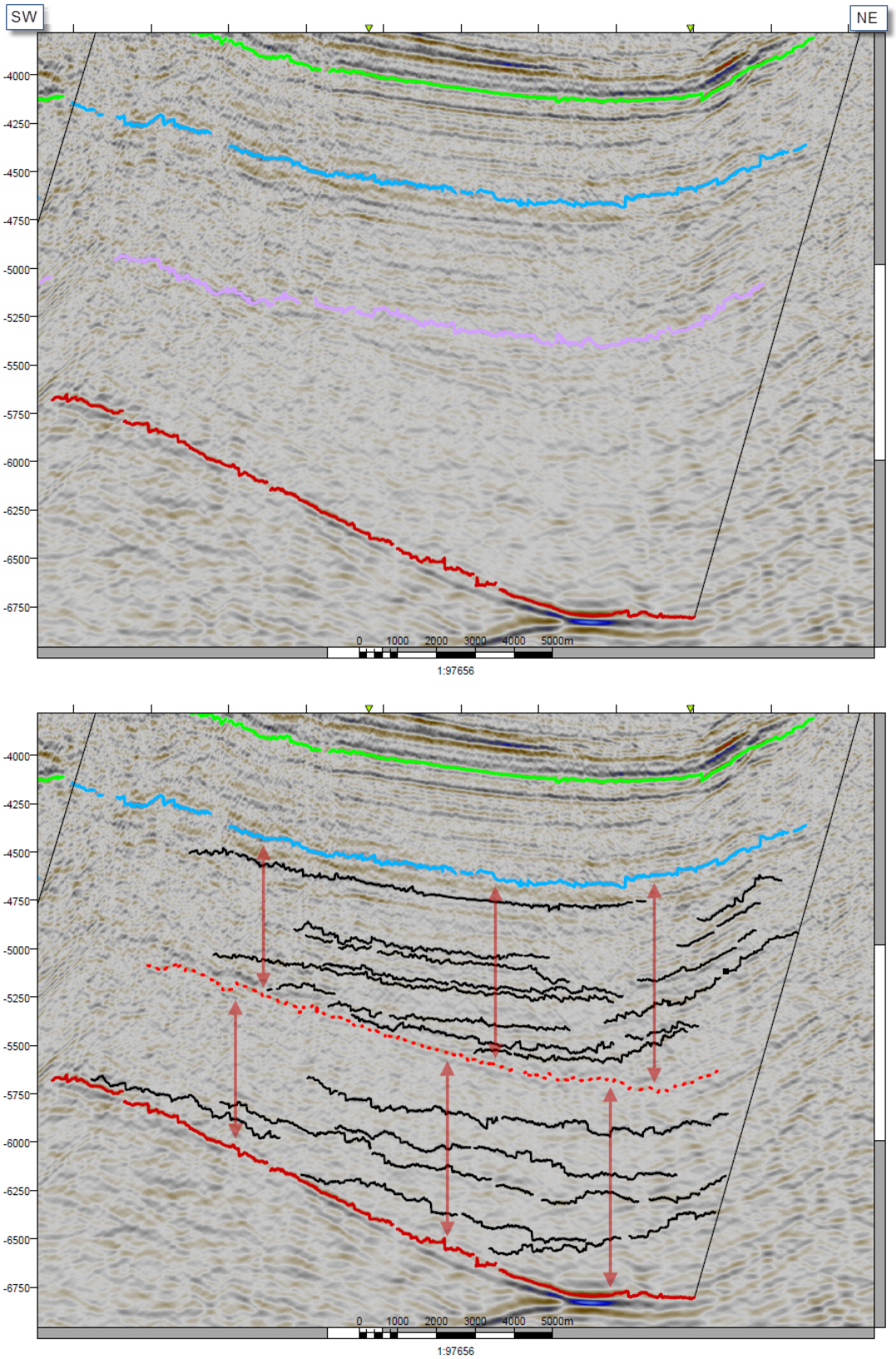

Fig. 3.19 Detailed interpretation of the interval between the Permian through Jurassic reflections displaying wedge geometries. The Permian reflection marks the lower boundary of the first sequence, whereas the red dotted line represents the lower boundary of the second sequence.

The master fault system is the main controlling structural feature as it separates the two subareas. It strikes roughly north-south (Fig. 3.11), i.e. the line does not depict the true geometry of the fault given its northeast-southwest direction. The master fault dips towards west and displaces the base Cretaceous reflection by ca. 2330 ms TWT. The line is very proximal to line V and naturally displays a similar structuring. The master fault is segmented into two branches (F1a and F1b). Both of the segments are interpreted as being planar to sub-planar. The area situated between the two segments is very disturbed, and possibly relates to the fault zone and the complex internal structure that it may have developed (Gabrielsen, 2010). The Triassic and Permian reflections in the footwall are seen to dip steeply between the two fault branches. This may be related to drag. It is difficult to pinpoint the lower termination of both fault branches as they are very deep. They may extend beyond -7000 ms TWT. All of the reflections between -5500 ms TWT and -3000 ms TWT onlapping the western fault branch (F1a) display signs of normal drag.

Line III This line (Fig. 3.20) displays a northeast-southwest-oriented section through the southern segment, i.e. segment 3, of the Leirdjupet Fault Complex (Fig. 3.11). The line is parallel to lines I and II. This segment of the Leirdjupet Fault Complex displays a rather different geometry compared to the other segments; while the central and northern segments are characterized by a single fault with large displacement, the southern region is dominated by smaller rotated normal faults. Hence, the displacement that is observed to occur over a narrow zone in lines I and II, is now distributed over a larger area. The faults (F1-F4) are all synthetic to the master fault observed in seismic lines in the other segments of the fault complex. The line is included mainly to demonstrate the change in style of faulting; all of the southern seismic lines are very incoherent, and present very few distinct features other than this. As demonstrated by Barrère (2009) and emphasized by Glørstad-Clark (2011) in their regional studies of the western Barents Sea, it is difficult to distinguish the crystalline basement from the deeply buried and compacted sediments in the Bjørnøya Basin.

The different subareas are not as clearly delineated on this line compared to the other

lines. The major features involving deepening towards the central part of subarea B and the shallower platform constituting subarea A are, however, evident.

The central part of the section is very obscured and none of the reflections can be mapped with confidence. All the mapped reflections are offset by 1000 to 2300 ms TWT during this 5 km interval, inferring the presence of one or more faults (F4?), although no clear definitions of faulting are, however, apparent and no distinct reflection discontinuities can be seen.

Line IV Line IV (Fig. 3.21) displays a northwest-southeast-oriented section through the central and southern segments, i.e. segment 2 and 3 (Fig. 3.11) of the Leirdjupet Fault Complex. The line displays a considerable thickening of the strata towards the master fault between the Aptian reflections and the reflection mapped above (black), as seen in line I (Fig. 3.12 and Fig. 3.13) and line II (Fig. 3.15 and Fig. 3.18). The height of the red arrow to the northwest is approximately 250 ms TWT, while the arrow to the southeast (i.e. closest to the fault) is about 475 ms TWT in height; i.e. there is a considerable thickening of the strata towards the fault. Similar sediment thickening is seen between base Cretaceous - Aptian and Permian - Triassic. A thin sequence between the Jurassic and Triassic reflections is also present.

The general fault geometry is very similar to that of line II. The major fault consists of two fault branches, F1a and F1b, which both appear to be planar.

Very proximal to the fault plane, some intervals show signs of folds (Fig. 3.22). These structures are recurring throughout segment 1 and 2 (Fig. 3.11) of the study area (e.g. Fig. 3.12 and Fig. 3.17 for a similar structure in segment 1).

Line V This line (Fig. 3.23) displays a west-east-oriented section through the central segment, i.e. segment 2 (Fig. 3.11), of the Leirdjupet Fault Complex. The fault geometry is similar to that of line II and line IV; it consists of two fault branches, F1a and F1b which are planar. This line displays a very pronounced wedge geometry where the Aptian reflection defines the lower boundary (Fig. 3.24). Slight thickening is also seen in the Triassic - Jurassic interval, and a clear thickening in the Permian - Triassic interval.

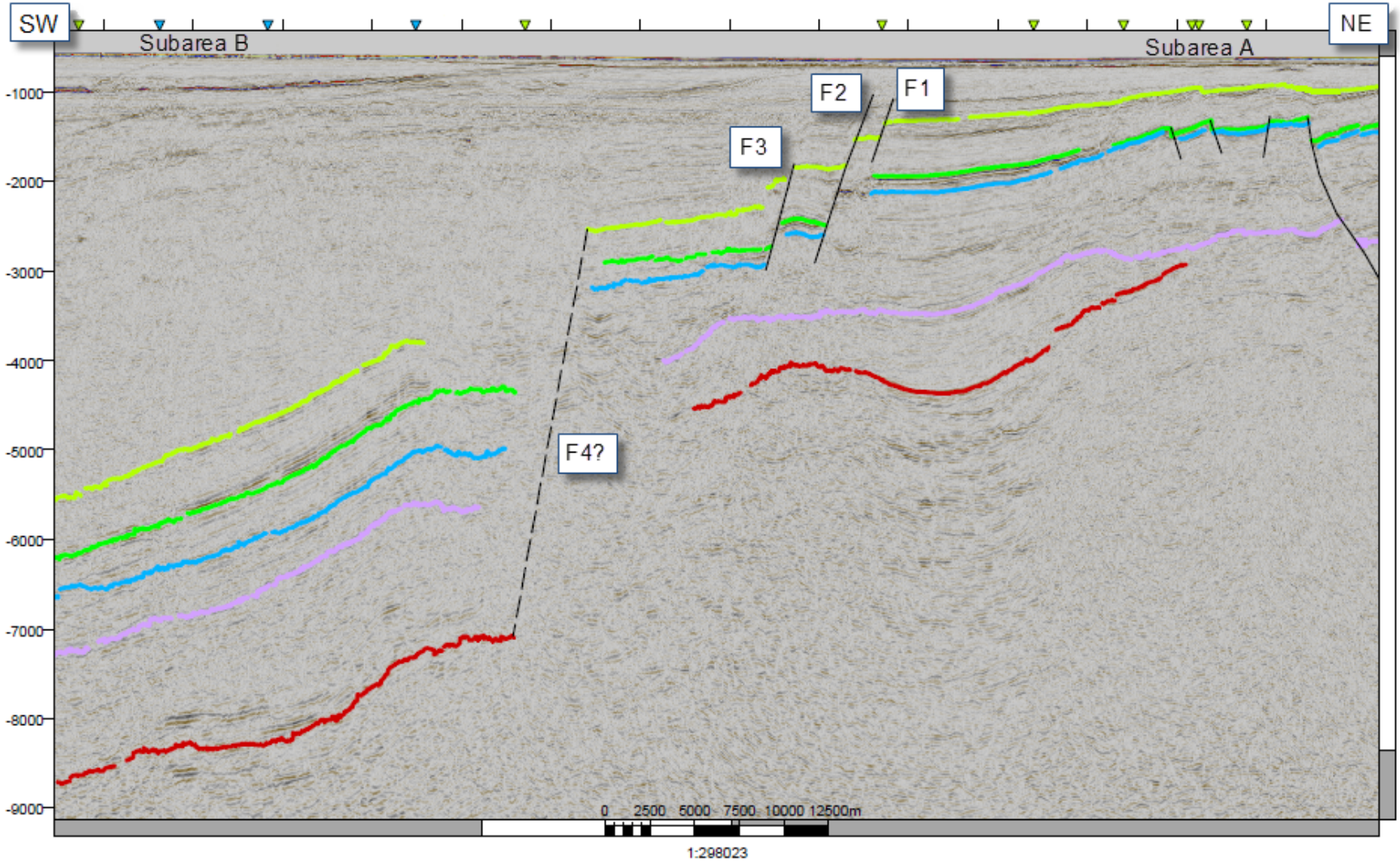

Fig. 3.20 Interpretation of line III. See Fig. 3.11 for location of line and Fig. 3.4 for color codes.

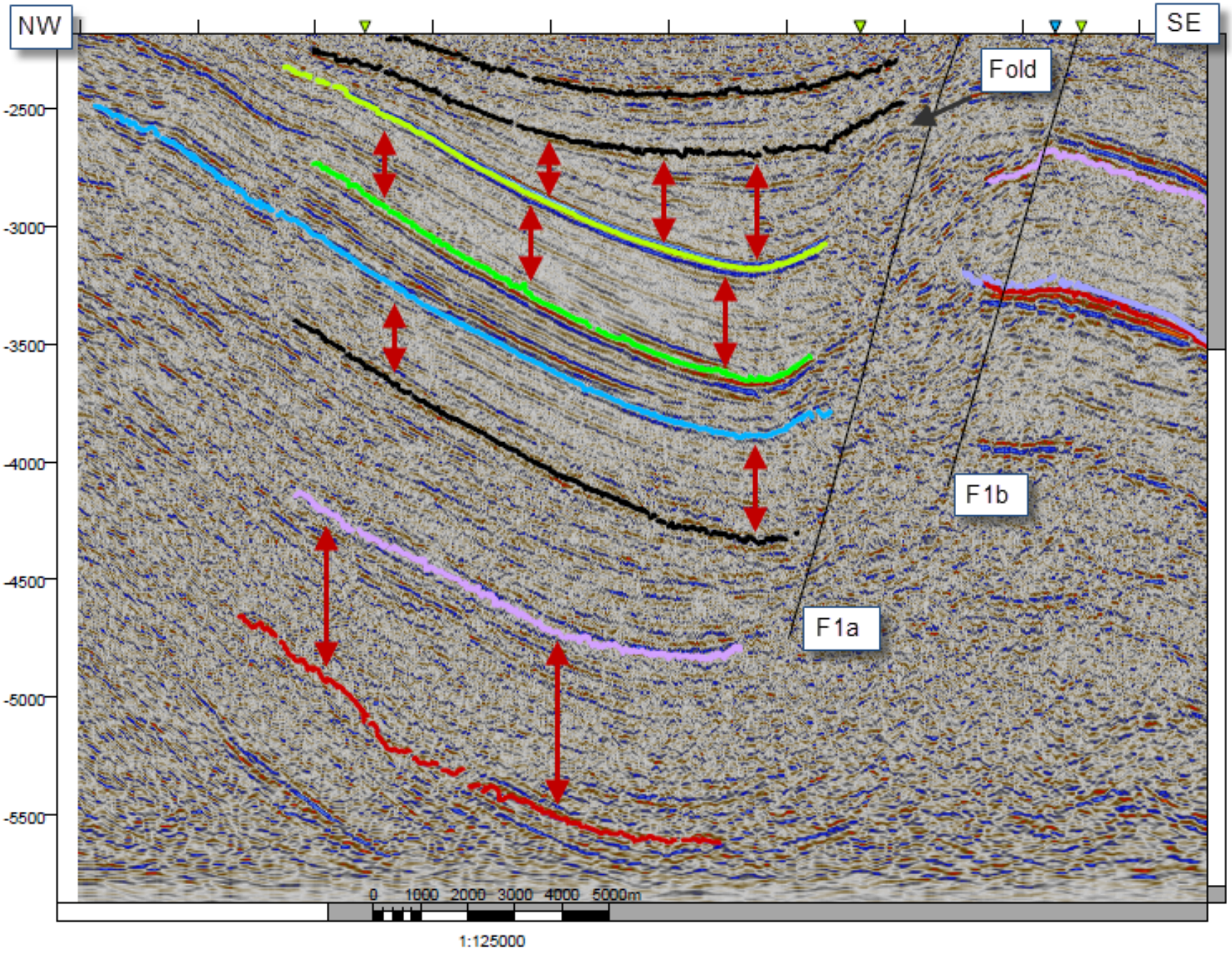

Fig. 3.21 Interpretation of line IV. See Fig. 3.11 for location of line. Note the wedge thickening towards the fault. See Fig. 3.22 for larger image of folds close to the fault plane.

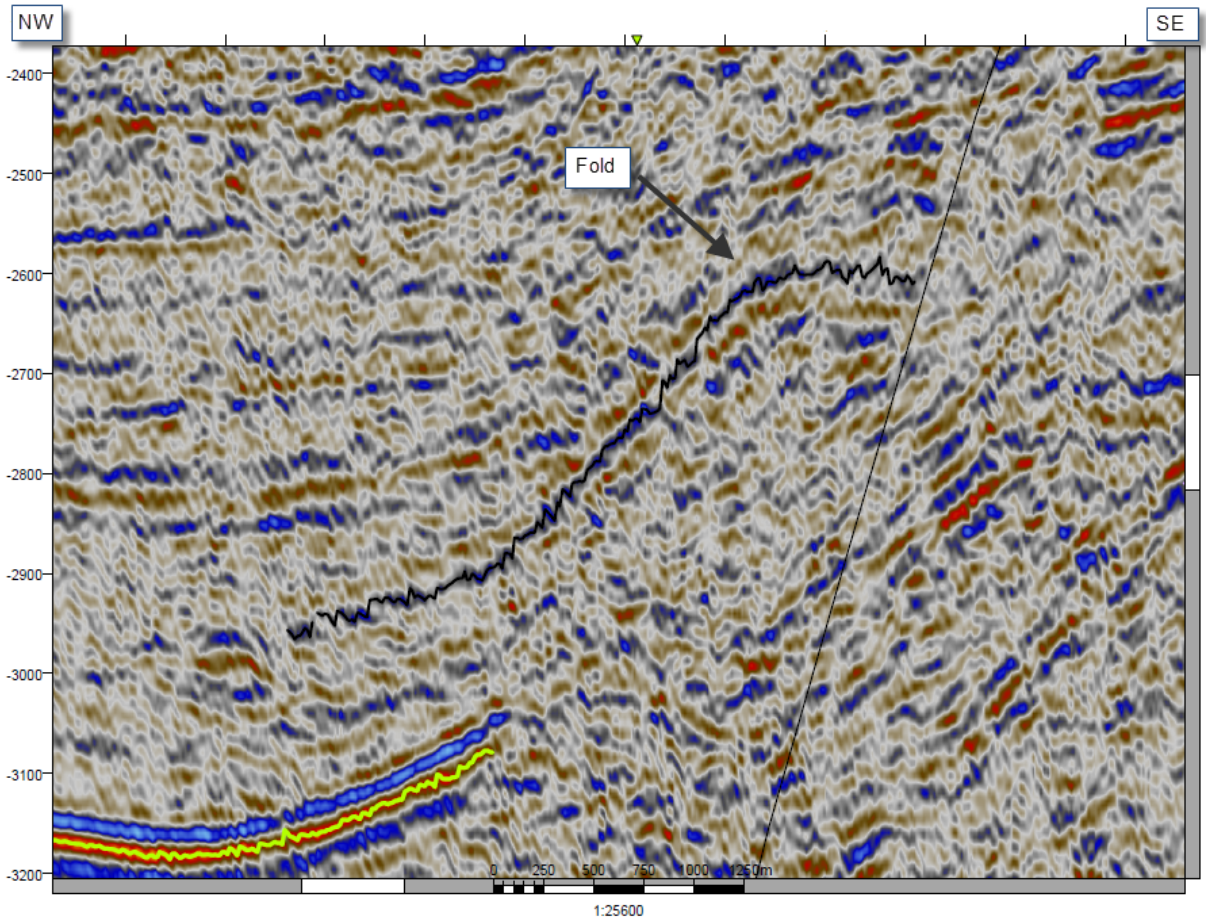

Fig. 3.22 Strata close to the fault plane showing a fold.

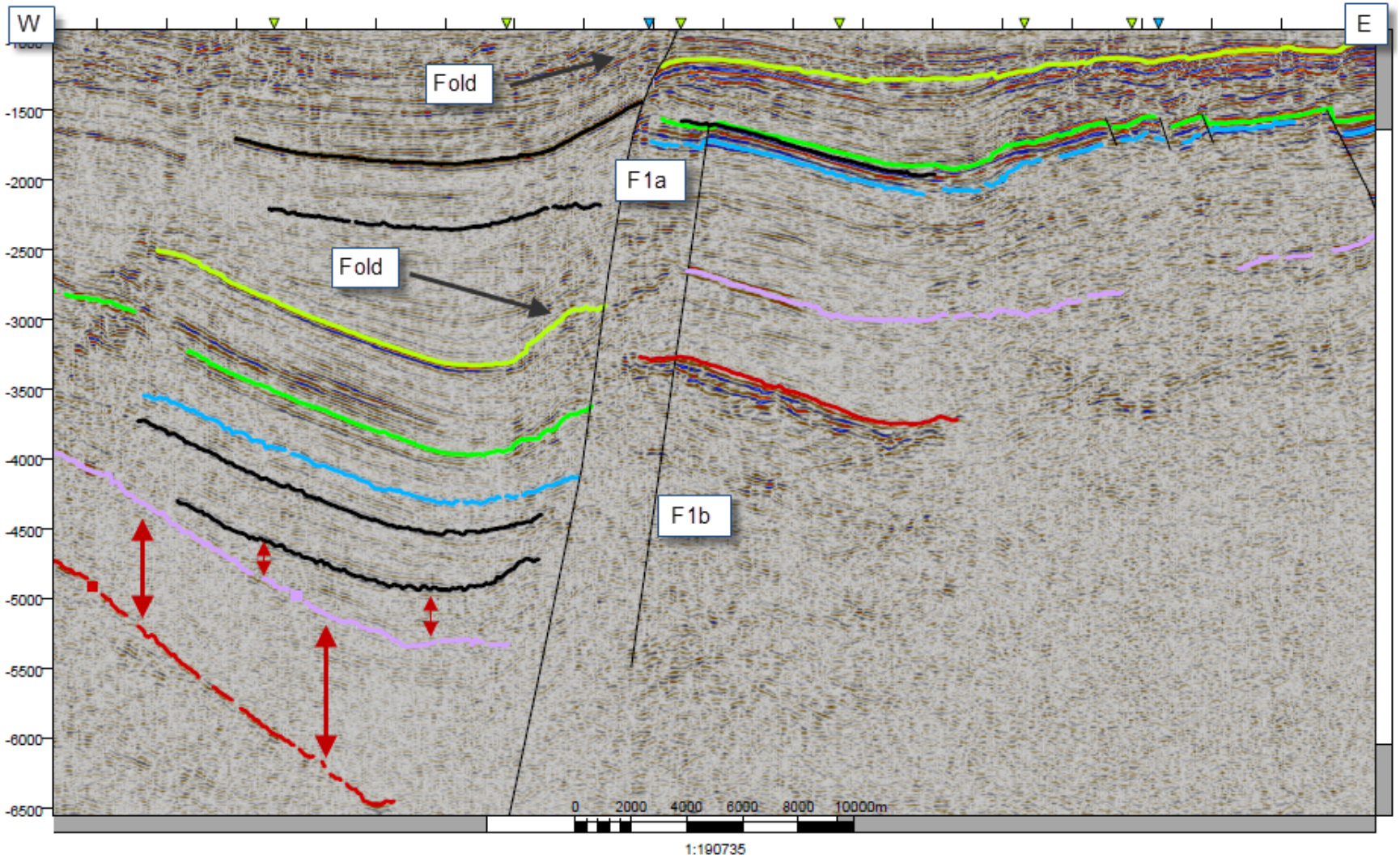

Fig. 3.23 Interpretation of line V. See Fig. 3.11 for location of line. See Fig. 3.4 for color codes.

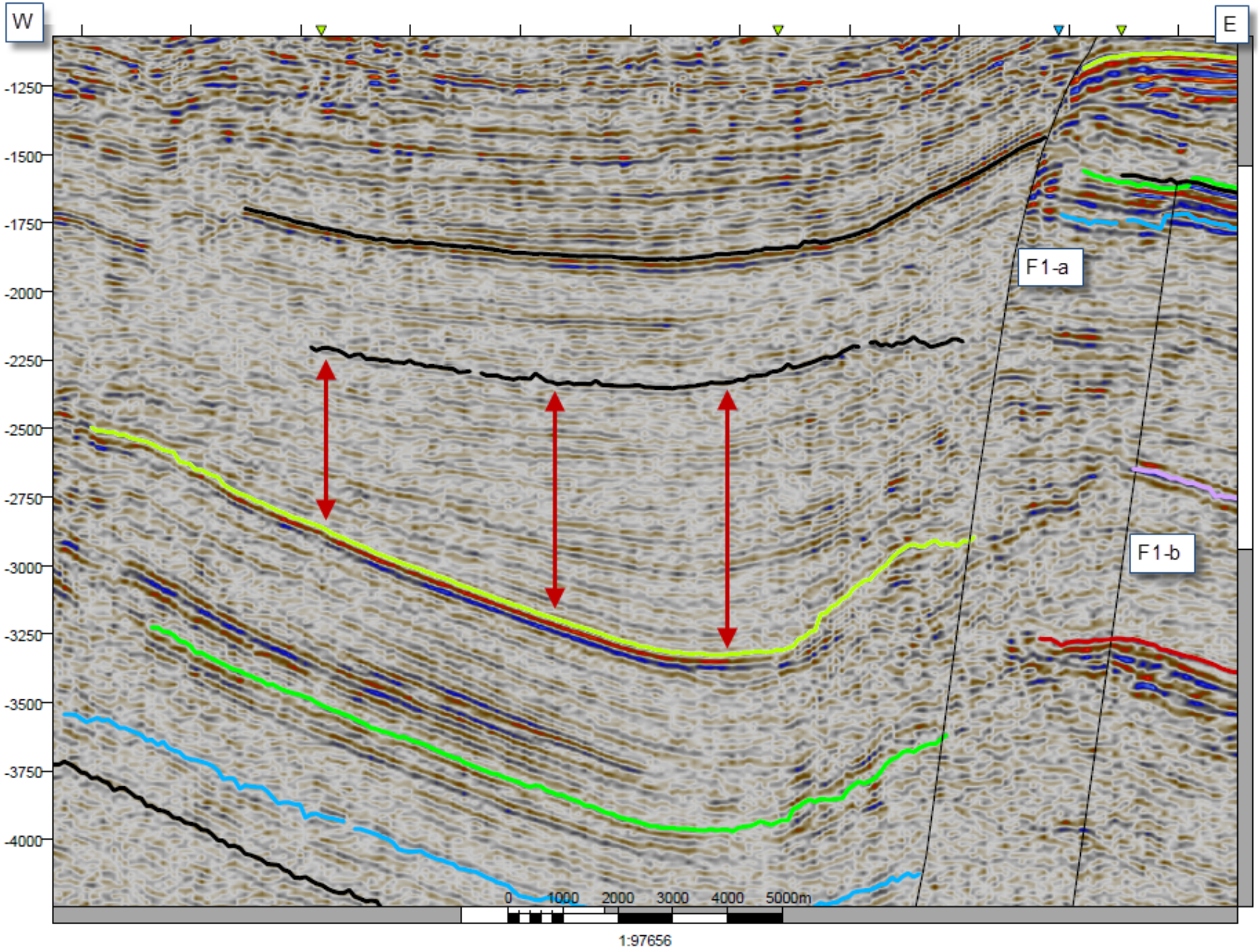

Fig. 3.24 A very pronounced wedge geometry is seen where the Aptian reflection defines the lower boundary.

Depth converted lines

Line I and line II were depth converted and are shown in Figs. 3.25 and 3.26, respectively.

The most noticeable differences are seen in line II (Fig. 3.26) close to the fault zone. Whereas the reflections between the fault branches in time domain dip towards to SW, they form a bulge-like structure and dipping towards NE in depth domain. Both of the fault branches are fairly planar in depth domain, as they were in time domain (Figs 3.12 and 3.15). The seismic data appear to be very distorted close to the fault. This is interpreted as being an artifact from the depth conversion scheme.

3.2.3 Time-structure and fault maps

In the following section, time-structure maps and associated fault maps of the interpreted reflections will be presented and described. The major structural feature dictating the overall geometry of the area is the major fault. This fault has affected all the reflections mapped, thus the individual fault maps exhibit great similaritites. Some differences are however apparent, and these will be pointed out. The solid black lines on the time-structure maps are meant to indicate the major structural trends. Fault annotations (i.e. F1 and F2) refers to the major faults seen in Fig. 3.12. Faults involving the individual surfaces are displayed in the associated fault map. Conversely, time-thickness maps have been derived from the time-structure maps, as shown in Fig. 3.32. It should be noted that the gridding process tends to smooth out important details which might be crucial in order to obtain an increased understanding of the geology in the area; this is especially the case when trying to assess the possibility of several faults being present and linked. In order to ensure that hard data is respected, a set of maps displaying the fault throw for individual seismic lines in segment 2 have been constructed (Fig. 4.6).

Base Permian In general, the clearly defined faults which are readily observed in the shallower reflections, are to a certain degree obscured in the time-structure map at this level (Fig. 3.27). The major structural features (subareas and fault segments) defined in the general description and principal fault map (Fig. 3.11), are recognizable however.

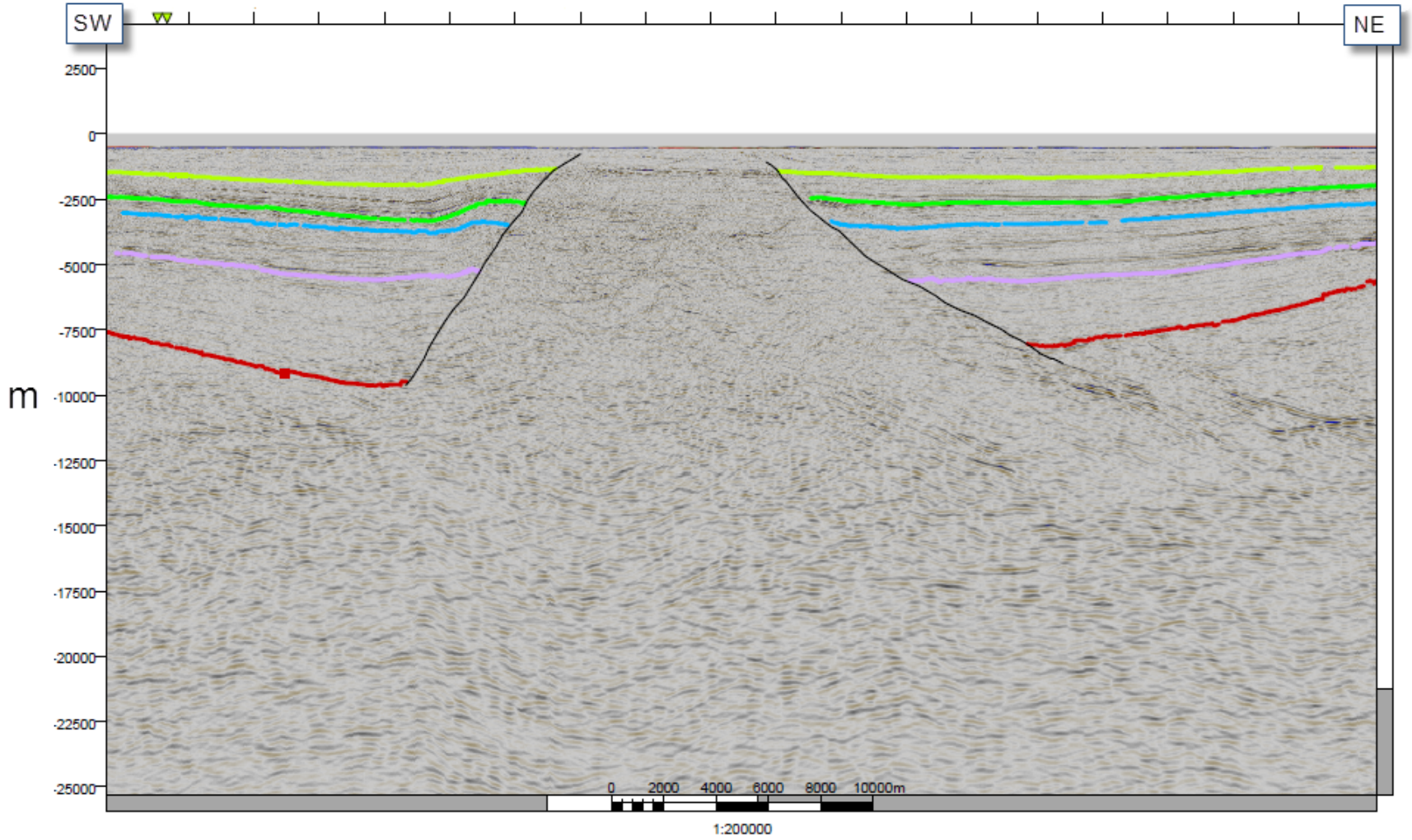

Fig. 3.25 Line I after depth conversion. See Fig. 3.11 for location of line. Note vertical scale in meters.

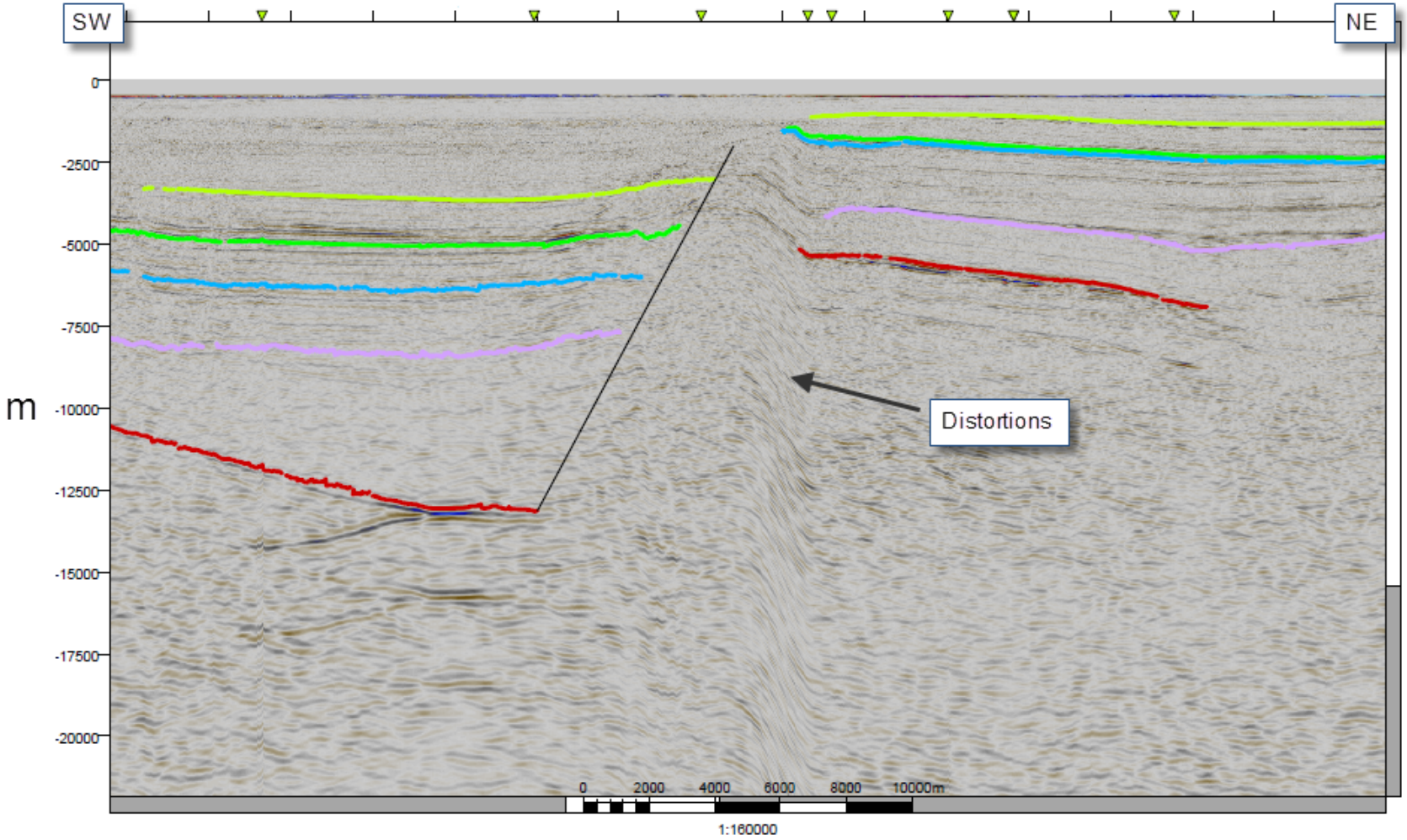

Fig. 3.26 Line II after depth conversion. See Fig. 3.11 for location of line. Note vertical scale in meters.

Starting in the east, the platform area (subarea A) reveals a smooth relief, generally unaffected by faults. Some structural highs and lows are apparent within the area.

The major fault is clearly seen, separating the platform area (subarea A) from the deeper areas of subarea B to the west. The major fault trends N-S in the central part of the map, and turns into a more NNW-SSE trend towards the south (segment 3). Segment 1 to the north is characterized by a more gentle relief as it borders the horst structure separating the two subareas (line I, Fig. 3.12).

To the north, a structural area delineated by an ENE-WSW striking trend is seen to separate the deeper parts of subarea B, interpreted as being the shallowing-up towards the southeastern part of Stappen High (Fig. 2.3).

Base Triassic Compared to the base Permian time-structure map, the base Triassic time-structure map (Fig. 3.28) displays more of the structuring of the fault complex. The overall N-S striking master fault of segment 2 is now readily recognizable. Towards segment 1, the strike of the fault is seen to extend farther north and undulate ever so slightly, going from NNW-SSE to NNE-SSW. This applies for all of the following time-structure maps. The eastern platform area maintains its smooth relief, though the structural highs and lows from the base Permian time-structure map now appear to be more pronounced. The shallow area to the northwest has a larger extent and strikes NE-SW. The major fault is accompanied by synforms in subarea B. These are approximately parallel to sub-parallel to the fault (see fault map, Fig. 3.28).

The antiform and associated faults are seen to the southwest, affecting the Triassic through base Cretaeous reflections.

Middle Jurassic Similar to the base Triassic time-structure map, the master fault is readily recognized on the Jurassic time-structure map (Fig. 3.29). The master fault in segment 2 maintains its strike of N-S, while the southern segment (segment 3) turns into a more NNW - SSE direction going southwards. The northern segment (segment 1) maintains its undulating trend. Some structural highs are seen close to the master fault in segment 1.

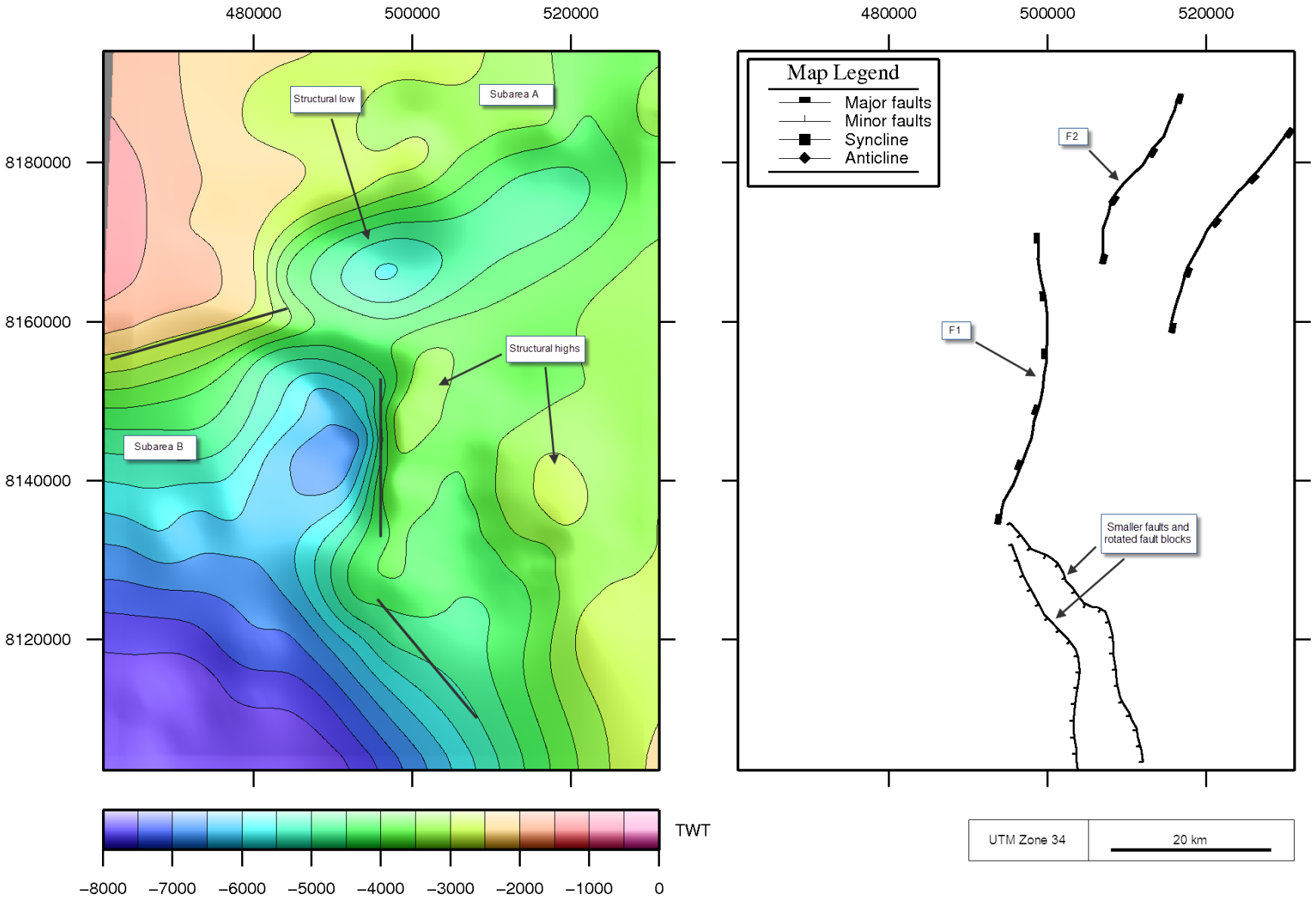

Fig. 3.27 Time-structure map of base Permian.

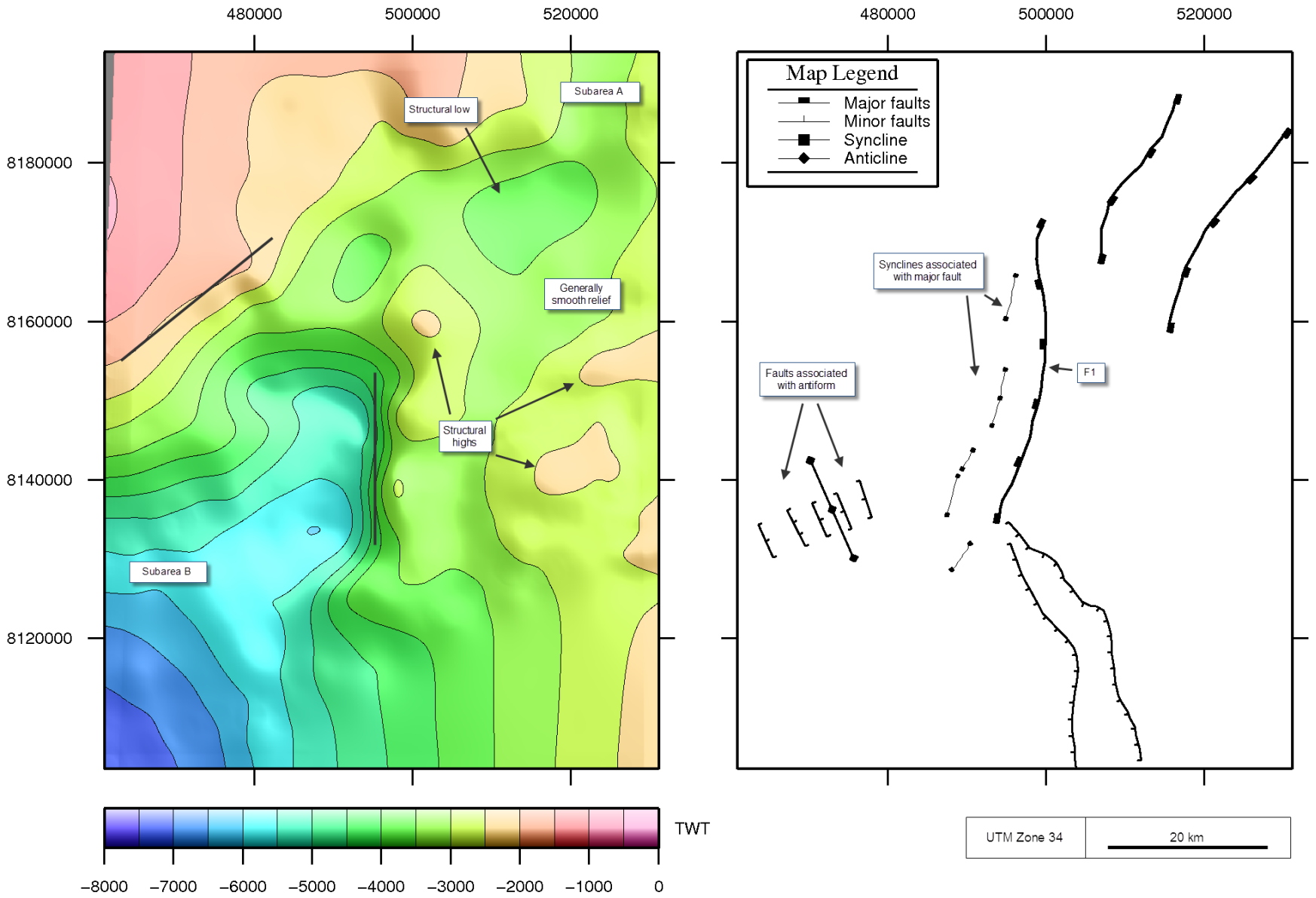

Fig. 3.28 Time-structure map of base Triassic.

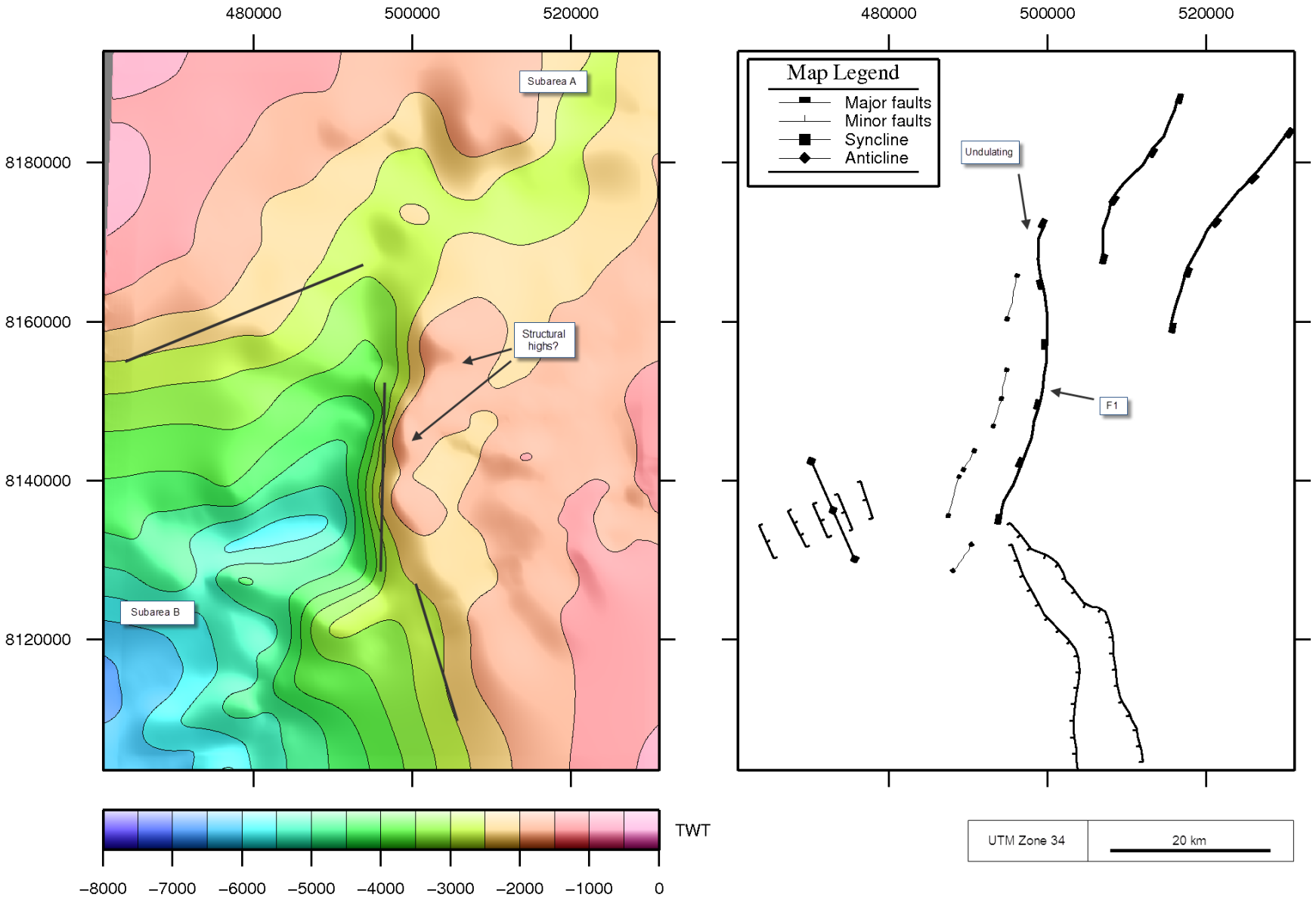

Fig. 3.29 Time-structure map of Middle Jurassic.

Base Cretaceous The segmentation of the fault complex as defined in this study (see Fig. 3.11) is now recognizable. A raised horst-like structure clearly separates subarea A from subarea B (ca. north of N8160000 at E500000), defining segment 1. The structural low in the northeast (E520000,N8180000) appears as a more restricted, isolated subbasin compared to the Jurassic time-structure map. At E500000 between ca. N8165000 and N8130000 the master fault is seen striking roughly N - S, although some undulation is apparent, and defining segment 2. The southern segment (segment 3) is recognized as the relatively abrupt transition from steeply dipping to more shallow dippping reflections at the southern end of segment 2. The strike of the faults in segment 3 maintain their NNW-SSE trend towards the south. Other structural features in subarea B are very identical to that of the Jurassic time-structure map, and no major changes occur between this interval.

Aptian Similar to base Cretaceous, the segmentation is clearly recognizable in the Aptian time-structure map (Fig. 3.31). The relief is somewhat more uniform, exhibiting less variation compared to that of base Cretaceous. This is especially the case in subarea A. The structural low in the northeast is seen to be separated by the horst-like structure. South of this depression in subarea A, i.e. between ca. N8162000 and N8130000, the topography is seen to be more or less uniformly leveled, defining a platform type of relief. The strike of the master fault is seen to go from a N - S direction in the northern part of segment 2, into a more NE - SW trend towards the southern end of the segment. This southern area of segment 2 is seen to comprise a structural high in the transition zone between segment 2 and segment 3. This feature is very hard to observe on the time-thickness map, due to the smoothing caused by the gridding algorithm. The faults in segment 3 maintain the NNW - SSE trend.

3.2.4 Time-thickness maps

Time-thickness maps were made between each of the interpreted reflections (see Fig. 3.32). None of the time-thickness maps are able to display the clear trend of sediment thickening as the seismic lines do.

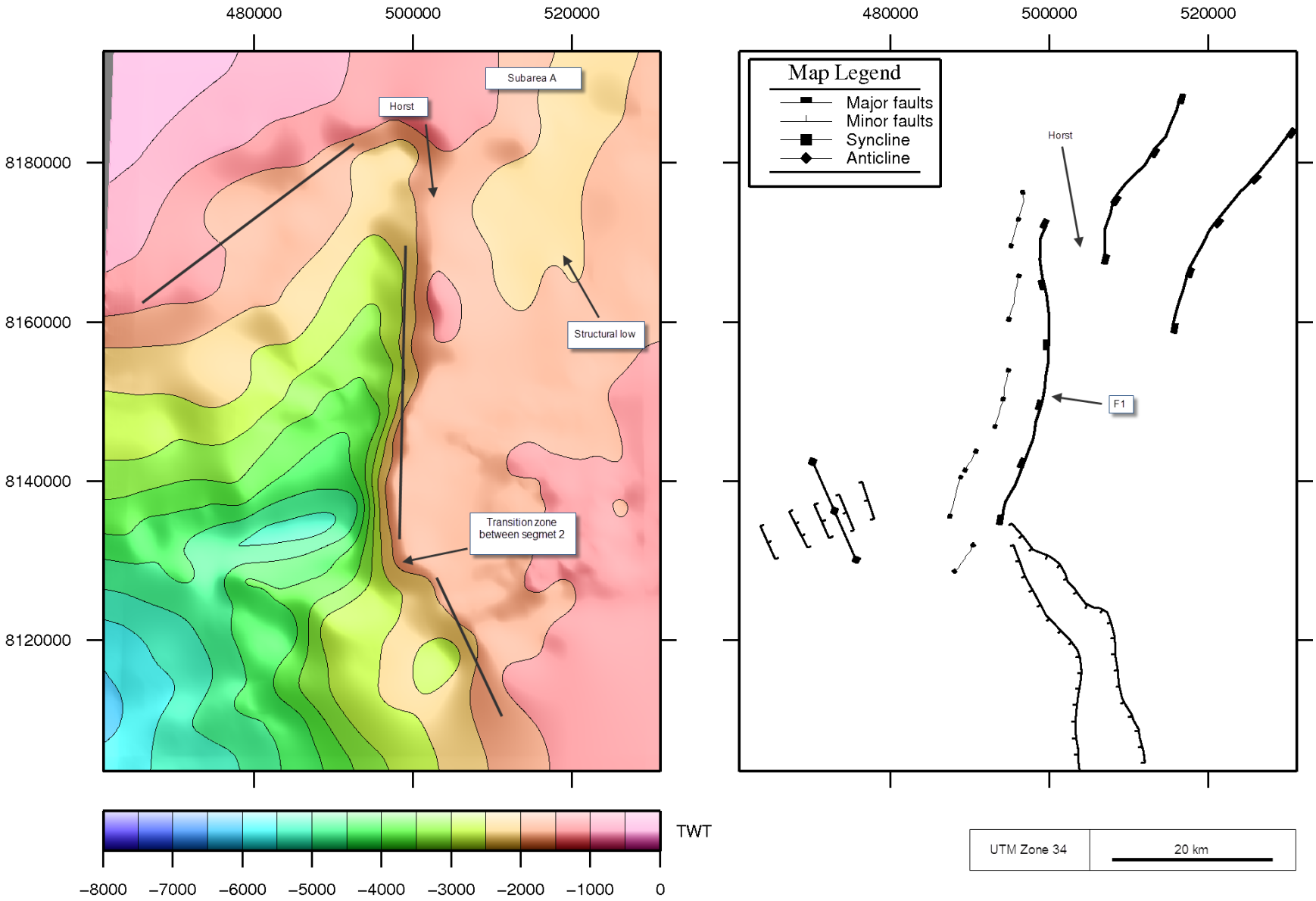

Fig. 3.30 Time-structure map of base Cretaceous.

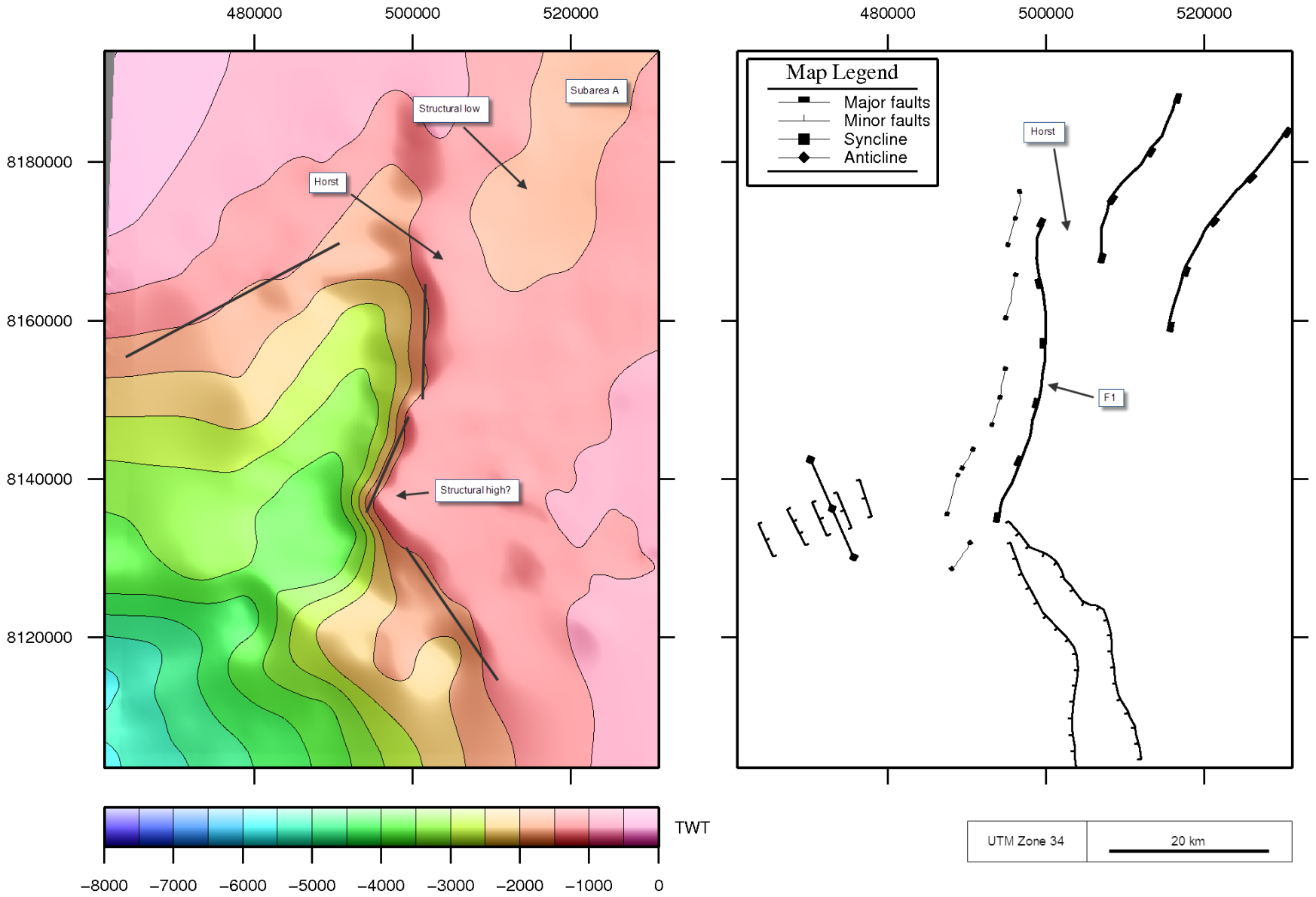

Fig. 3.31 Time-structure map of Aptian.

The Aptian - Base Cretaceous time-thickness map show very little thickness variation. An elongated area in subarea B is however, apparent. In addition some small patches of thickening are seen. The Aptian and base Cretaceous reflections are seen to be quite parallel to each other in most of the seismic sections - thus little variation is seen on the time-thickness map. Common for all the maps are the relatively constant thicknesses observed in the northwestern part towards the Stappen High.

The Base Cretaceous - Middle Jurassic reflections are seen to be very close in the seismic sections. In subarea A there are almost no significant variations. In the northern part of the map an elongated thickening pattern is seen. In the transition zone between segment 2 and 3, a narrow thickening trend is seen to extend towards subarea B.

The Middle Jurassic - Base Triassic time-thickness map shows more variation in both subareas. Most of subarea A is seen to display thickening, which increases towards the south. The central part of subarea B also displays significant thickening in some areas.

The Base Triassic - Base Permian time-thickness map covering the Permian succession shows a very distinct thickening in the upper part of the map (segment 1). This may be related to the gridding process in areas where the Permian reflections are below seismic recording length, i.e. these areas should be interpreted with caution. In the far south thickening is seen to extend southwards.

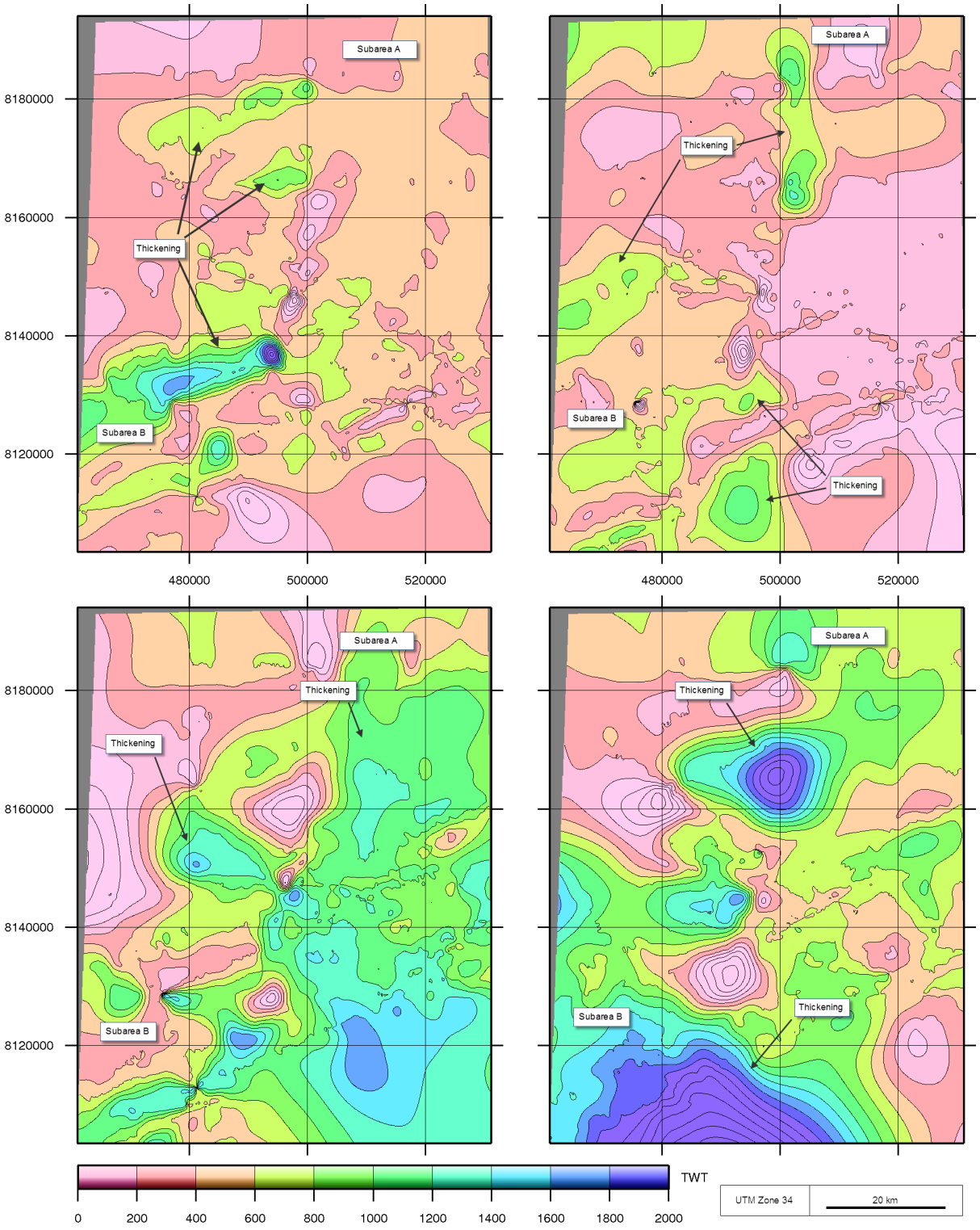

Fig. 3.32 Time-thickness maps between each of the interpreted reflections. Upper left: Aptian - Base Cretaceous, upper right: Base Cretaceous - Middle Jurassic, lower left: Middle Jurassic - Base Triassic, lower right: Base Triassic - Base Permian.

4 Discussion

In general, the Bjørnøya Basin together with the Fingerdjupet Subbasin separated by the master fault segment (F1), constitutes a well known structural style and configuration for areas that have undergone extension.

Following the terminology by Gabrielsen (2010), the Bjørnøya Basin represents the major down thrown segment characterized as the sub-platform. The Fingerdjupet Subbasin with its platform-like geometry and sub-horizontal sedimentary sequences corresponds to the platform (Fig. 4.1). Within each of these structural elements, local deformation and faulting is likely to take place. Although the main controlling feature dictating the overall geometry is the major down thrown fault, the complex is likely to constitute several subordinate faults, folds and other structural elements as observed in the seismic lines presented (e.g. Figs. 4.4, 4.15 and 4.17). These are usually, but need not be, related to the movement, deformation and development of the master fault through time.

The horst structure separating the Bjørnøya Basin from the Fingerdjupet Subbasin in the northern segment (segment 1, Fig. 4.3) may be referred to as an antithetic interbasin ridge (Gawthorpe and Hurst, 1993), as shown in Fig. 4.2. In principle, it could also represent a transfer fault linking border faults of opposite polarity. This would, however, imply that the linkage takes place over a narrow zone, which consequently is absent in the seismic lines due to the relatively wide line spacing.

4.1 Extensional deformation

The Leirdjupet Fault Complex is clearly extensional in nature, and the gross structuring leaves little doubt of this fact and has been well established through several earlier studies of the area (Rønnevik and Jacobsen, 1984; Gabrielsen et al., 1990b; Faleide et al., 1993b).

Line I and II (Fig. 4.4) demonstrate this and show how all reflections mapped have been faulted down towards the west, defining a N-S trending fault system (Fig. 4.3). The eastern margin of the Bjørnøya Basin displays some characteristics of a half-graben (Fig. 4.1) as recognized by Gabrielsen et al. (1990b).

The common subsidence history of the Tromsø and Bjørnøya basins during Late Jurassic-

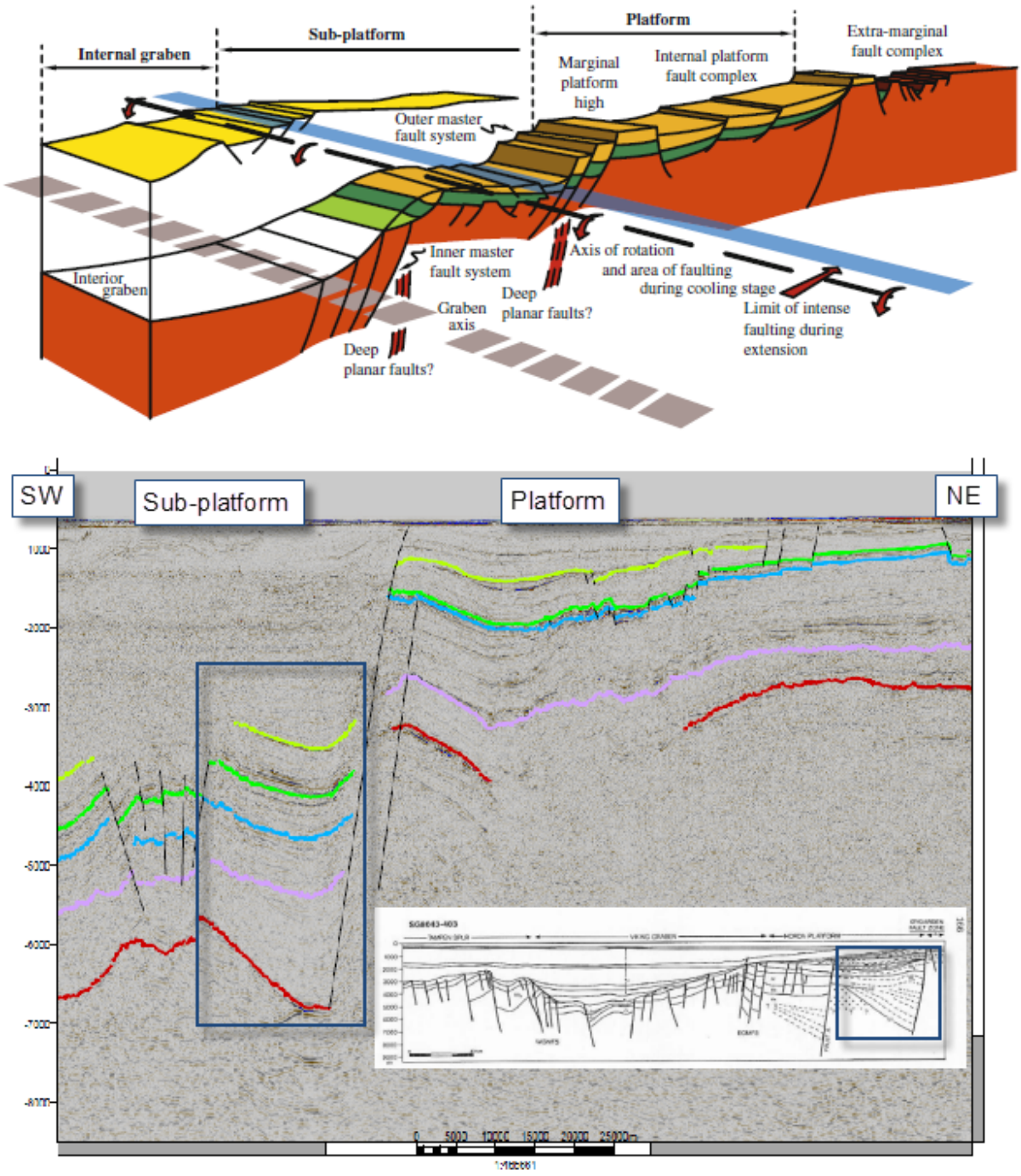

Fig. 4.1 Upper: A principal sketch of the major structural elements in graben systems. The Bjørnøya Basin corresponds to the sub-platform segment, while the Fingerdjupet Sub-basin corresponds to the structurally elevated platform area. From Gabrielsen (2010). Lower: Line II displaying the corresponding structural elements observed. The figure shows the eastern margin of the Bjørnøya Basin with its half-graben geometry. A geoseismic section across the northern Viking Graben (Gabrielsen et al., 1990a) is included as an analogue.

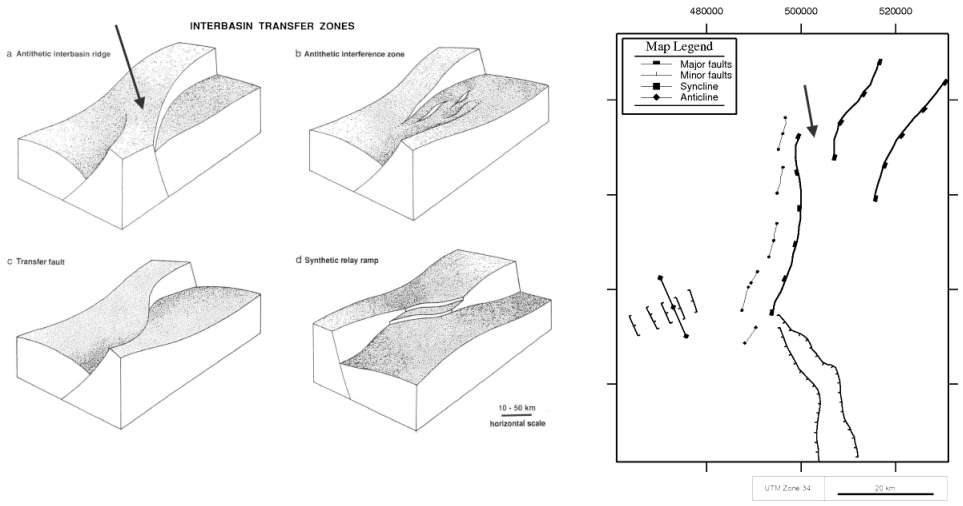

Fig. 4.2 Left: A diagrammatic representation of the main geometries of interbasin transfer zones. (a) Antithetic interbasin ridge. (b) Antithetic interference zone. (c) Transfer fault (linking border faults of opposite polarity). (d) Synthetic relay ramp. From Gawthorpe and Hurst (1993). The horst structure present in segment 1 is interpreted as being an antithetic interbasin ridge as depicted in (a). Right: The Aptian fault map.

Early Cretaceous and the similar sediment thickness deposited in Middle Jurassic through mid-Cretaceous indicate that the basins were affected by much the same processes (Breivik et al., 1998). In addition, thick Lower Cretaceous strata within the eastern part of the Veslemøy High have demonstrated continuity between these two basins prior to late Cretaceous - early Tertiary structuring (Faleide et al., 1993a). The Bjørnøya, Tromsø and Hammerfest basins are all structures which were active in late Jurassic - early Cretaceous as the rifting progressed westwards towards the incipient margin (Breivik et al., 1998; Faleide et al., 2010).

4.1.1 Continuous versus segmented faults

In order to identify possible fault segmentation in the central segment (segment 2), contour maps displaying the throw of the master fault (F1) for the Aptian through Triassic reflections were made (Fig. 4.6). The map displays a clear trend of large throws for all reflections in the south, decreasing towards the north. In the central part (ca. N8150000),

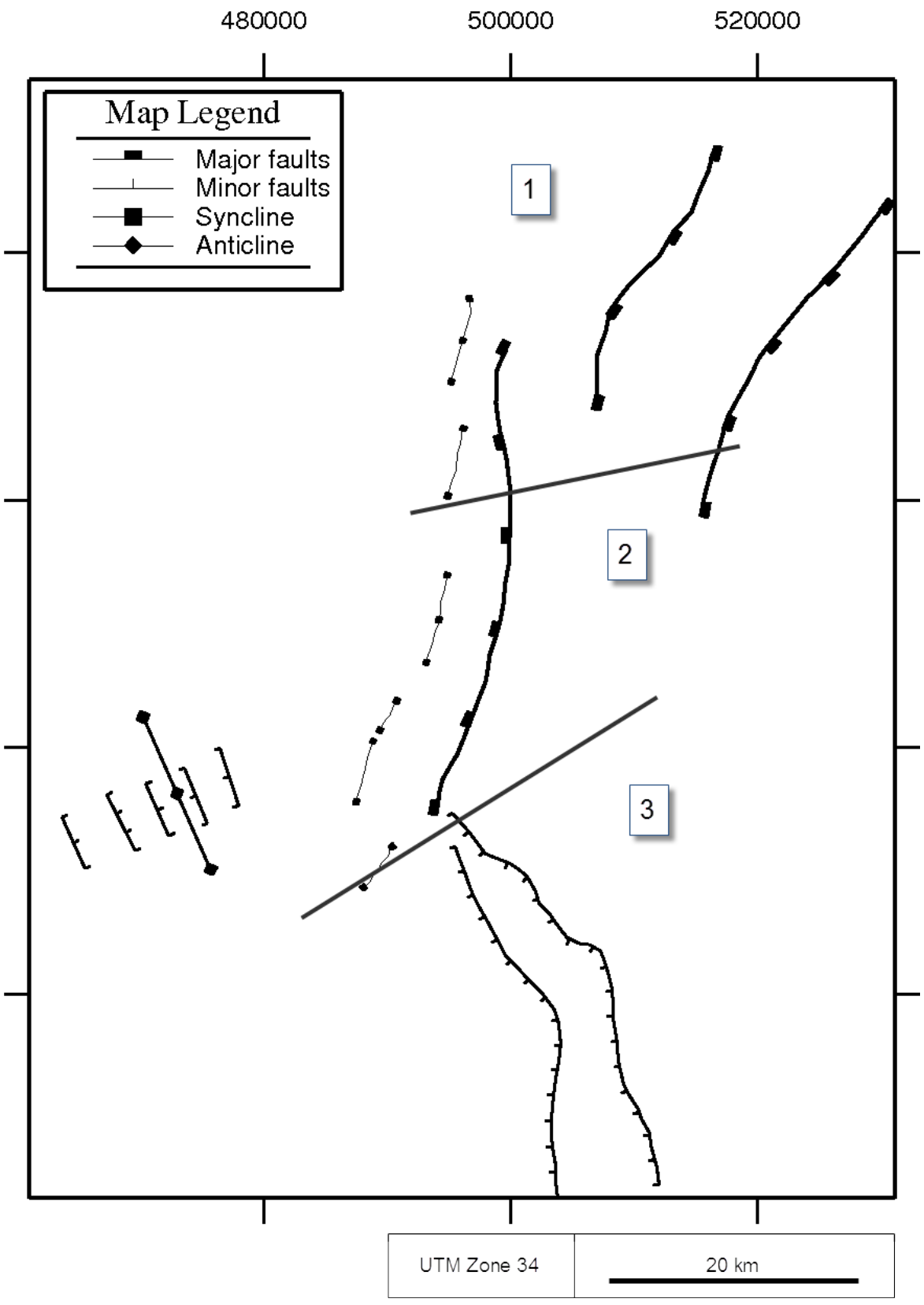

Fig. 4.3 Principal fault map of the Leirdjupet Fault Complex and the three segments as defined in this study.

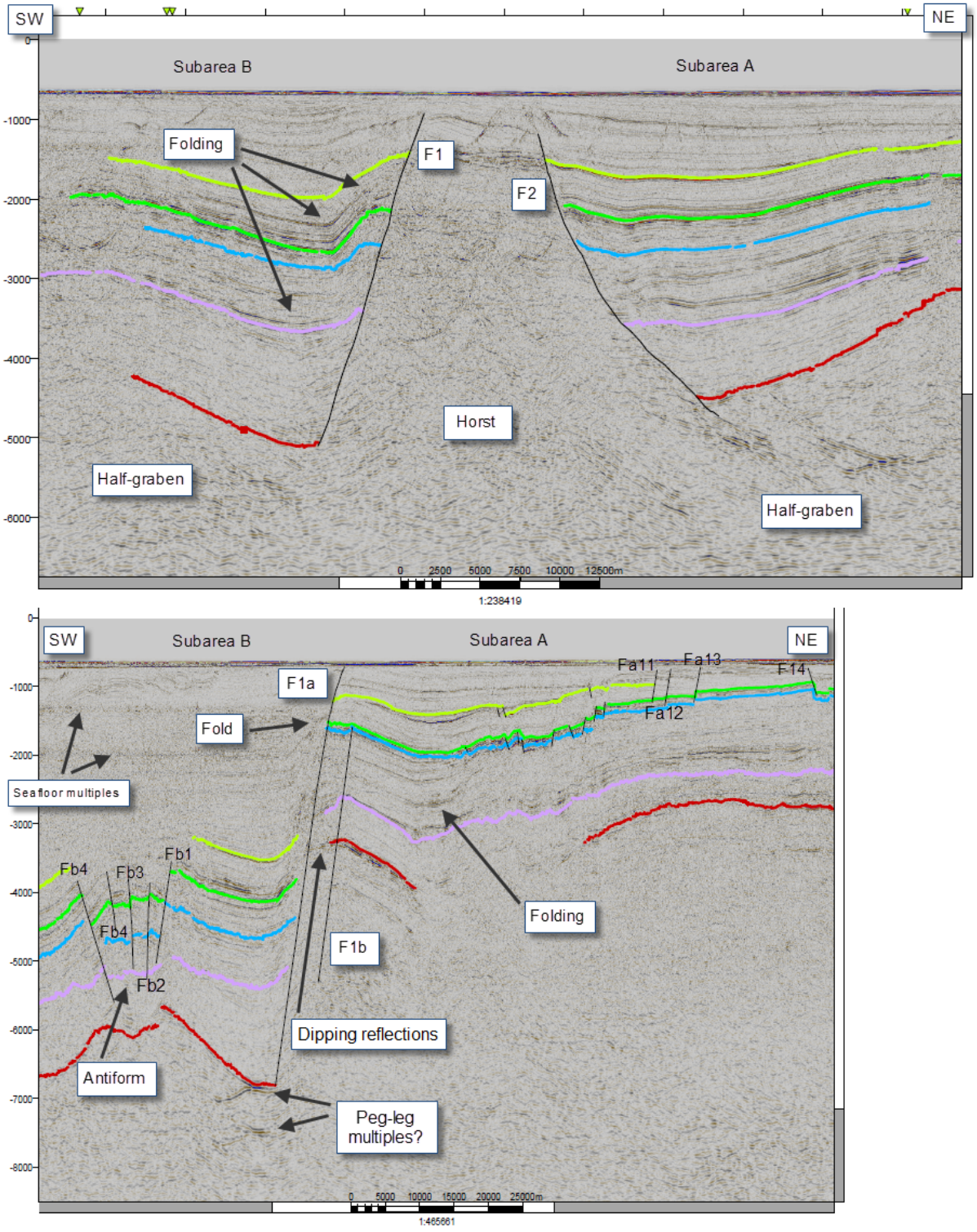

Fig. 4.4 Line I and II displaying the major structural elements of the fault complex.

however, there are some inconsistencies and the throw varies much, considering the short distance.

A single normal fault will generate a different geometry compared to a system of faults (Fig. 4.5) which subsequently link up.

Whereas an ideal single normal fault will follow a displacement pattern on the fault surface which is systematic and predictable (Fig. 4.7), this relationship is more complex by the presence of multiple faults. This is well illustrated by the displacement curve for a set of faults pre-interaction and the resultant displacement curve after interaction and linkage have taken place (Fig. 4.8). Note the importance of fault interaction and linkage and the effect it yields for the final displacement curve.

The Leirdjupet Fault Complex has in earlier studies been depicted as a single through-going fault going from the Loppa High and terminating at the northeastern end of the Bjørnøya Basin.

The variations in the displacement can in principle indicate that this area is in a displacement zone for a breached relay, i.e. in the area between two fault segments where the throw changes (Fig. 4.9), or some type of transfer or linkage zone where faults are interacting.

Davison (1994) defined a linked fault system as "a network of broadly contemporaneous branching faults, which link up over a length scale much greater than individual fault segments". These systems of linked faults may occur in extensional, strike-slip and contractional regimes i.e. they are ubiquitous, and the Leirdjupet Fault Complex could

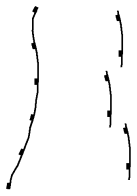

Fig. 4.5 Schematic map view of a continuous fault (left) and a system of segmented faults (right). The left figure displays the master fault as it is defined in this study. Although depicted as a continuous structural feature, some indications of segmentation are present (see text for details).

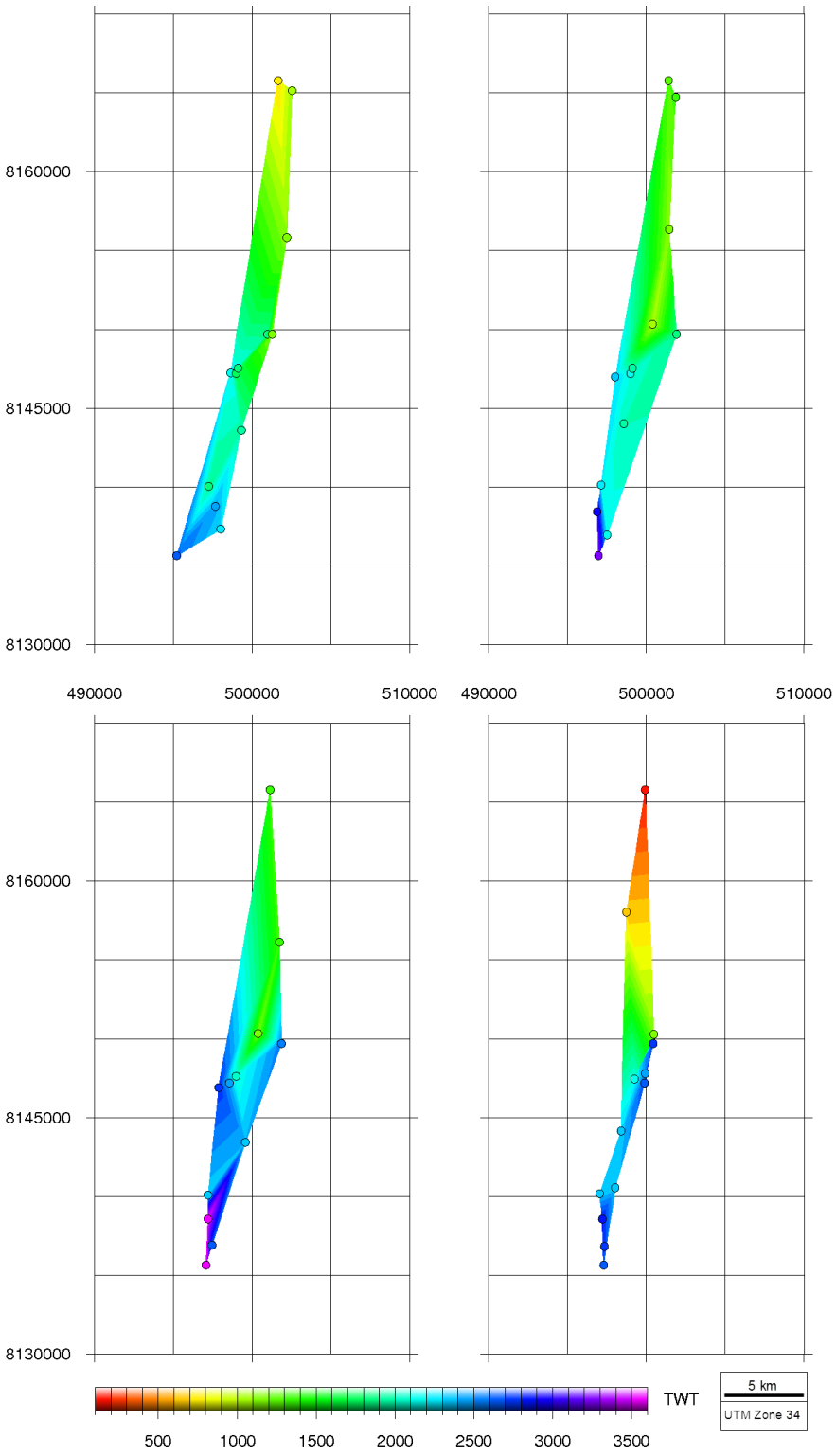

Fig. 4.6 Map indicating the amount of throw along the master fault. Each dot represents a measurement of the fault throw along a 2D seismic line. The amount of throw is indicated by the color coding. Upper left: Aptian, upper right: base Cretaceous, lower left: Jurassic, lower right: Triassic.

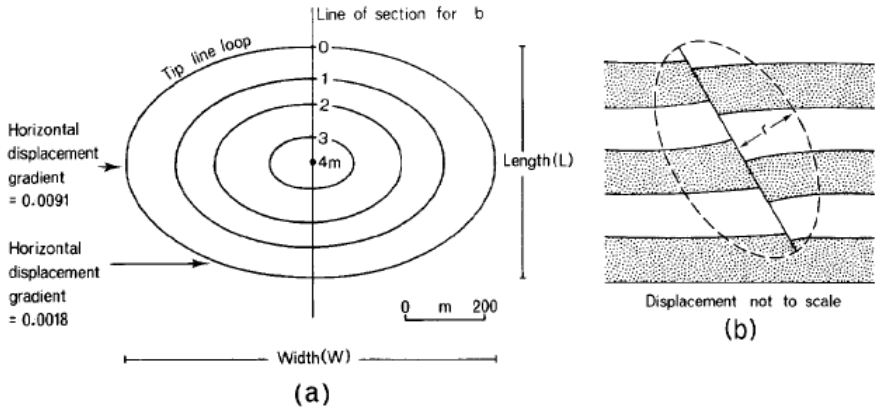

Fig. 4.7 Schematic displacement diagram for a single normal fault. Note that maximum displacement occurs at the center of the fault, whereas the displacement diminishes towards the edge or tip-line. From Barnett et al. (1987).

represent such a linked fault system.

There are several uncertainties with this analysis; due to the relatively widely spaced seismic lines, there are few data points and the lower (and possibly upper) termination of the fault may be erroneously mapped due to varying seismic quality, especially at great depth. Thus, the contour map should be interpreted with caution and no definite conclusion should be drawn based solely on the map. A denser grid of seismic lines would decrease the uncertainty and possibly reveal other zones fault segmentation and linkage. The varying displacement, however, is a good indication that the master fault might be segmented and comprise at least two fault segments.

4.1.2 Extent of fault system and fault displacement

Whether the master fault is segmented and assuming hard linkage, the resultant displacement curve should converge to that of a single fault (Fig. 4.8). The importance of fault segmentation and the influence by individual fault segments will in this context have a limited significance.

Studies which have compared the relationship between the length of faults versus the amount of displacement have found that there is a correlation between the two parameters. Schlische et al. (1996) carried out a study of the geometry and scaling relations of

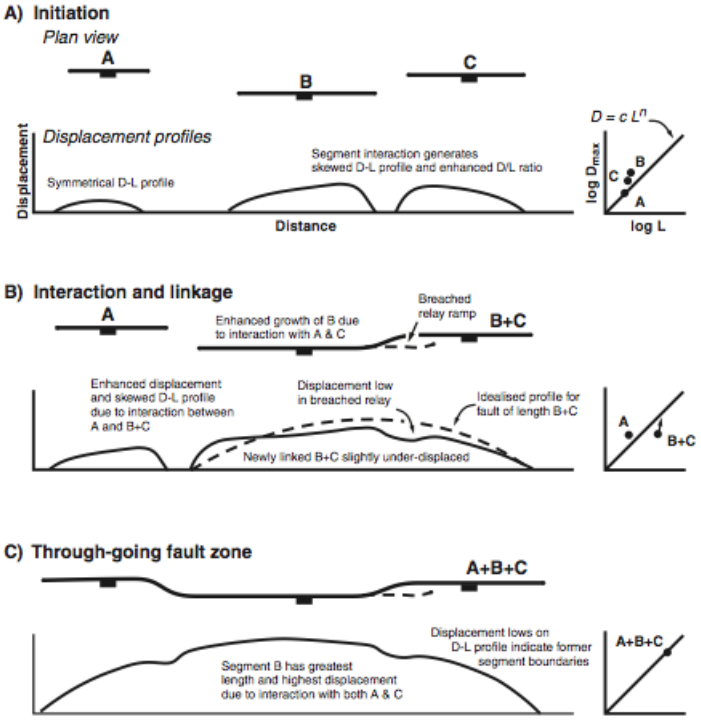

Fig. 4.8 Schematic development of three fault segments which ultimately link up to form a continuous and through-going fault zone. A) Fault initiation stage, B) interaction and linkage and C) through-going fault zone. Note how the interaction and linkage affects the displacement profile for the individual fault segments and compare with Fig. 4.7 which shows an idealized displacement curve for a single fault. Note how the final displacement curve for the through going fault zone displays characteristics of an isolated fault segment. From Gawthorpe and Leeder (2000).

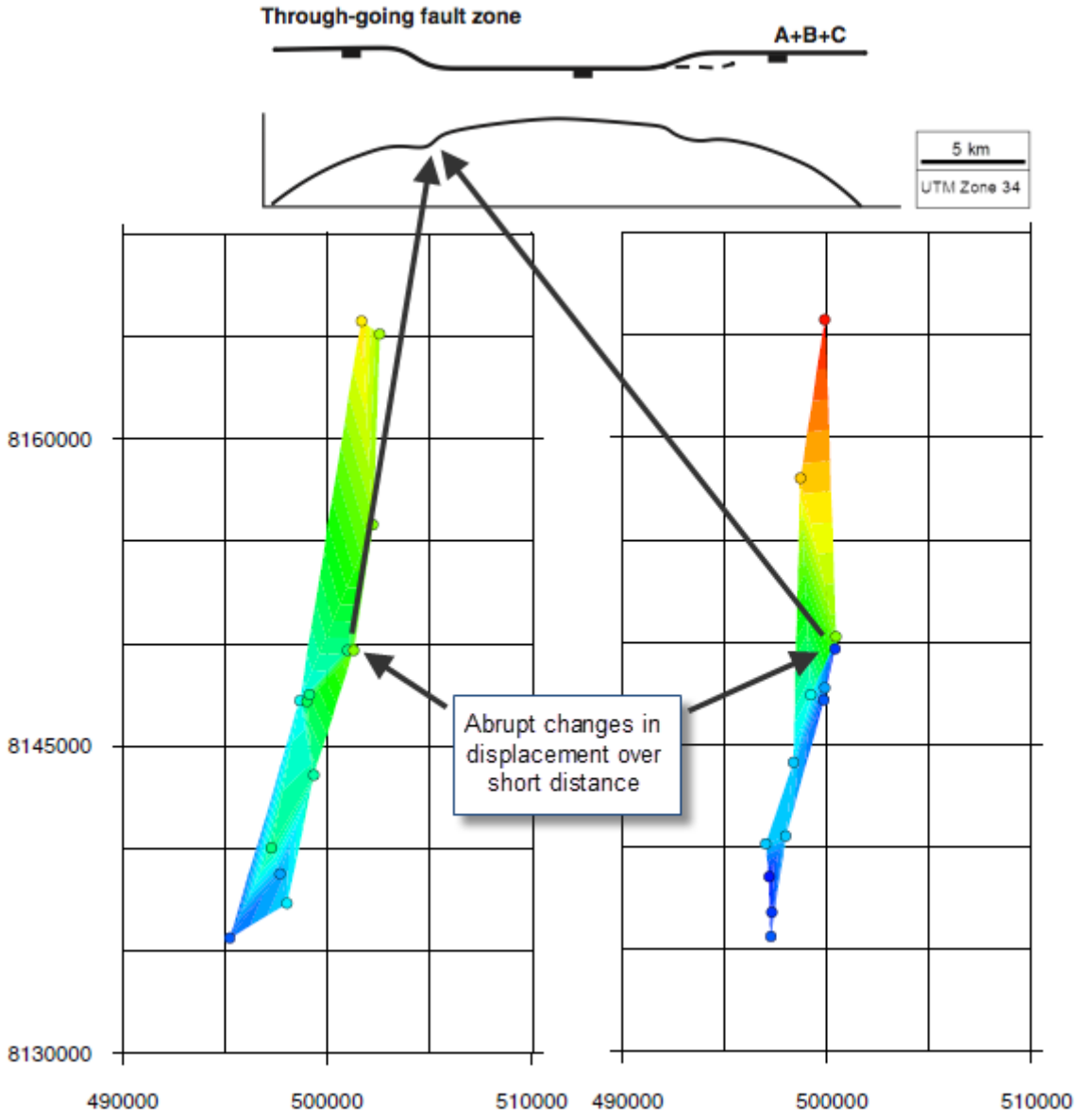

Fig. 4.9 Contour map of the displacement affecting the Aptian reflections (lower left) and Triassic reflections (lower right). The upper image (modified from Gawthorpe and Leeder (2000)) shows how the variations in displacement may be related to the displacement curve of a fault system comprising several faults which subsequently interact and link up. See Fig. 4.6 for all contour maps and Fig. 4.8 for a schematic overview of how faults interact and link up.

a population of very small rift-related normal faults and compared this to earlier studies. The general conclusion is that the displacement increases as a function of the length of a fault, i.e. faults with large horizontal extent are assumed to cause large displacements (Fig. 4.10).

Assuming that the major fault (F1) can be considered as a continuous fault spanning through segment 1 and 2 (Fig. 4.3), an estimate for its total horizontal extent is about 65 km. The scaling relation is given as

$$D = 0.03L^{1.06}$$

where D and L denotes the displacement and length of the fault, respectively (Schlische et al., 1996). This yields a displacement of $D \approx 3791$ m. This relation seems to be in good harmony with the observation in the study area (e.g. Aptian reflection in seismic line II, Fig. 4.11). For the other reflections however, this figure is too low, i.e. the reflections below have experienced larger displacement. Relating this to the displacement diagram (Fig. 4.7), this may indicate that the Aptian reflection is situated in an area which is represented by the upper half of the diagram. This implies that the fault represents a deep structure. The Permian reflection is displaced by ca. 8000 m (Fig. 4.11); solving with respect to L, this yields a fault length of ≈ 131.47 km, indicating a fault system of broad extent. This supports the notion of the Leirdjupet Fault Complex being a branch of a much larger system with broad extent. It is important to note that this most definitely is an estimate - the interpretation in e.g. the southern segment (segment 3) has a lot of uncertainties associated with it due to very incoherent seismic data. It is also important to take into account possible phases of reactivation. Line II (Fig. 4.4) also shows that the fault is cut by the base Quaternary, i.e. the area has been subjected to erosion (Dimakis et al., 1998) and the fault may have cut through successions of sedimentary strata now absent.

Barrère et al. (2009) considered the Leirdjupet, Bjørnøyrenna and Ringvassøy-Loppa fault complexes all to be prolongations of the Billefjorden Fault Zone caused by a Caledonian deep-seated weak zone. This is in agreement with Gabrielsen (1984) who related the ENE - WSW and NE - SW structural trends to a Caledonian structural grain. This

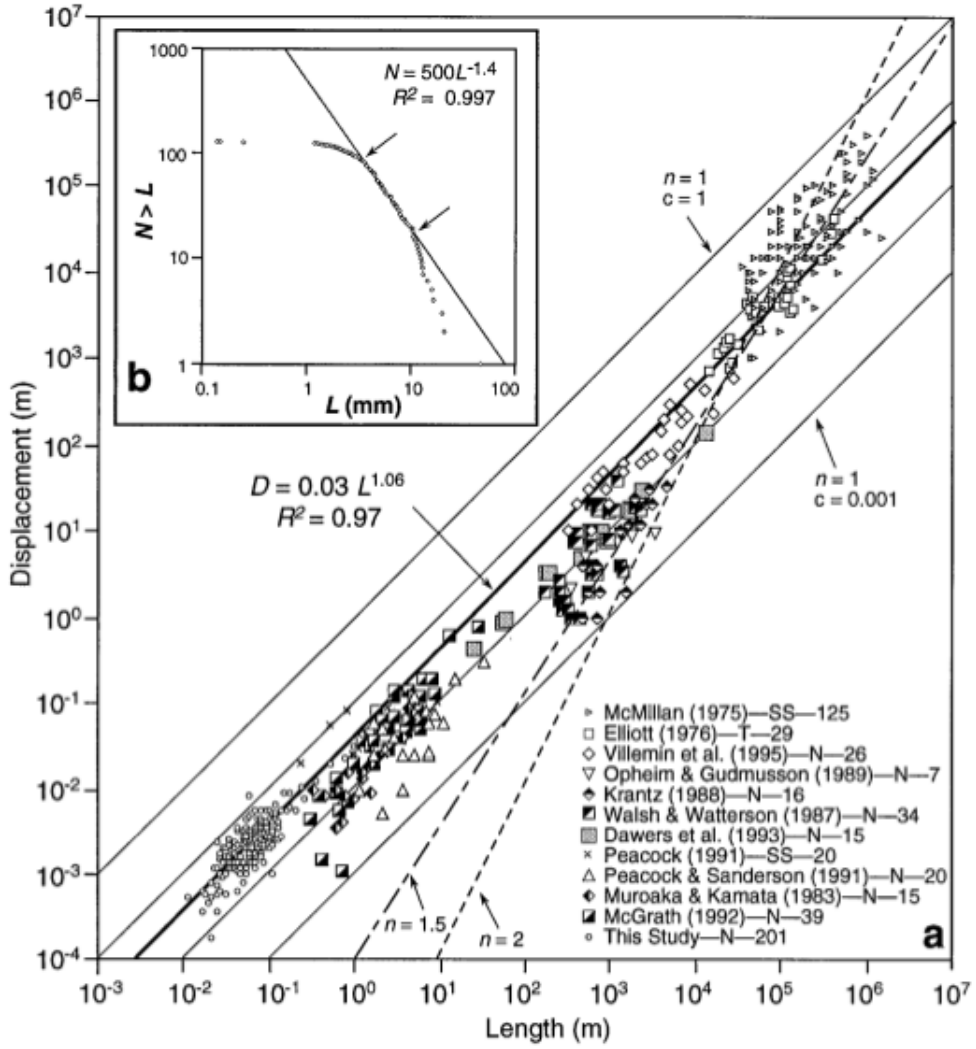

Fig. 4.10 A log plot of fault displacement versus length for several fault populations. (N - normal faults, T - Thrust faults, SS - Strike-slip faults. Best fit for the data set as a whole is denoted by the heavy solid line. From Schlische et al. (1996).

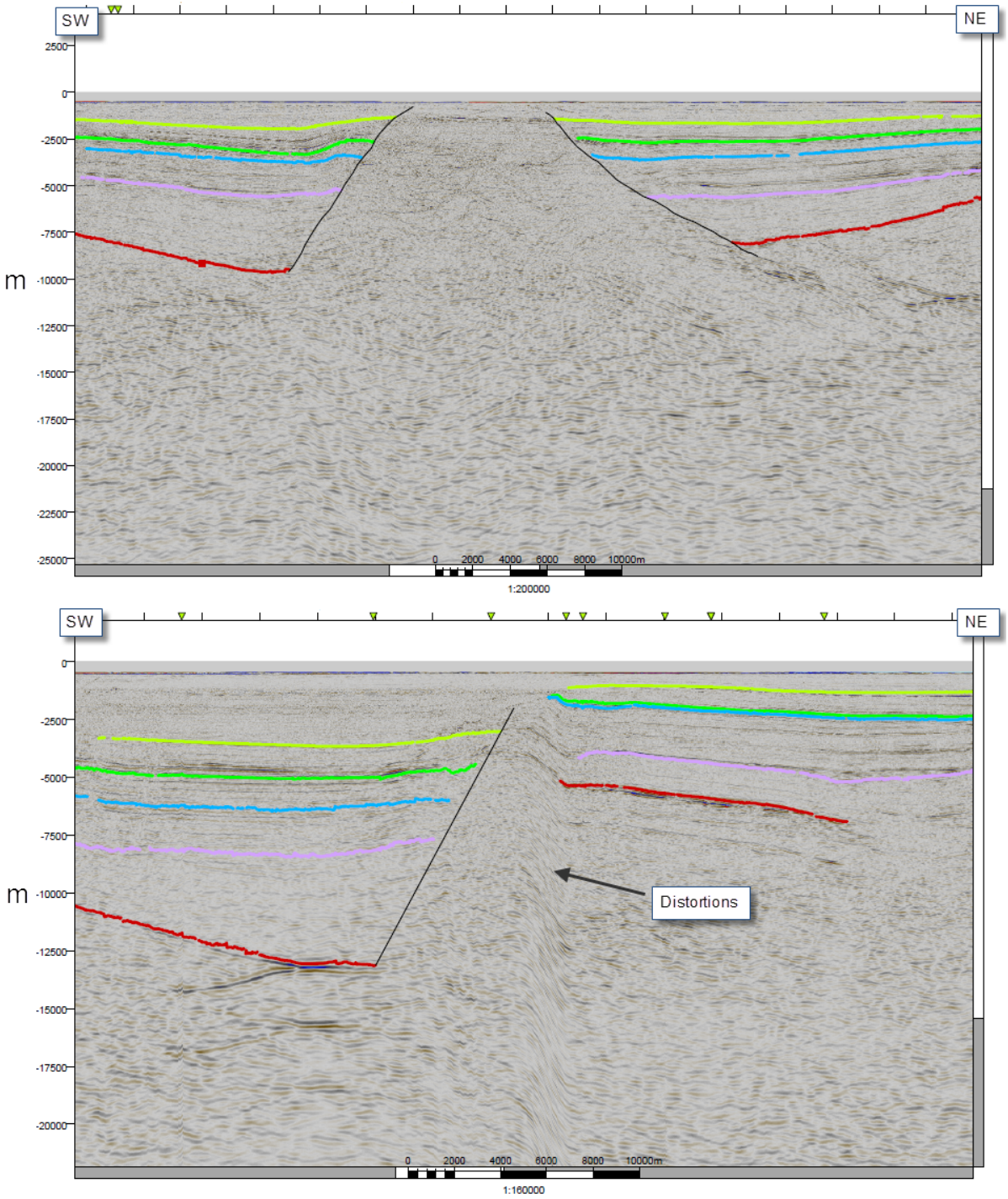

Fig. 4.11 Line I and line II after depth conversion. Note vertical scale in meters.

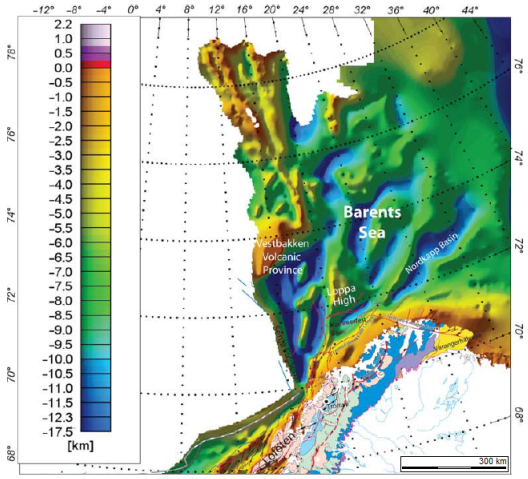

Fig. 4.12 Top basement map of the Barents Sea. The map also demonstrates how onshore features continues offshore and illustrates the link between margin segmentation and onshore geology as pointed out by Gabrielsen (1984). Modified from Ebbing and Olesen (2010) only to incude the Barents Sea area.

implies a fault system spanning across most of the western Barents Sea. Due to its excellent exposure in Svalbard, the Billefjorden Fault Zone is one of the most studied Carboniferous basins on Spitsbergen and has been thoroughly studied (Johannessen and Steel, 1992; Maher and Braathen, 2010).

As seen in e.g. seismic line I and II in time (Fig. 4.4) and depth domain, the master fault (F1) represents a very deep fault. It is likely that the fault continues deeper than mapped in this study, but due to the deteriorating seismic reflections at great depth, this has not been indicated. Ebbing and Olesen (2010) compiled a top basement map for the entire Norwegian shelf (Fig. 4.12) which shows that the top basement is situated at a depth of c. 11.5 km along the eastern part, including the margin, of the Bjørnøya Basin (i.e. hanging wall) and ranging from ca. 9 to 11 km for the Fingerdjupet Subbasin (i.e. foot wall). This may imply that the Leirdjupet Fault Complex is a basement involved structure.

Gabrielsen (1984) proposed a fault classification scheme based on regional significance and the degree of tectonic implications (Table 4.1 and Fig. 4.13). This would make the Leirdjupet master fault a class 1 fault, having regional significance and being basement

Table 4.1 Fault classification scheme proposed by Gabrielsen (1984). Faults are classified according to their regional signficance and tectonic implications. See Fig. 4.13 for a schematic representation of each fault class.

First class	Basement involved	Regional significance	Reactivated	Separate areas of different tectonic outline
Second class	Basement involved	Semi-regional	Reactivated/not reactivated	Separate areas of different tectonic outline
Third class	Basement detached	Local significance	Not reactivated	Does not separate areas of different tectonic outline

involved. This is reasonable taking into account that the Leirdjupet Fault Complex defines an eastern boundary separating the western basin province from the area to the east which is dominated by platforms and terraces. In this respect, the Bjørnøya Basin and Fingerdjupet Subbasin falls into two separate regions as recognized by Rønnevik (1981); the Bjørnøya Basin being located in the province west 20°E and the Fingerdjupet Subbasin in the province between 20°- 25°E.

4.2 Influence of oblique-slip and inversion

Studies which have included the Swaen Graben (located on the Loppa High, Fig. 2.3), the Asterias Fault Complex and the Bjørnøyrenna Fault Complex (i.e. some of the master fault systems of the western Barents Sea) have shown that the area has been subject to several phases of deformation. Being principally extensional features, they are thought to all have been subject to reactivation and subsequent inversion (Gabrielsen et al., 1992). The inversion is manifested by different geometrical expressions related to regional stress configurations. The notion of reactivation being an important factor in the region is well established in the literature. Gabrielsen et al. (1992) suggested three phases of inversion occurring in ?late Jurassic - early Cretaceous, late Cretaceous and (?)early Tertiary.

The tectonic configuration affiliated with the inversion is disputed. Several structures related to strike-slip domains, such as positive and negative flower structures have been associated with the Bjørnøyrenna Fault Complex (Gabrielsen et al., 1992).

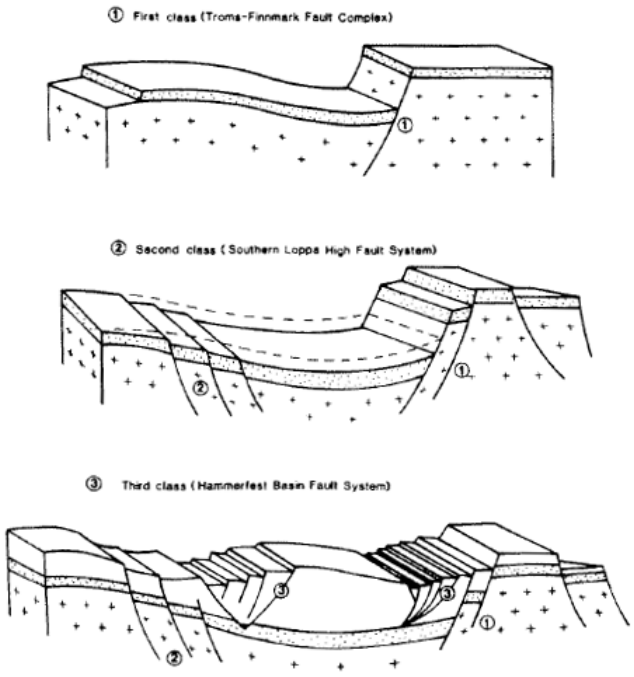

Fig. 4.13 A schematic representation of the relation of first, second and third class fault systems (Table 4.1). From Gabrielsen et al. (1990b).

By simply looking at the major fault traces which constitute the Leirdjupet Fault Complex in map view, it shows similarities to an anastomosing or braided structural geometry (Fig. 4.14). Although ambiguous, these types of branching and interconnected fault geometries are commonly encountered in strike-slip regimes.

The Leirdjupet Fault Complex is thought to be closely related to the Bjørnøyrenna Fault Complex. Gabrielsen et al. (1997) divided the Bjørnøyrenna Fault Complex into regions according to structural style, in which Leirdjupet Fault Complex constituted the northern segment. In this respect the Leirdjupet Fault Complex can be described as a continuation of the Bjørnøyrenna Fault Complex, in agreement with Barrère et al. (2009). Hence, they should be affected by much of the same deformation. The Bjørnøyrenna Fault Complex was affected by northwest-southeast-directed extension during the late Jurassic-early Cretaceous, a phase of early Cretaceous dextral shear (transtension?), late Cretaceous - early Tertiary northwest-southeast contraction (inversion) and Tertiary uplift and erosion (Gabrielsen et al., 1997).

Several of the features observed in the seismic lines (Figs. 4.15 and 4.17) support

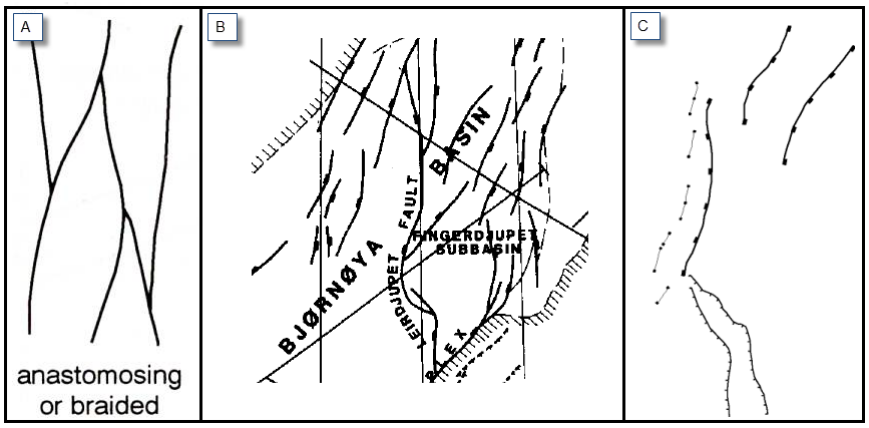

Fig. 4.14 A)Example of an anastomosing or braided fault system. These systems are ambiguous and are found in extensional, contractional and strike-slip regimes. From Woodcock and Schubert (1994). B) Figure of Bjørnøya Basin, Fingerdjupet Subbasin, Leirdjupet Fault Complex and other structural elements from Gabrielsen et al. (1990b). C) Faults mapped in this study.

these observations from the Bjørnøyrenna Fault Complex; wedges are clearly defined in the Early Cretaceous interval, though more subtle within the Jurassic successions. The northwest-southeast-directed extension suggested by Gabrielsen et al. (1997) would infer an oblique slip in the central segment of the Leirdupet Fault Complex. An increasing degree of oblique slip would cause the major fault to be more steep compared to that of e.g. pure dip-slip. Given the N - S strike of the major fault in both segment 1 and 2, the slip sense should be about the same. Consequently the major fault displays a very similar dip in both of the seismic key lines representing the two segments (Fig. 4.4).

In general, inversion of provinces that have undergone extensional deformation requires a major change in the regional stress direction. This is not necessarily the case for a strike-slip dominated system. In such systems basin inversion may arise under similarly oriented crustal stresses, that is, a small rotation in the regional stresses. This may cause a switch from what was originally a transtensile zone, to a transpressional zone (Woodcock and Schubert, 1994).

The importance of the opening of the Norwegian-Greenland Sea is regarded as an important control on the regional geology in the area. Faleide et al. (2008) proposed that

the pre-break up structure, geometry of the plate boundaries and the direction of relative plate motions were main controlling parameters for later structural development. Much of the compressional deformation in and along the Norwegian-Greenland Sea margins is thought to be related to this event. The change in plate motion through time may be a cause for change in deformation style, i.e. the change from extension to compression through strike-slip motion.

In earliest Oligocene the plate motion had a major change, and earlier studies have related several of the compressional features to this event (Lundin and Doré, 2002). Fig. 2.2 shows the tectonic map of the Norwegian-Greenland Sea and the location of compressional structures (i.e. domes and anticlines). By this time there was a considerable counter-clockwise shift of the opening direction, going from a NNW-SSE trend to NW-SE. The NW-SE opening direction has been unchanged to the present. This implies a 30° rotation. The compressional domes found along the mid-Norwegian continental shelf was caused by this shift, leading to sinistral reactivation (Lundin and Doré, 2002, p. 88).

The Bjørnøya - Spitsbergen margin segment was also affected by oblique continent-continent shear and some continent-ocean shear in Eocene times (Faleide et al., 2008). This comprised both transtensional and transpressional components. It is possible that these events affected an extended area in the southwestern part of the Barents Sea.

4.2.1 Inversion

The southwestern Barents Sea was early recognized as being a province which has been subjected to inversion and subsequent uplift. These events have had big implications for the petroleum potential in the area (see chapter 1). Several of the characteristic features associated with inversion are observed in the study area. Grunnaleite (2002) did a regional study of inversion structures in the area including the greater part of the southwestern Barents Sea. In the study, all the major fault complexes, including the Knølegga Fault Zone, Bjørnøyrenna Fault Complex, Leirdjupet Fault Complex and Hoop Fault Complex show signs of inversion. Inverted normal faults are distributed in the whole region accompanied with reverse faulting and folding. Thus, inversion seems to be common and associated to most of the significant fault systems of the western

Barents Sea.

The folds observed close to the fault plane in line II, IV (Fig. 4.15) and V (Fig. 4.17) are interpreted as being inversion related structures. The folds are present throughout the northern and central area of the fault complex, and the fold axis appears to be almost perpendicular to the fault (Fig. 4.16). This indicates that the area was subjected to head-on contraction. This is in agreement with a phase of head-on inversion along the Bjørnøyrenna Fault Complex in late Cretaceous - early Tertiary (Gabrielsen et al., 1997). The Bjørnøya Basin and Bjørnøyrenna Fault Complex was also subjected to inversion in the Hauterivian - Aptian (Gabrielsen et al., 1997), and it is plausible that the Leirdjupet Fault Complex was subjected to this as well.

Inversion in extensional fault systems typically genererate folding and backthrusting in a still downthrown hanging wall block (Hayward and Graham, 1989). In areas that have undergone inversion, this may cause clearly defined pre-inversion wedges to be obscured in present day cross sections (Fig. 4.18), which appears to be the case in line I, V (Fig. 4.17) and IV (Fig. 4.15).

In addition to the inversion related structures, Faleide et al. (1993b) suggested that the half-graben geometry of the Bjørnøya Basin may have been accentuated by inversion, subsequently tilting the basin infill when the Stappen High was uplifted in the Tertiary.

4.3 Timing of faulting

The presence of wedges, growth faults and thickness variations across faults, i.e. sediment thickening towards the fault plane, can be used in order to determine syndepositional fault activity and constrain periods of tectonic activity from periods of tectonic quiescence (Osmundsen et al., 1998). Fault growth may also have a significant influence on the depositional patterns (Leeder and Jackson, 1993; Nøttvedt et al., 2000; Gawthorpe and Leeder, 2000; Braathen et al., 2011; Maher and Braathen, 2011). Prosser (1993) divided the evolution of an ideal basin into four *system tracts*; i)Rift initiation, ii)rift climax, iii)immediate post-rift and iv)late post-rift. Each of these system tracts have their own characteristic seismic expression (Fig. 4.19).

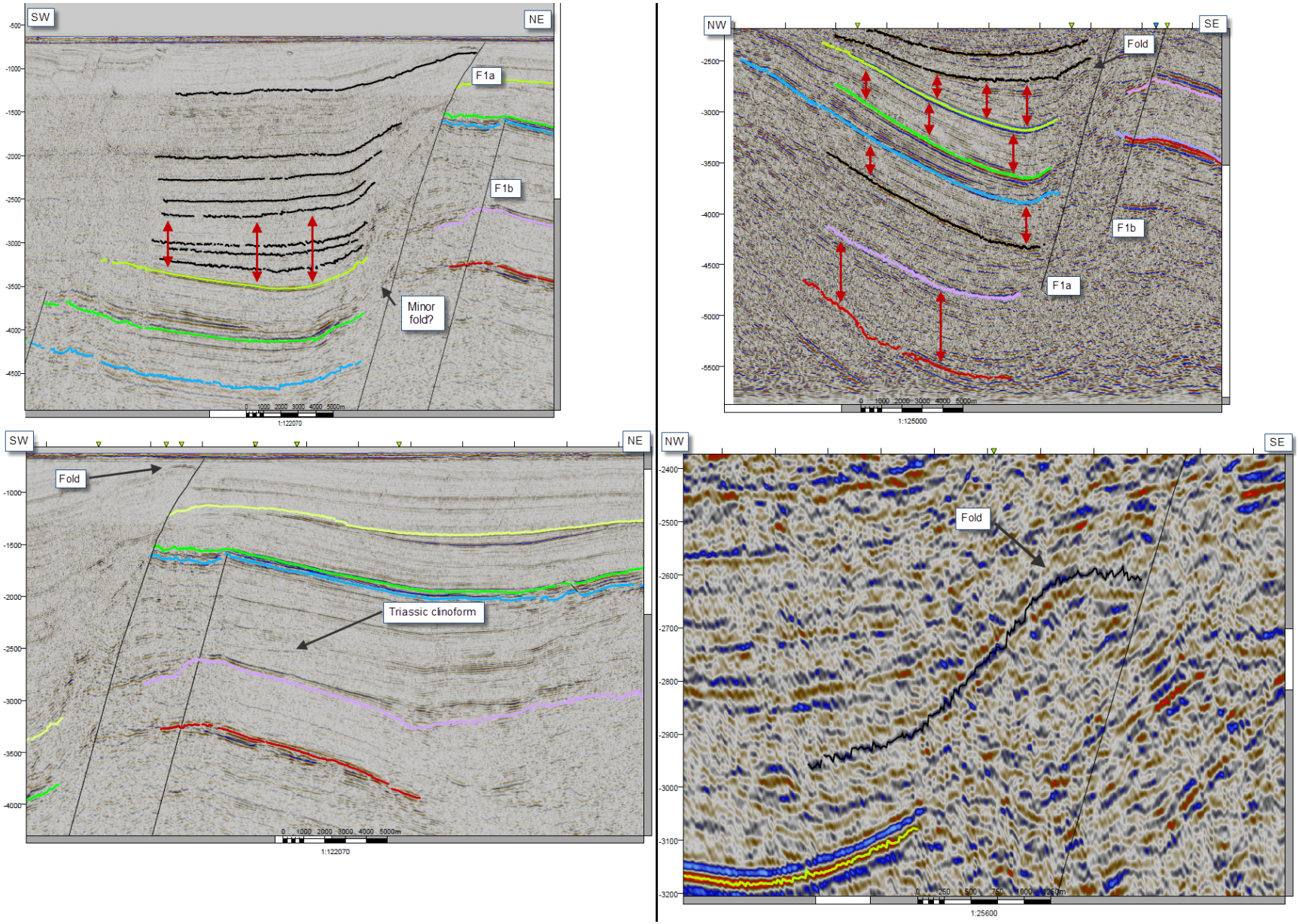

Fig. 4.15 Inversion structures and sediment thickening observed in the study area. Left: Line II (Figs. 3.17 and 3.18). Right: Line IV (Figs. 3.21 and Fig. 3.22). The red arrows indicate the wedge shape and infers the upper boundary of this unit. Note that the black lines in these figures only are meant as markers - they are not associated with any defined time lines.

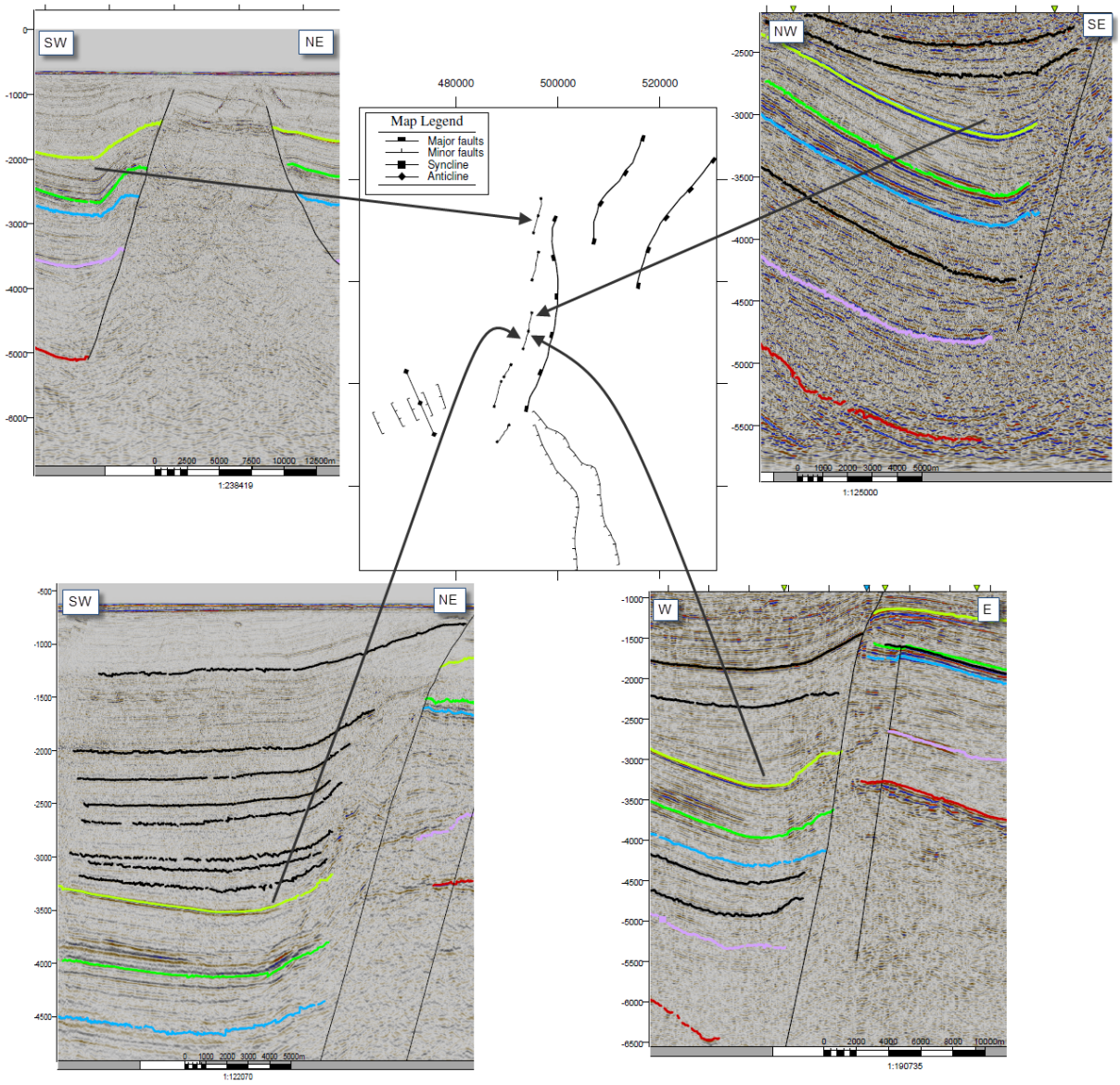

Fig. 4.16 Upper left: Line I, upper right: Line IV, lower left: Line II, lower right: Line V. The folds appear to be perpendicular to the fault in both segment 1 and 2.

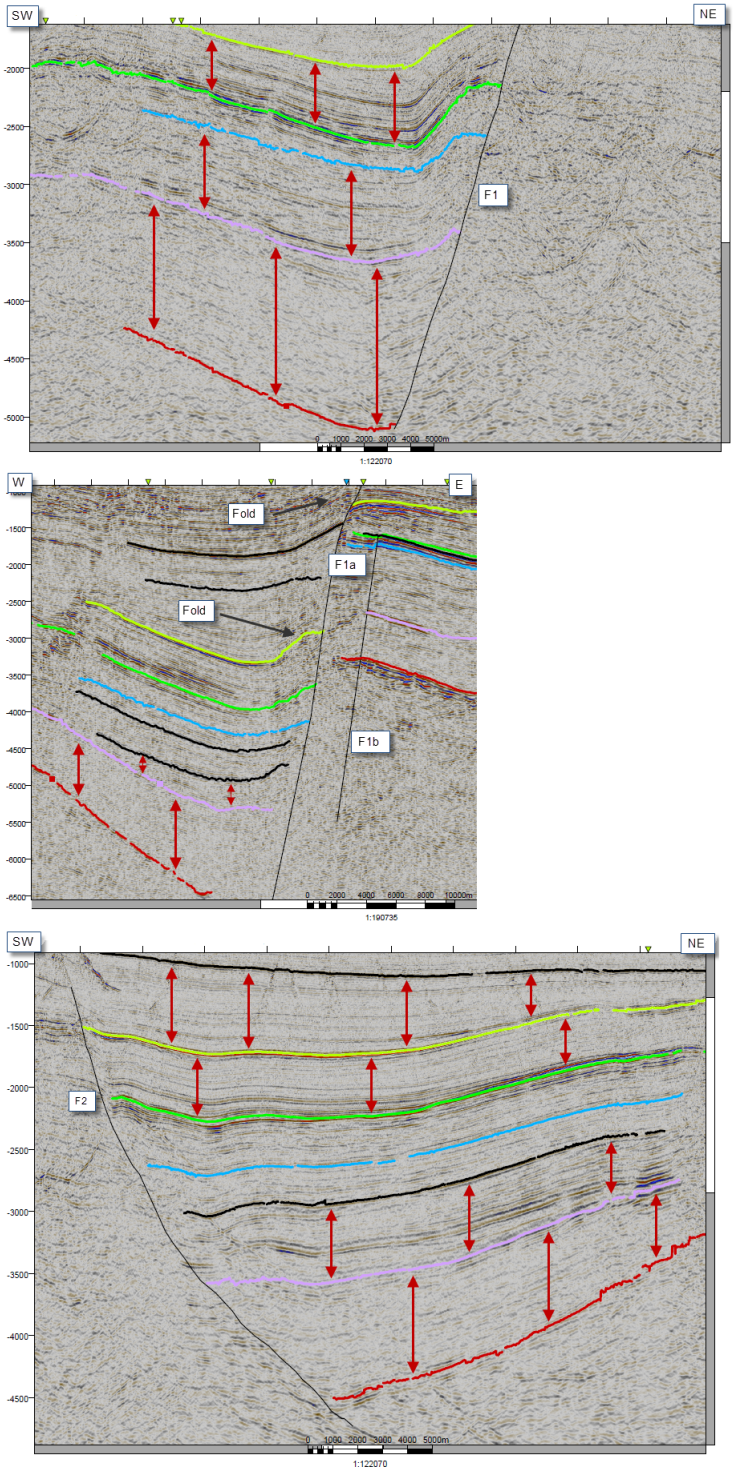

Fig. 4.17 Folds observed in line I (upper) and line V (lower left) and sediment thickening in line I (lower right).

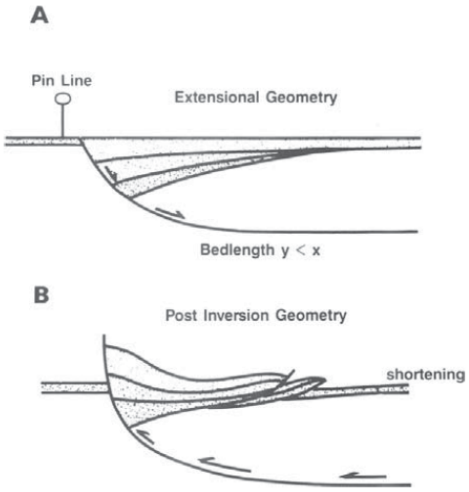

Fig. 4.18 Left: A) Formation of a half-graben during extension. Wedges develop during active faulting. B) Subsequent inversion causing accomodation structures. Note how this affects the previously clear wedge geometry. From (Hayward and Graham, 1989).

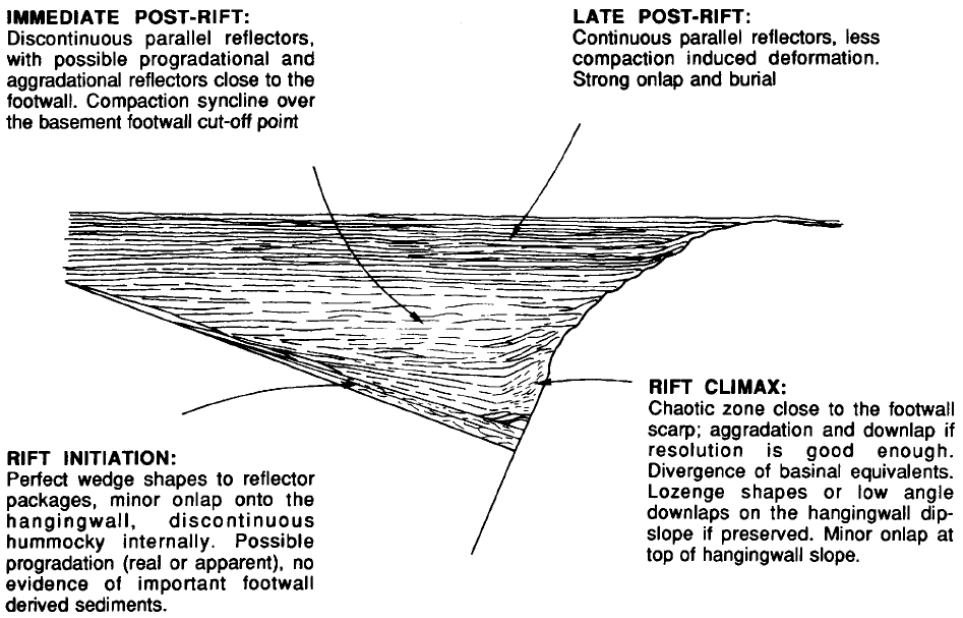

Fig. 4.19 An idealized section through an ideal basin showing the four different systems tracts and their associated characteristic seismic expression. From Prosser (1993).

The Aptian reflections in line II and IV (Fig. 4.15) mark the lower boundary of a unit which thickens toward the master fault. Corresponding features are observed in the northeastern part of line I (Fig. 4.17). The thick succession of post-Aptian sediment infill (see e.g. Fig. 4.20) in subarea B cause ambiguity in terms of determining the duration of this phase and potential later phases of movement. A very important observation, however, is that the fault is seen to cut all reflections up to the Quaternary unconformity in some of the seismic sections (Fig. 4.15).

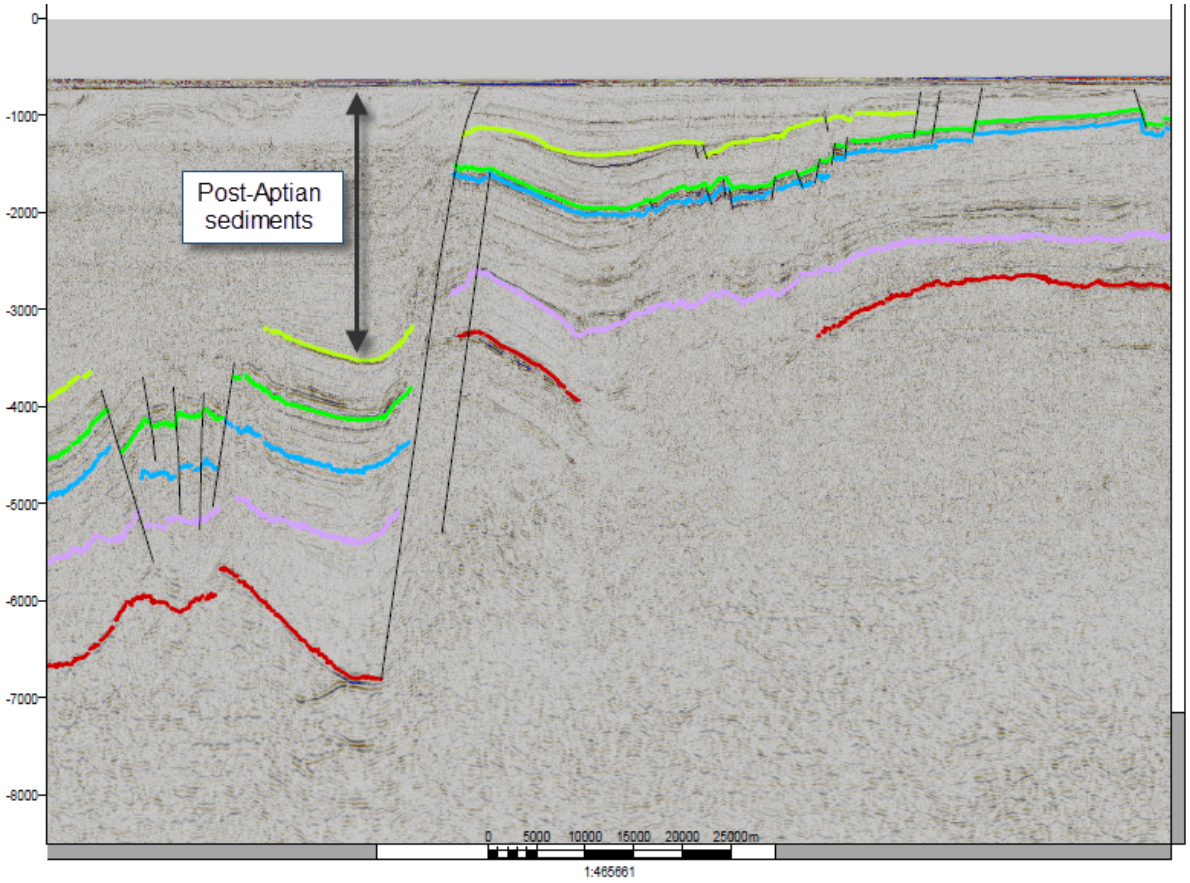

Fig. 4.20 Line II displaying the thick post-Aptian sediment package.

Line I (Fig. 4.17) and IV (Fig. 4.15) also display this sediment thickening between the base Cretaceous and Aptian reflection, indicating early Cretaceous movement as suggested by Faleide et al. (1984) and Gabrielsen et al. (1990b). Signs of movement in this interval in line II are more subtle. Some indications of movement are also seen within the Jurassic succession.

Between the (base) Permian and Jurassic reflections in line II, two sequences, possibly representing two phases of movement, have been mapped (Fig. 4.21). Several of the characteristic seismic signatures related to different rift phases as defined by Prosser (1993) can be recognized (Fig. 4.19). The lower sequence is missing a clearly defined late post-rift stage. This could imply that the first phase of fault movement rapidly was succeeded by renewed activity. Nevertheless, it indicates two discrete phases of tectonic activity, as opposed to continuous movement. Line I displays similar features in the Permian and Triassic interval (Fig. 4.17), indicating movement during Permian and (early?) Triassic. This is in agreement with Gabrielsen et al. (1990b) and Gudlaugsson et al. (1998). The northeastern part of line I (Fig. 4.17) also shows a significant thickening of the Permian and Triassic interval, supporting the belief of Permian - Early Triassic extension in the Fingerdjupet Subbasin (Gudlaugsson et al., 1998).

Fig. 4.22 shows a compilation of earlier studies addressing timing of tectonic movements in the study area.

4.4 Continuation of the Selis Ridge

The development of the Loppa High and the relict structural high which was initiated during Late Paleozoic, the Selis Ridge (Fig. 4.23), have been important structures since Late Paleozoic. Glørstad-Clark (2011) made a clear distinction between the two structures; Loppa High was formed in the latest Jurassic - early Cretaceous times while the Selis Ridge is defined as a Late Paleozoic to Early Triassic high. The reflections observed in line II (Fig. 4.15) are interpreted to be a prograding clinoform, relating the area to the regional development of the southwestern Barents Sea during Triassic and illustrates that the Selis Ridge was as a structural high and a western sediment barrier during Late Paleozoic - Early Mesozoic in agreement with Glørstad-Clark et al. (2010) and Glørstad-Clark (2011). The Selis Ridge being defined as a narrow N - S trending high bounded in the west by the Jason Fault Complex, the Leirdjupet Fault Complex might bound a northern continuation of this ridge. Gabrielsen et al. (1990b) did not discriminate between the Loppa High and the relict Selis Ridge, but considered the pre-Ladinian

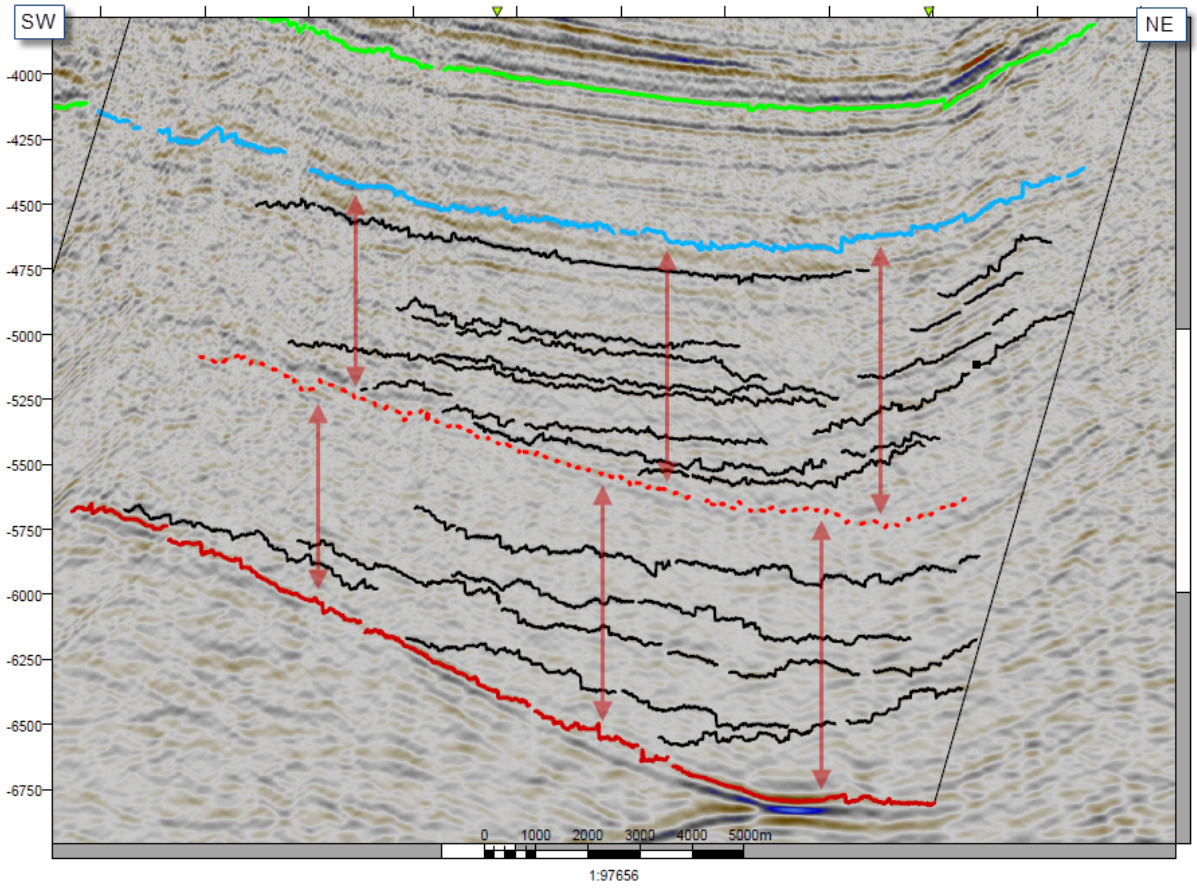

Fig. 4.21 Detailed interpretation of the interval between the Permian through Jurassic reflections displaying wedge geometries. The Permian reflection marks the lower boundary of the first sequence, whereas the red dotted line represents the lower boundary of the second sequence.

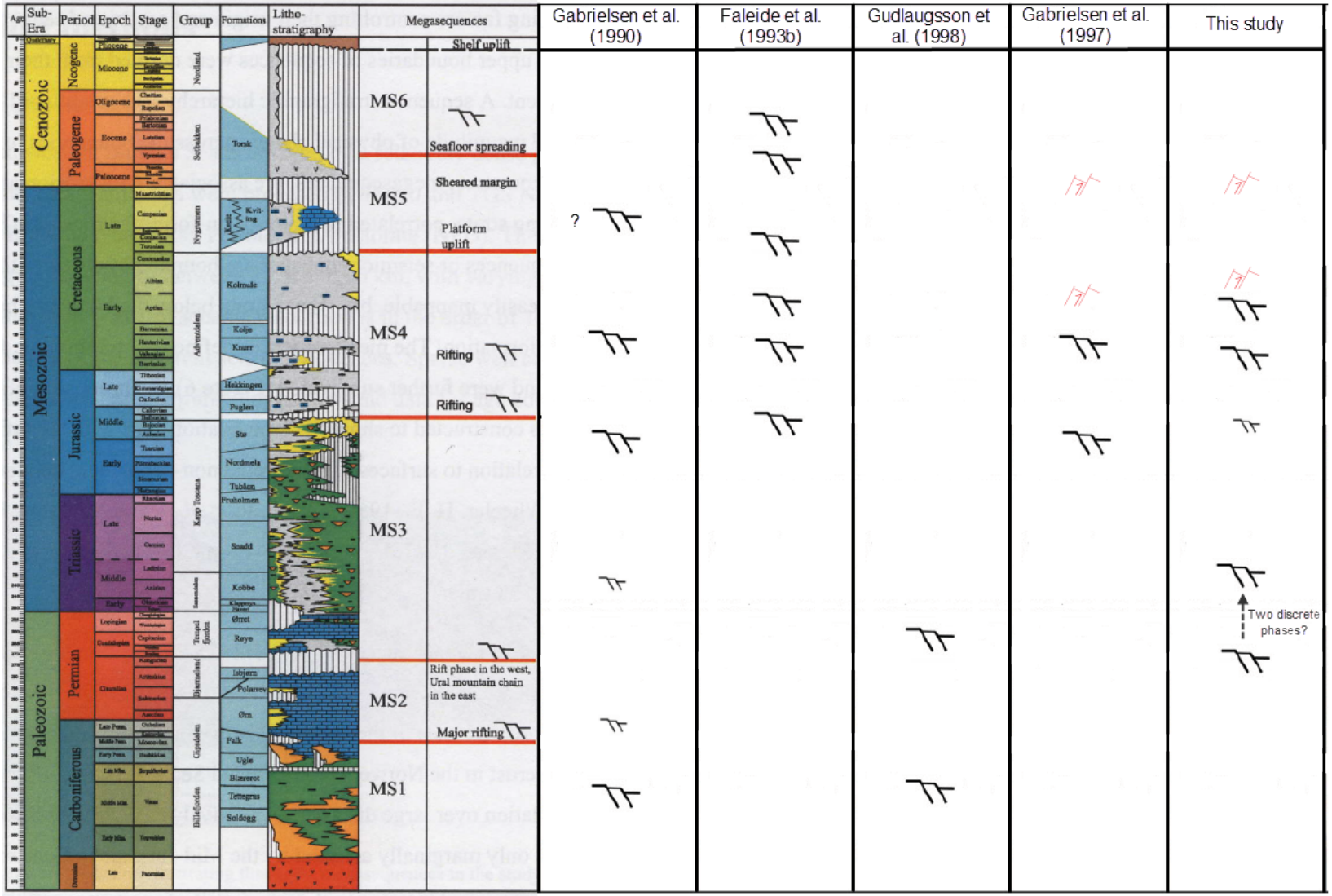

Fig. 4.22 Lithostratigraphy (modified from Glørstad-Clark et al. (2010)) and compilation of tectonic phases in the southwestern Barents Sea as presented in other studies. Glørstad-Clark et al. (2010) includes the whole western Barents Sea, Gabrielsen et al. (1990b) is more localized to the Leirdjupet Fault Complex, Faleide et al. (1993b) includes events of regional scale during Late Mesozoic - Cenozoic, Gudlaugsson et al. (1998) includes events during Late Paleozoic, Gabrielsen et al. (1997) considers the Bjørnøyrenna Fault Complex which includes the Leirdjupet Fault Complex.

evolution of Fingerdjupet Subbasin to be closely associated to the development of what later became the Loppa High. The presence and faulted succession of Permian strata further strengthen this notion of a northern continuation of the Selis Ridge. This further implies that the Leirdjupet Fault Complex has been active through several periods and has exerted a regional tectonic influence qualifying as a class 1 fault (Table 4.1 and Fig. 4.13).

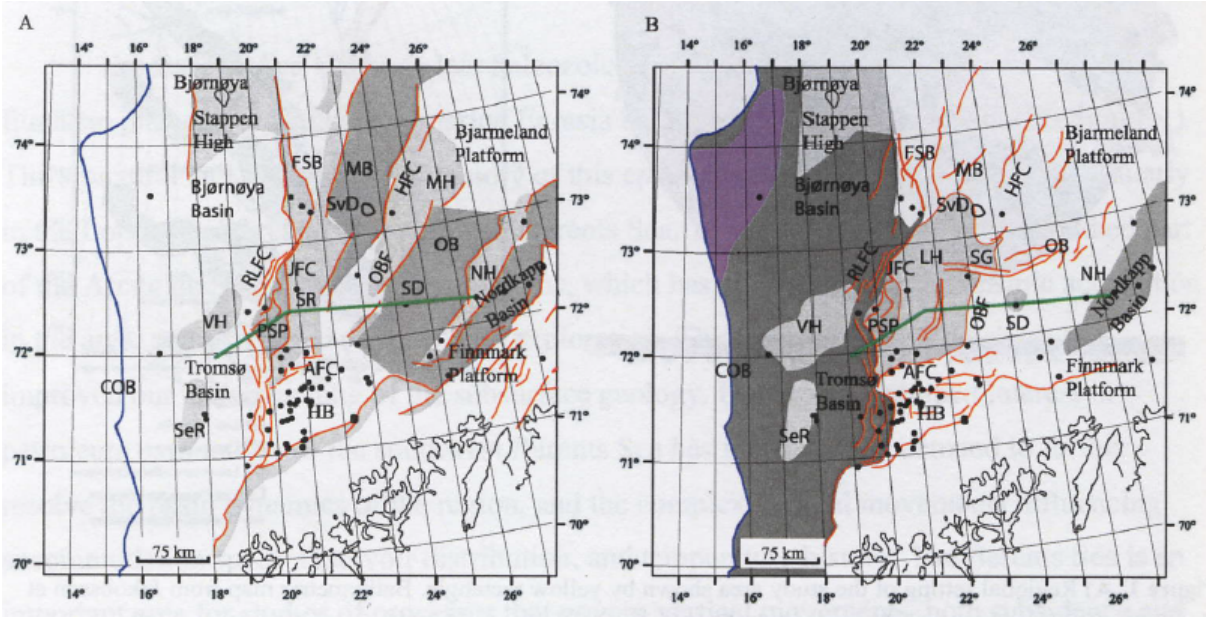

Fig. 4.23 Structural elements of the southwestern Barents Sea. A) Late Paleozoic structural elements, illustrating the Selis Ridge. B) Present day structural elements with the broader Loppa High. AFC = Asterias Fault Complex, BFC = Billefjorden Fault Complex, COB = Continent-Ocean-Boundary, HB = Hammerfest Basin, HFC = Hoop Fault Complex, FSB = Fingerdjupet Sub-basin, LH = Loppa High, MB = Maud Basin, MH = Mercurius High, NH = Norsel High, OB = Ottar Basin, OBF = Ottar Basin bounding faults, PSP = Polheim Sub-Platform, RLFC = Ringvassøy-Loppa Fault Complex, SD = Samson Dome, SG = Swaen Graben, SHF = Sørkapp-Hornsund Fault zone, SR = Selis Ridge, SvD = Svalis Dome, SeR = Senja Ryggen, VH = Veslemøy High, JFC = Jason Fault Complex. From Glørstad-Clark (2011).

5 Conclusion

The Leirdjupet Fault Complex is an extensional feature which has been affected by several periods of extension, and subordinate phases of inversion. The fault complex experienced rifting in the Late Permian extending into the Triassic and was affected by at least two later phases of extension in the Late Jurassic - Early Cretaceous and during the Cretaceous (intra-Aptian). The folds are associated with inversion and may have been caused by a phase of head-on contraction in late Cretaceous - early Tertiary. The fault complex is likely to have been developed due to pre-existing zones of weakness inherited from earlier tectonic movement and related to a Caledonian structural grain. The Leirdjupet Fault Complex is likely to represent a fault system of broad extent and is part of large complicated network of fault complexes in the southwestern Barents Sea.

The fault complex shows some indications of fault segmentation, although definite signs of this are hard to obtain with the data at hand.

The presence of Permian sediments, prograding clinoforms in the Triassic interval and the similar north-south trend of the controlling fault implies that the Leirdjupet Fault Complex may bound a northern continuation of the Selis Ridge. Furthermore, this would strengthen the notion that the Leirdjupet Fault Complex can be regarded as a class 1 fault. This would imply that the complex has had a regional significance, representing the eastern boundary separating the western basin province from the eastern province which is dominated by platforms and terraces.

References

Arlov, T.B. 2003, *Svalbards historie*. Tapir akademisk forlag.

Barnett, J.A.M., Mortimer, J., Rippon, J.H., Walsh, J.J., and Watterson, J. 1987, Displacement Geometry in the Volume Containing a Single Normal Fault. *The American Association of Petroleum Geologists Bulletin* 71, pp. 925–937.

Barrère, C. 2009, *Integrated geophysical modelling and tectonic evolution of the western Barents Sea*. Ph.D. thesis, Norwegian University of Science and Technology.

Barrère, C., Ebbing, J., and Gernigon, L. 2009, Offshore prolongation of Caledonian structures and basement characterisation in the western Barents Sea from geophysical modelling. *Tectonophysics* 470, pp. 71–88.

Bjørlykke, K. and Egeberg, P.K. 1993, Quartz Cementation in Sedimentary Basins. *The American Association of Petroleum Geologists Bulletin* 77, pp. 1538–1548.

Bjørlykke, K. 2006, Effects of compaction processes on stresses, faults, and fluid flow in sedimentary basins: examples from the Norwegian margin. In: Buiter, S.J.H. and Schreurs, G. (Eds.) *Analogue and Numerical Modelling of Crustal-Scale Processess*, Geological Society London, Special Publications, vol. 253, pp. 359–379.

Bjørlykke, K. and Jahren, J. 2010, Sandstones and Sandstone Reservoirs. In: Bjørlykke, K. (Ed.) *Petroleum Geoscience: From Sedimentary Environments to Rock Physics*, Springer Verlag, pp. 113–140.

Braathen, A., Bælum, K., Maher, H., and Buckley, S.J. 2011, Growth of extensional faults and folds during deposition of an evaporite-dominated half-graben basin; the Carboniferous Billefjorden Trough, Svalbard. *Norwegian Journal of Geology* 91, pp. 137–160.

Breivik, A.J., Faleide, J.I., and Gudlaugsson, S.T. 1998, Southwestern Barents Sea margin: late Mesozoic sedimentary basins. *Tectonophysics* 293, pp. 21–44.

Breivik, A.J., Gudlaugsson, S.T., and Faleide, J.I. 1995, Ottar Basin, SW Barents Sea: a major Upper Palaeozoic rift basin containing large volumes of deeply buried salt. *Basin Research* 7, pp. 299–312.

Brown, A.R. 2004, *Interpretation of Three-Dimensional Seismic Data, 6th Edition*, vol. 42. The American Association of Petroleum Geologists and the Society of Exploration Geophysicists.

Bugge, T., Elvebakk, G., Fanavoll, S., Mangerud, G., Smelror, M., Weiss, H.M., Gjelberg, J., Kristensen, S.E., and Nilsen, K. 2002, Shallow stratigraphic drilling applied in hydrocarbon exploration of the Nordkapp Basin, Barents Sea. *Marine and Petroleum Geology* 19, pp. 13–37.

Christiansson, P., Faleide, J.I., and Berge, A.M. 2000, Crustal structure in the northern North Sea: an integrated geophysical study. In: *Dynamics of the Norwegian margin*, Geological Society London. Special Publication, vol. 167, pp. 15–40.

Dalland, A., Worsley, D., and Ofstad, K. 1988, A lithostratigraphic scheme for the Mesozoic and Cenozoic succession offshore mid- and northern Norway. *Norwegian Petroleum Directorate Bulletin* 4, p. 65.

Davison, I. 1994, Linked Fault Systems; Extensional,Strike-Slip and Contractional. In: Hancock, P.L. (Ed.) *Continental Deformation*, Pergamon Press, pp. 121–142.

Dimakis, P., Braathen, B.I., Faleide, J.I., Elverhøi, A., and Gudlaugsson, S.T. 1998, Cenozoic erosion and the preglacial uplift of the Svalbard - Barents Sea region. *Tectonophysics* 300, pp. 311–327.

Ebbing, J. and Olesen, O. 2010, New compilation of top basement and basement thickness for the Norwegian continental shelf reveals the segmentation of the passive margin system. In: Vining, B.A. (Ed.) *Petroleum Geology: From Mature Basins to New Frontiers – Proceedings of the 7th Petroleum Geology Conference*, pp. 885–897, doi:10.1144/0070885.

Egeland, A. and Deehr, C.S. 2011, Roald Amundsen's contributions to our knowledge of the magnetic fields of the Earth and the Sun. *Hist. Geo Space. Sci.* 2, pp. 99–112, doi:10.5194/hgss-2-99-2011.

Eidvin, T., Jansen, E., and Riis, F. 1993, Chronology of Tertiary fan deposits off the western Barents Sea: Implications for the uplift and erosion history of the Barents Shelf. *Marine Geology* 112, pp. 109–131.

England, W.A. 1994, Secondary Migration and Accumulation of Hydrocarbons. In: Magoon, L.B. and Dow, W.G. (Eds.) *The petroleum system—from source to trap*, AAPG Memoir, vol. 60, pp. 211–217.

Evans, D., Graham, C., Armour, A., and Bathurst, P. 2002, *Millennium Atlas: Petroleum Geology of Central & Northern North Sea*. Geological Society London.

Faleide, J.I., Vågnes, E., and Gudlaugsson, S.T. 1993a, Late Mesozoic-Cenozoic evolution of the southwestern Barents Sea. In: Parker, J.R. (Ed.) *Petroleum Geology of Northwest Europe: Proceedings of the 4th Conference*, The Geological Society, London, pp. 933–950.

Faleide, J.I., Bjørlykke, K., and Gabrielsen, R.H. 2010, Geology of the Norwegian Continental Shelf. In: Bjørlykke, K. (Ed.) *Petroleum Geoscience: From Sedimentary Environments to Rock Physics*, Springer Verlag, pp. 467–499, doi: 10.1007/978-3-642-02332-3_22.

Faleide, J.I., Gudlaugsson, S.T., and Jacquart, G. 1984, Evolution of the western Barents Sea. *Marine and Petroleum Geology* 1, pp. 123–150.

Faleide, J.I., Solheim, A., Fiedler, A., Hjelstuen, B.O., Andersen, E.S., and Vanneste, K. 1996, Late Cenozoic evolution of the western Barents Sea-Svalbard continental margin. *Global and Planetary Change* 12, pp. 53–74.

Faleide, J.I., Tsikalas, F., Breivik, A.J., Mjelde, R., Ritzmann, O., Øyvind Engen, Wilson, J., and Eldholm, O. 2008, Structure and evolution of the continental margin off Norway and the Barents Sea. *Episodes* 31, pp. 82–91.

Faleide, J.I., Vågnes, E., and Gudlaugsson, S.T. 1993b, Late Mesozoic-Cenozoic evolution of the south-western Barents Sea in a regional rift-shear tectonic setting. *Marine and Petroleum Geology* 10, pp. 186–214.

Fawad, M., Mondol, N.H., Jahren, J., and Bjørlykke, K. 2011, Mechanical compaction and ultrasonic velocity of sands with different texture and mineralogical composition. *Geophysical Prospecting* 59, pp. 697–720, doi:10.1111/j.1365-2478.2011.00951.x.

Fjeldskaar, W., ter Voorde, M., Johansen, H., Christiansson, P., Faleide, J.I., and Cloetingh, S.A.P.L. 2004, Numerical simulation of rifting in the northern Viking Graben: the mutual effect of modelling parameters. *Tectonophysics* 382, pp. 189–212.

Gabrielsen, R.H. 1984, Long-lived fault zones and their influence on the tectonic development of the southwestern Barents Sea. *J. geol. Soc. London* 141, pp. 651–662.

Gabrielsen, R.H., Faerseth, R.B., Steel, R.J., Idil, S., and Kløvjan, O.S. 1990a, Architectural styles of basin fill in the northern Viking Graben. In: Blundell, D.J. and Gibbs, A.D. (Eds.) *Tectonic evolution of the North Sea rifts*, Oxford University Press, pp. 158–179.

Gabrielsen, R.H., Færseth, R.B., Jensen, L.N., Kalheim, J.E., and Riis, F. 1990b, Structural elements of the Norwegian continental shelf - part I: the Barents Sea Region. *Norwegian Petroleum Directorate Bulletin* 6, p. 33.

Gabrielsen, R.H., Grunnaleite, I., and Ottesen, I. 1992, Reactivation of fault complexes in the Loppa High area, southwestern Barents Sea. In: Vorren, T.O., Bergsager, E., Dahl-Stamnes, .A., Holter, E., Johansen, B., Lie, E., and Lund, T.B. (Eds.) *Arctic Geology and Petroleum Potential*, Elsevier Science, pp. 631–641.

Gabrielsen, R.H., Grunnaleite, I., and Rasmussen, E. 1997, Cretaceous and

Tertiary inversion in the Bjørnøyrenna Fault Complex, south-western Barents Sea. *Marine and Petroleum Geology* 14, pp. 165–178.

Gabrielsen, R.H. 2010, The Structure and Hydrocarbon Traps of Sedimentary Basins. In: Bjørlykke, K. (Ed.) *Petroleum Geoscience: From Sedimentary Environments to Rock Physics*, Springer Verlag, pp. 299–327, doi:10.1007/978-3-642-02332-3_12.

Gawthorpe, R.L. and Leeder, M.R. 2000, Tectono-sedimentary evolution of active extensional basins. *Basin Research* 12, pp. 195–218.

Gawthorpe, R. and Hurst, J.M. 1993, Transfer zones in extensional basins: their structural style and influence on drainage development and stratigraphy. *Journal of the Geological Society* 150, pp. 1137–1152.

Gjelsvik, T. 1976, Utforskningen av kontinentalsokkelen i Barentshavet — fra Fridtjof Nansens tid til i dag. *Norwegian Academy of Science and Letters* pp. 5–42.

Glørstad-Clark, E., Birkeland, E., Nystuen, J., Faleide, J., and Midtkandal, I. 2011, Triassic platform-margin deltas in the western Barents Sea. *Marine and Petroleum Geology* 28, pp. 1294–1314, doi:10.1016/j.marpetgeo.2011.03.006.

Glørstad-Clark, E. 2011, *Basin analysis in the western Barents sea area: The interplay between accomodation space and depositional systems*. Ph.D. thesis, University of Oslo.

Glørstad-Clark, E., Faleide, J.I., Lundschien, B.A., and Nystuen, J.P. 2010, Triassic seismic sequence stratigraphy and paleogeography of the western Barents Sea area. *Marine and Petroleum Geology* 27, pp. 1448–1475, doi:10.1016/j.marpetgeo.2010.02.008.

Green, P.F. and Duddy, I.R. 2010, Synchronous exhumation events around the Arctic including examples from Barents Sea and Alaska North Slope. In: Vining, B.A. and Pickering, S.C. (Eds.) *Petroleum Geology: From Mature Basins to New Frontiers — Proceedings of the 7th Petroleum Geology Conference*, Geological Society, London, vol. 7, pp. 633–644, doi:10.1144/0070633.

Grunnaleite, I. 2002, *Inversion in the Norwegian continental shelf with particular emphasis on the areas N of 62°N*. Ph.D. thesis, University of Bergen.

Gudlaugsson, S.T., Faleide, J.I., Johansen, S.E., and Breivik, A.J. 1998, Late palaeozoic structural development of the South-western Barents Sea. *Marine and Petroleum Geology* 15, pp. 73–102.

Hayward, A.B. and Graham, R.H. 1989, Some geometrical characteristics of inversion. In: Cooper, M.A. and Williams, G.D. (Eds.) *Inversion Tectonics*, Geological Society Special Publications, vol. 44, pp. 17–39, doi:10.1144/GSL.SP.1989.044.01.03.

Hjelstuen, B.O., Eldholm, O., and Faleide, J.I. 2007, Recurrent Pleistocene mega-failures on the SW Barents Sea margin. *Earth and Planetary Science Letters* 258, pp. 605–618.

Johannessen, E.P. and Steel, R.J. 1992, Mid-carboniferous extension and rift-infill sequence in the Billefjorden Trough, Svalbard. *Norsk Geologisk Tidsskrift* 72, pp. 35–48.

Klemme, H.D. 1994, Petroleum Systems of the World Involving Upper Jurassic Source Rocks. In: Magoon, L.B. and Dow, W.G. (Eds.) *The petroleum system—from source to trap*, AAPG Memoir, vol. 60, pp. 51–72.

Knutsen, S.M., Augustson, J.H., and Pål, H. 2000, Exploring the Norwegian part of the Barents Sea — Norsk Hydro's lessons from nearly 20 years of experience. In: Ofstad, K., Kittilsen, J.E., and Alexander-Marrack, P. (Eds.) *Improving the Exploration Process by Learning from the Past*, Elsevier Science B.V., pp. 99–112.

Leeder, M.R. and Jackson, J.A. 1993, The interaction between normal faulting and drainage in active extensional basins, with examples from the western United States and central Greece. *Basin Research* 5, pp. 79–102.

Lundin, E. and Doré, A.G. 2002, Mid-cenozoic post-breakup deformation in the 'passive' margins bordering the Norwegian-Greenland Sea. *Marine and Petroleum Geology* 19, pp. 79–93.

Magoon, L.B. and Dow, W.G. 1994, The Petroleum System. In: Magoon, L.B. and Dow, W.G. (Eds.) *The petroleum system—from source to trap*, AAPG Memoir, vol. 60, pp. 3–24.

Maher, H.D. and Braathen, A. 2010, Løvehovden fault and billefjorden rift basin segmentation and development, spitsbergen, norway. *Geological Magazine* 148, pp. 154–170, doi:10.1017/S0016756810000567.

Maher, H.D. and Braathen, A. 2011, Løvehovden fault and Billefjorden rift basin segmentation and development, Spitsbergen, Norway. *Geol. Mag.* 148, pp. 154–170, doi:10.1017/S0016756810000567.

Mondol, N.H., Bjørlykke, K., Jahren, J., and Høeg, K. 2007, Experimental mechanical compaction of clay mineral aggregates — Changes in physical properties of mudstones during burial. *Marine and Petroleum Geology* 24, pp. 289–311, doi:10.1016/j.marpetgeo.2007.03.006.

Mussett, A.E. and Khan, M.A. 2000, Refraction seismology. In: *Looking Into The Earth: An Introduction to Geological Geophysics*, Cambridge University Press, pp. 65–83.

Nøttvedt, A., Gabrielsen, R.H., and Steel, R.J. 1995, Tectonostratigraphy and sedimentary architecture of rift basins, with reference to the northern north sea. *Marine and Petroleum Geology* 12, pp. 881–901.

Nøttvedt, A., Berge, A.M., Dawers, N.H., Færseth, R.B., Häger, K.O., Mangerud, G., and Puigdefabregas, C. 2000, Syn-rift evolution and resulting play models in the Snorre-H area, northern North Sea. In: Nøttvedt, A. (Ed.) *Dynamics of the Norwegian Margin*, Geological Society, London, Special Publications, vol. 167, pp. 179–218.

Odinsen, T., Christiansson, P., Gabrielsen, R.H., Faleide, J.I., and Berge. 2000, The geometries and deep structure of the northern North Sea rift system. In:

Nøttvedt, A. (Ed.) *Dynamics of the Norwegian margin*, Geological Society London, Special Publication, pp. 41–57.

Ohm, S.E., Karlsen, D.A., and Austin, T.J.F. 2008, Geochemically driven exploration models in uplifted areas: Examples from the Norwegian Barents Sea. *AAPG Bulletin* 92, pp. 1191–1223.

Osmundsen, P.T., Andersen, T.B., S., M., and Svendby, A.K. 1998, Tectonics and sedimentation in the hangingwall of a major extensional detachment: the Devonian Kvamshesten Basin, western Norway. *Basin Research* 10, pp. 213–234.

Prosser, S. 1993, Rift-related linked depositional systems and their seismic expression. *Geological Society, London, Special Publications* 71, pp. 35–66, doi:10.1144/GSL.SP.1993.071.01.03.

Ritzmann, O. and Faleide, J.I. 2007, Caledonian basement of the western Barents Sea. *Tectonics* 26, p. 20, doi:10.1029/2006TC002059.

Rønnevik, H.C. 1981, Geology of the barents sea. In: Illing, L.V. and Hobson, G.D. (Eds.) *Petroleum Geology of the Continental Shelf of North-West Europe*, Heyden & Son LTD, pp. 395–406.

Rønnevik, H. and Jacobsen, H.P. 1984, Structural highs and basins in the western Barents Sea. In: Spencer, A.M., Holter, E., Johnsen, S.O., Mørk, A., Nysæther, E., Songstad, P., and Spinnangr, n. (Eds.) *Petroleum Geology of the North European Margin*, Graham & Trotman, pp. 19–32.

Rüpke, L.H., Schmalholz, S., Schmid, D.W., and Podladchikov, Y. 2008, Automated thermotectonostratigraphic basin reconstruction: Viking Graben case study. *AAPG Bulletin* 92, pp. 309–326.

Ryseth, A., Augustson, J.H., Charnock, M., Haugerud, O., Stig-Morten, Knutsen, Midbøe, P.S., Opsal, J.G., and Sundsbø, G. 2003, Cenozoic stratigraphy and evolution of the Sørvestsnaget Basin, southwestern Barents Sea. *Norwegian Journal of Geology* 83, pp. 107–130.

Schlische, R.W., Young, S.S., Ackermann, R.V., and Gupta, A. 1996, Geometry and scaling relations of a population of very small rift-related normal faults. *Geology* 24, pp. 683–686.

Smelror, M., Petrov, O.V., Larssen, G.B., and Werner, S. 2009, *Atlas: Geological History of the Barents Sea*. Geological Survey of Norway.

Stewart, D.J., Berge, K., and Bowlin, B. 1995, Exploration trends in the Southern Barents Sea. In: Hanslien, S. (Ed.) *Petroleum Exploration and Exploitation in Norway*, Norwegian Petroleum Society, pp. 253–276.

Østvedt, O.J., Blystad, P., and Magnus, C. 2005, Assessment of undiscovered resources on the Norwegian Continental Shelf. In: Doré, A.G. and Vining, B.A. (Eds.) *Petroleum Geology: North-West Europe and Global Perspectives—Proceedings of the 6th Petroleum Geology Conference*, Geological Society, London, pp. 55–62.

Tissot, B.P., Pelet, R., and Ungerer, P. 1987, Thermal History of Sedimentary Basins, Maturation Indices and Kinetics of Oil and Gas Generation. *The American Association of Petroleum Geologists Bulletin* 71, pp. 1445–1466.

Waples, D.W. 1994, Maturity Modeling: Thermal Indicators, Hydrocarbon Generation, and Oil Cracking. In: Magoon, L.B. and Dow, W.G. (Eds.) *The petroleum system—from source to trap*, AAPG Memoir, vol. 60, pp. 285–306.

Wessel, P. and Smith, W.H.F. 1998, New, improved version of Generic Mapping Tools released. *EOS Trans. Amer. Geophys. U.* 79, p. 579.

Woodcock, N.H. and Schubert, C. 1994, Continental Strike-Slip Tectonics. In: Hancock, P.L. (Ed.) *Continental Deformation*, Pergamon Press, pp. 251–263.

Worsley, D. 2008, The post-Caledonian development of Svalbard and the western Barents Sea. *Polar Research* 27, pp. 298–317, doi:10.1111/j.1751-8369.2008.00085.x.